TECHNICAL UNIVERSITY OF LIBEREC
Faculty of Mechanical Engineering

DIAGNOSTIC SYSTEM FOR LOW-SPEED BEARINGS

Dissertation thesis

Study programme:	P2302 – Machines and Equipment
Study branch:	2302V010 – Machine and Equipment Design
Author:	**Dipl.-Ing. Michael Oeljeklaus**
Supervisor:	prof. Ing. Lubomír Pešík, CSc.

Liberec 2019

Declaration

I hereby certify that I have been informed that Act 121/2000, the Copyright Act of the Czech Republic, namely article 60 – Schoolwork, applies to my thesis in full.

I acknowledge that the Technical University of Liberec (TUL) does not infringe my copyrights by using my thesis for TUL's internal purposes.

I am aware of my obligation to inform TUL if I have charged for the use of my thesis or sold a licence to use it; in such a case TUL can ask to be reimbursed for the costs incurred when supervising this thesis.

I have written my thesis myself using the literature listed therein and in consultation with my supervisor and my tutor.

I also confirm that the printed version of my thesis is consistent with an electronic version, submitted via IS STAG.

Date:

Signature:

Supplementary statement

I hereby declare that this thesis is the result of my own work, having been supported by my employer ŠKODA AUTO a.s. and the Technical University of Liberec under the guidance of my doctoral supervisor prof. Lubomír Pešík, CSc. and having used the literature cited in the appendix.

Date:

Signature:

Abstract

This thesis resolves the current issue of running diagnostics on low-speed bearings and has resulted from urgent industry requirements.

The central concept of the design solution is the introduction of a reference element into the sprocket shaft bearing assembly of a chain conveyor used in the ŠKODA AUTO a.s. paint shop.

Using two pairs of roller bearings each, this reference element is connected to both the shaft as well as the frame. With this design, the reference element can freely rotate, thereby making it possible to run diagnostics on the bearings.

Firstly, this design makes it possible to rotate the reference element at a high speed and – just like for high-speed bearings – establish the frequency of the vibrations, determining the level of damage in doing so. Secondly, it makes it possible to identify and measure the resistance when rotating the reference element.

This design solution has been successfully patented at a European level.

In the course of this thesis, various designs have been developed, one of which has been realised as a prototype and integrated into the conveyor system at the ŠKODA AUTO a.s. paint shop in Mladá Boleslav.

Keywords

Low-speed bearings, damage identification, monitoring of bearings, diagnostics of bearings, resistance diagnostics, vibration diagnostics.

Acknowledgements

Firstly, I would especially like to thank my doctoral supervisor prof. Ing. Lubomír Pešík, CSc. for his involvement in realising this thesis over the past four years, both personally and indirectly through the support with graphic design and technical work provided by staff from the Department of the Design of Machine Elements and Mechanism of the Technical University of Liberec led by prof. Ing. Ladislav Ševčík, CSc.

I would also like to thank the maintenance team from the ŠKODA AUTO a.s. paint shop in Mladá Boleslav, headed by Mr Václav Havelka, for their expert support.

Furthermore, I would like to thank the Internal Repairs team at ŠKODA AUTO a.s. in Mladá Boleslav, headed by Ing. René Fichna, for preparing and making the prototypes.

Without the extensive involvement of Ing. Zbyněk Kobylka from the ŠKODA AUTO a.s. patent department, it would not have been possible to successfully register my two European patents, which form the scientific basis of my thesis.

Not least, I would like to formally thank my employer ŠKODA AUTO a.s., firstly for giving me the opportunity to realise this scientific work over the past four years and secondly for financing this entire doctoral project.

Finally, I would like to thank my future wife Arwa who, over the past four years, frequently had to spend her weekends without me.

Contents

List of the symbols used **8**

1 Introduction **16**

2 Research **18**

3 Aim of thesis and processing methods **23**

4 Low-speed bearings in conveyor systems **25**

4.1 Kinematic diagram of the conveyor 25

4.2 Drive units and gear systems 26

4.2.1 Right-hand side EM2 drive unit 29

4.2.2 Left-hand side EM2 drive unit 30

4.2.3 The drive units' chain drive 31

4.2.4 The gear system's spring suspension 33

4.3 Sprocket shaft bearing assembly 36

4.3.1 Bearing parameters 37

4.3.2 Seal 39

5 Strength of the current sprocket shaft bearing assembly **40**

5.1 Forces acting on the conveyor chain 40

5.1.1 Dynamic calculation of the conveyor's drive unit 40

5.1.2 Spring displacement in the suspension of the drive unit 45

5.1.3 Data from the frequency converter 47

5.1.4 Malfunction 48

5.2 Sprocket shaft 48

5.2.1 Load on the sprocket shaft 49

5.2.2 Calculating stress and strain 51

5.2.3 Measuring the strain on the sprocket shaft 54

5.2.4 Comparison of calculations and measurements 56

5.3 Bearings 56

5.3.1 Load on the bearing 56

5.3.2 Calculation of load rating 57

6 Diagnosing damage in ball and roller bearings **59**

6.1 Kinematic conditions of ball and roller bearings 59

6.2 Kinematic analogy of rolling-element bearings and planetary gear systems ... 61
6.3 Vibration frequencies caused by bearing damage ... 64
6.3.1 Damage to the outer ring ... 65
6.3.2 Damage to the inner ring ... 66
6.3.3 Damage to the rolling element ... 67

7 Diagnostic device for low-speed ball and roller bearings ... 68
7.1 Running diagnostics based on measuring vibrations ... 68
7.1.1 Damage to the shaft bearing's inner ring ... 72
7.1.2 Damage to the shaft bearing's rolling element ... 73
7.1.3 Damage to the shaft bearing's outer ring ... 74
7.1.4 Damage to the frame bearing's inner ring ... 75
7.1.5 Damage to the frame bearing's rolling element ... 76
7.1.6 Damage to the frame bearing's outer ring ... 77
7.2 Running diagnostics based on identifying increased rolling resistance ... 78
7.2.1 Shaft bearing ... 80
7.2.2 Frame bearing ... 82

8 Design of the diagnostic device for low-speed bearings ... 84
8.1 Design of a new sprocket shaft bearing assembly ... 84
8.2 Stress analyses for a new assembly ... 86
8.2.1 The shaft's load, stress and safety factor ... 86
8.2.2 The reference element's load, stress and safety factor ... 87
8.2.3 Stress analysis using FEM ... 89
8.2.4 Load rating of the bearings ... 89
8.3 Design variants ... 89
8.3.1 Design variant I ... 90
8.3.2 Design variant II ... 94
8.3.3 Design variant III ... 98
8.3.4 Assessment of the design variants ... 102
8.4 Optimised design variant of the sprocket shaft bearing assembly ... 103
8.4.1 Design variant II, optimised ... 103
8.4.2 Assessment of the optimised design variant ... 107
8.5 Design of the optimised sprocket shaft bearing assembly ... 107
8.5.1 Parameters of the spherical roller bearing ... 109

8.5.2 Replacing the bearings in the event of repair 111

9 Laboratory test of the diagnostic device 114

9.1 Fatigue test on the first prototype 114

9.2 Load test on the first prototype 115

9.3 Diagnostic test on the second prototype 120

10 Conclusion 122

Literature 124

Appendix 126

A On attached CD 126

List of the symbols used

Chapter 4

a [m]	Dimension of bearing housing
b [m]	Dimension of bearing housing
B [m]	Width of the bearing
C [N]	Dynamic load rating
C_0 [N]	Static load rating
D [m]	Outer diameter
d_1 [m]	Pitch diameter
d_{1H} [m]	Inner diameter of bearing
d_2 [m]	Pitch diameter
d_3 [m]	Pitch diameter
d_4 [m]	Pitch diameter
e [−]	Calculation factor
h [m]	Height of bearing housing
i_{12} [−]	Reduction ratio
i_{34} [−]	Reduction ratio
n_1 [s^{-1}]	Rotational speed
n_2 [s^{-1}]	Rotational speed
n_3 [s^{-1}]	Rotational speed
n_3 [s^{-1}]	Rotational speed
p_{12} [m]	Pitch of the chain links
p_{34} [m]	Pitch of the chain links
R_k [Pa]	Yield strength
R_m [Pa]	Ultimate strength
Y_0 [−]	Calculation factor
Y_1 [−]	Calculation factor
Y_2 [−]	Calculation factor
z_1 [−]	Number of teeth

z_2 [−]	Number of teeth
z_3 [−]	Number of teeth
z_4 [−]	Number of teeth

Chapter 5

a [m]	Distance
b [m]	Distance
b_A [Nsm^{-1}]	Damping coefficient
β [rad]	Angle
C [N]	Dynamic load rating
d [m]	Diameter
d_5 [m]	Pitch diameter
e [m]	Distance
ε_{BB} [−]	Strain
ε_{BP} [−]	Strain
f_W [−]	Resistance due to friction
F [N]	Force
F_8 [N]	Maximum force
F_{B1} [N]	Bending force acting on shaft
F_{B2} [N]	Bending force acting on shaft
F_{B3} [N]	Bending force acting on shaft
F_{Bi} [N]	Bending force acting on shaft
F_{gK} [N]	Overall force acting on both conveyor chains
F_K [N]	Force acting on one conveyor chain
F_{K1} [N]	Force acting on one conveyor chain
F_{K2} [N]	Force acting on one conveyor chain
F_{K3} [N]	Force acting on one conveyor chain
F_{Ki} [N]	Force acting on one conveyor chain
F_W [N]	Transformed force due to resistance
φ_A [rad]	Angle of actuating movement

$\dot{\varphi}_A$ [rad s^{-1}]	Angular velocity of actuating movement
$\ddot{\varphi}_A$ [rad s^{-2}]	Angular acceleration of drive sprocket
i_{14}[Nm^{-1}]	Reduction ratio
J_A [kg m^2]	Mass moment of inertia of drive unit
J_I [kg m^2]	Transformed mass moment of inertia of conveyed objects
k_A [Nm^{-1}]	Overall spring rate
L [Mil]	Bearing life
m [−]	Calculation coefficient of bearing
M_1 [Nm]	Torque
M_4 [Nm]	Torque
M_5 [Nm]	Torque
M_A [Nm]	Moment of acceleration
M_b [Nm]	Damping moment
M_{Bi} [Nm]	Bending moment
M_{B2} [Nm]	Bending moment
M_i [Nm]	Moment of drive unit due to inertia
M_I [Nm]	Transformed moment of inertia due to conveyed objects
M_k [Nm]	Reaction moment of the drive unit's spring suspension
M_N [Nm]	Nominal torque
M_W [Nm]	Transformed moment due to resistance of conveyed objects
n [s^{-1}]	Rotational speed
P [N]	Equivalent dynamic bearing load
q_i [−]	Operational proportion of load
q_1 [−]	Operational proportion of load
q_2 [−]	Operational proportion of load
q_3 [−]	Operational proportion of load
r_1 [m]	Pitch radius
R_{Ai} [N]	Reaction force in bearing
R_{A1} [N]	Reaction force in bearing
R_{A2} [N]	Reaction force in bearing

R_{A3} [N]	Reaction force in bearing
R_{Bi} [N]	Reaction force in bearing
σ_{Bi} [Pa]	Bending stress
σ_{B2} [Pa]	Bending stress
v_1 [m s^{-1}]	Velocity
W_B [m^3]	Section modulus for bending
y_8 [m]	Maximum displacement of spring
y [m]	Deflection
z_1 [−]	Number of teeth
z_2 [−]	Number of teeth
z_3 [−]	Number of teeth
z_4 [−]	Number of teeth

Chapter 6

a_{A21} [m s^{-2}]	Acceleration
a_{A31} [m s^{-2}]	Acceleration
a_{A32} [m s^{-2}]	Acceleration
ε_{21} [rad s^{-2}]	Angular acceleration
ε_{31} [rad s^{-2}]	Angular acceleration
ε_{32} [rad s^{-2}]	Angular acceleration
ε_R [rad s^{-2}]	Angular acceleration of Résal
f [Hz]	Frequency
f_{DI} [Hz]	Damaged bearing frequency
f_{DO} [Hz]	Damaged bearing frequency
f_{DR} [Hz]	Damaged bearing frequency
φ_{21} [rad]	Angle
φ_{31} [rad]	Angle
φ_{32} [rad]	Angle
m [−]	Number of rolling elements
ω_{21} [rad s^{-1}]	Angular velocity

ω_{31} [rad s^{-1}]	Angular velocity
ω_{32} [rad s^{-1}]	Angular velocity
ω [rad s^{-1}]	Angular velocity
ω_C [rad s^{-1}]	Angular velocity
ω_I [rad s^{-1}]	Angular velocity
ω_O [rad s^{-1}]	Angular velocity
r_{A21} [m]	Radius vector
r_{A32} [m]	Radius vector
r_C [m]	Radius
r_I [m]	Radius
r_O [m]	Radius
r_R [m]	Radius
s_{A21} [m]	Distance
s_{A31} [m]	Distance
s_{A32} [m]	Distance
v_{A21} [m s^{-1}]	Velocity
v_{A31} [m s^{-1}]	Velocity
v_{A32} [m s^{-1}]	Velocity

Chapter 7

f_{DIF} [Hz]	Damaged bearing frequency
f_{DIS} [Hz]	Damaged bearing frequency
f_{DOF} [Hz]	Damaged bearing frequency
f_{DOS} [Hz]	Damaged bearing frequency
f_{DRF} [Hz]	Damaged bearing frequency
f_{DRS} [Hz]	Damaged bearing frequency
f_{IS} [Hz]	Frequency
f_{RE} [Hz]	Frequency
F_{PC} [N]	Circumferential force
F_{PG} [N]	Circumferential force

m_F [−]	Number of rolling elements
m_S [−]	Number of rolling elements
M_{Fr} [Nm]	Friction moment
M_{FB} [Nm]	Moment
M_{PC} [Nm]	Moment
M_{RG} [Nm]	Moment
M_{SB} [Nm]	Moment
ω_{CF} [rad s^{-1}]	Angular velocity
ω_{CS} [rad s^{-1}]	Angular velocity
ω_{DIF} [rad s^{-1}]	Angular velocity due to bearing damage
ω_{DIS} [rad s^{-1}]	Angular velocity due to bearing damage
ω_{DOF} [rad s^{-1}]	Angular velocity due to bearing damage
ω_{DOS} [rad s^{-1}]	Angular velocity due to bearing damage
ω_{DRF} [rad s^{-1}]	Angular velocity due to bearing damage
ω_{DRS} [rad s^{-1}]	Angular velocity due to bearing damage
ω_{IF} [rad s^{-1}]	Angular velocity
ω_{IS} [rad s^{-1}]	Angular velocity
ω_{OF} [rad s^{-1}]	Angular velocity
ω_{OS} [rad s^{-1}]	Angular velocity
ω_{RE} [rad s^{-1}]	Angular velocity
ω_{RF} [rad s^{-1}]	Angular velocity
ω_{RS} [rad s^{-1}]	Angular velocity
r_{CF} [m]	Radius
r_{CS} [m]	Radius
r_{IF} [m]	Radius
r_{IS} [m]	Radius
r_{OF} [m]	Radius
r_{OS} [m]	Radius
r_{PC} [m]	Radius
r_{RF} [m]	Radius

r_{RG} [m]	Radius
r_{RS} [m]	Radius
r_{SG} [m]	Radius

Chapter 8

a [m]	Distance
b [m]	Distance
B [mm]	Dimension of assembly
c [m]	Distance
C [N]	Dynamic load rating
C_0 [N]	Static load rating
d [m]	Inner diameter of bearing
d_C [m]	Inner diameter of reference element
D [m]	Outer diameter of bearing
D_C [m]	Outer diameter of reference element
e [m]	Distance
F [mm]	Dimension of assembly
F_{B2} [N]	Bending force acting on shaft
F_{B3} [N]	Bending force acting on shaft
F_{S2C} [N]	Shear force acting on reference element
L [mm]	Dimension of assembly
M_{B2C} [Nm]	Bending moment on reference element
R_{A2} [N]	Reaction force in bearing
R_{B2} [N]	Reaction force in bearing
R_{C2} [N]	Reaction force in bearing
R_{D2} [N]	Reaction force in bearing
s_{2C} [−]	Safety factor for the reference element
s_{3C} [−]	Safety factor for the reference element
s_{B2A} [−]	Safety factor for the shaft
s_{B2C} [−]	Safety factor for the reference element in bending

s_{B3A} [−]	Safety factor for the shaft in bending
s_{B3C} [−]	Safety factor for the reference element in bending
s_{S2C} [−]	Safety factor for the reference element in shear
s_{S3C} [−]	Safety factor for the reference element in shear
S_C [m^2]	Critical cross-sectional area of reference element
σ_{B2A} [Pa]	Bending stress on shaft
σ_{B2C} [Pa]	Bending stress on reference element
σ_{B3A} [Pa]	Bending stress on shaft
σ_{B3C} [Pa]	Bending stress on reference element
σ_{By} [Pa]	Yield strength in bending
σ_{BA}^{*} [Pa]	Fatigue strength in bending
τ_{S2C} [Pa]	Shearing stress on reference element
τ_{S3C} [Pa]	Shearing stress on reference element
τ_{Sy} [Pa]	Yield strength in shear
τ_{SC}^{*} [Pa]	Fatigue strength in shear
W_{BC} [m^3]	Section modulus

1 Introduction

In practice in industry, low-speed bearings can be found not only in the transportation sector, but also in manufacturing machines and systems using manufacturing technology closely associated with the conveying of material or processed products. This includes the metal-processing, mining, paper, and textile industries as well as, of course, the automotive industry.

In large industrial companies, production is currently largely carried out by numerous robots and complex production lines involving a high level of automation and computerised management. These lines often operate without human intervention and the complex production process is managed by monitoring systems. These systems gather data not only regarding productivity, but also regarding the functional status and operational wear of individual components. Fully automated, predictive diagnostics for machines and their components has become an integral part of industrial production.

In the automotive industry, chain conveyors are frequently used in chemical pretreatment processes and the cathodic dip coating of car bodies. Their chains' drive sprockets and guide wheels are mounted on shafts that are placed in two bearings on one side. Whilst the sprockets are found in the technological section of the painting line, the shaft bearings are located outside of this area and are not exposed to any chemicals, solvents or paints. The shafts and their corresponding bearings rotate at a rate of a few revolutions per minute and can therefore be described as low-speed. Running diagnostics on these bearings is of utmost importance. A damaged bearing must be identified before it completely fails, otherwise there is a risk of subsequent production downtime, which usually results in significant financial losses.

Although the layout of the sprocket shaft bearing assembly shields the bearings from any harmful environmental factors, the bearings have to meet significant requirements with regards to the strength of the entire construction. Extreme loads primarily occur close to the conveyor's main drive system, where the tensile forces acting on the chain are greatest.

Thus, chain conveyors constitute a complex transportation system in which the design of the drive system, in view of the loads arising from the transportation process, and the strength of the other components in the system are of great importance. These components are primarily the main conveyor chains, the carriers for the car bodies, the pendulums as well as the sprockets along with their shafts.

There is no doubt that the reliability of the chain conveyor's construction has a significant impact on production volume, particularly given that the paint shop usually is a bottleneck for the entire vehicle production process.

With regard to strength, the chain conveyor's components are subjected to stresses that display characteristics of quasi-static or dynamic load rating. In addition to the bearings, classic calculation methods and processes are used to determine the structural design of the chain conveyor's components. Here, the stresses in the observed critical cross sections are obtained using the finite element method and confronted with threshold values.

Bearings are generally designed based on manufacturer algorithms, and bearings defined in this manner have a certain probability to meet the requirements for reliable operation and a long lifespan. It cannot be ruled out that the bearing will sustain damage, even if it was designed correctly.

In car body conveyor systems and similar examples of constructions which require guaranteed continuous and smooth operation, it is necessary to constantly monitor the condition of the bearings and introduce efficient technical diagnostic methods. This is precisely the subject of this thesis.

While reliable diagnostic procedures based on measuring vibrations have been used for many years for high-speed bearings, issues relating to diagnostics for low-speed bearings remain unresolved. To this day, no suitable physics-based method has come to light that enables damaged low-speed bearings to be detected in good time.

The subject of this thesis is centred on resolving the issue of running diagnostics on low-speed roller bearings with a view to applying the findings to series operation at the ŠKODA AUTO a.s. paint shop in Mladá Boleslav.

2 Research

According to [1], it is possible to run diagnostics on low-speed ball and roller bearings by using the envelope method utilising wavelet transform (WT) denoising. Diagram as per *Fig. 2.1*

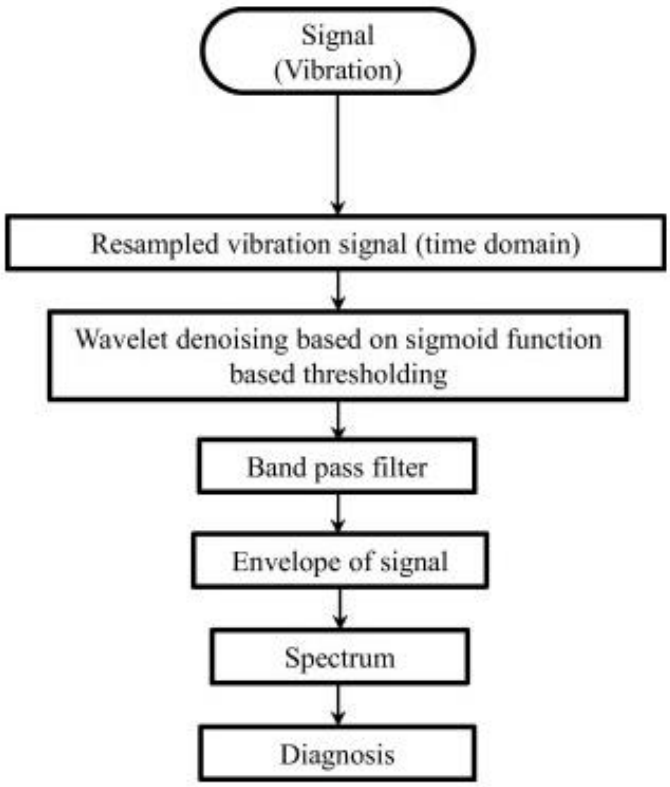

Fig. 2.1 Diagram of bearing diagnostics according to [1]

To ensure this method succeeds in detecting a bearing failure, it is important to select suitable parameters for the wavelet transform threshold. When running diagnostics on ball and roller bearings, it is sensible to use the sigmoid function as the threshold parameter.

According to [2], the sigmoid function exhibits a higher signal-to-noise ratio (SNR) i.e. the ratio between the effective load capacity and the level of the vibrational noise. The diagnostic method described in [1], however, is only suitable at relatively low bearing loads and at shaft speeds of over 30 rpm.

In line with the current industry trends of Industry 4.0, diagnostics can be run on ball and roller bearings using a deep-learning network. In [3], the author uses the LAMSTAR neural network to evaluate the recorded acoustic emission signal. In order to run diagnostics on the bearings, deep-learning networks can use test measuring signals for various types of bearing damage. Under laboratory conditions, this method has been validated for a shaft speed of 120 rpm.

In [4], the author makes use of the amplification of the acoustic emissions' useful signal and thus the increase of the SNR by 90 dB in order to run diagnostics on low-speed ball and roller bearings. Such an increase is sufficient to assess the acoustic emissions of damaged bearings using the envelope method. The article also mentions the possibility of running diagnostics on low-speed bearings by removing the noise from the recorded acoustic emission signal. This noise can be suppressed by the time limit value of the filtered signal's individual impulses (*Fig. 2.2*). The author further states that the idle time of the noise and the useful signal are different.

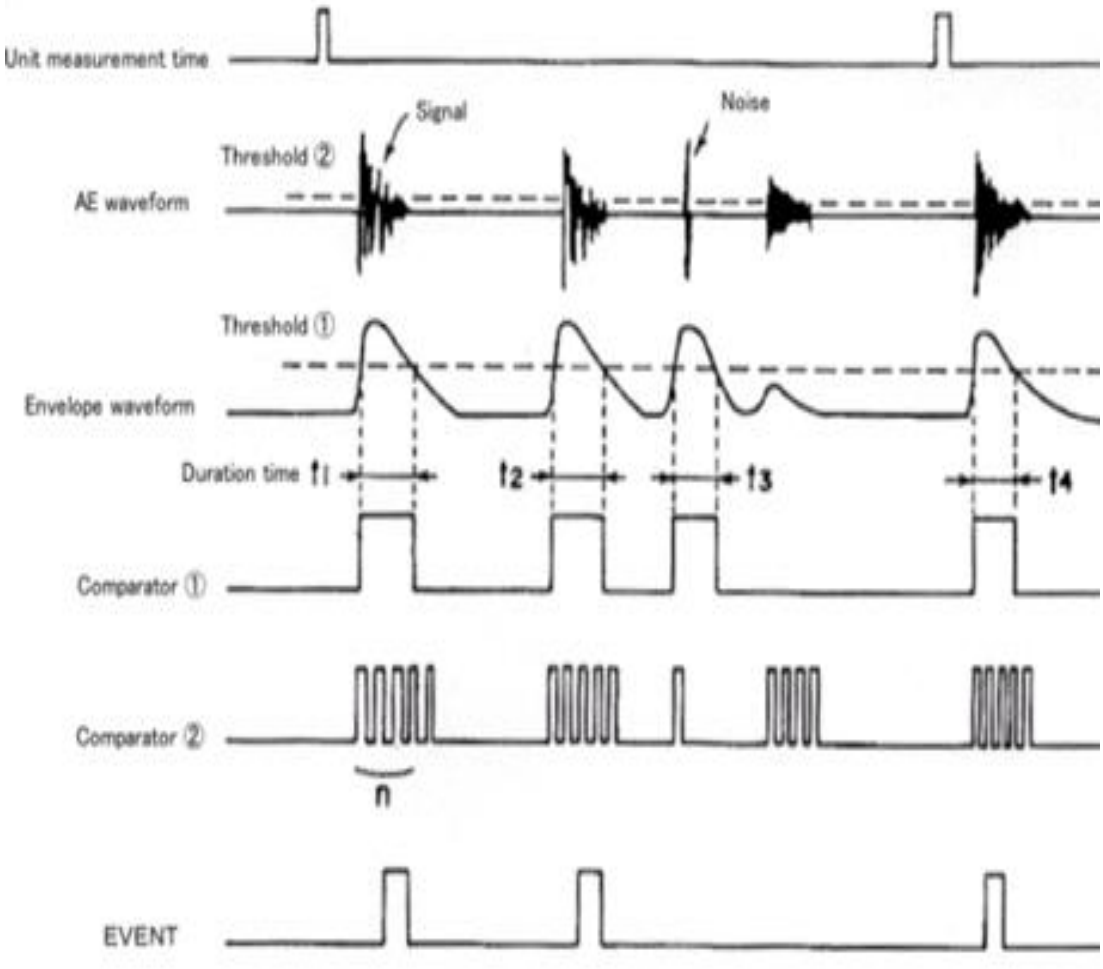

Fig. 2.2 Diagram of bearing diagnostics according to [4]

The methods described in [4] were tested on low-speed machines, such as those used in paper factories or rolling mills used for resin processing, and are effective at a shaft speed of 1 rpm.

Following a similar principle to that outlined in article [3], in [5] the author describes running diagnostics on low-speed roller bearings based on diagnostic rules ascertained using test measurements. In [5], this method is used on the recorded acceleration signal which is further processed using filters in the envelope spectra (*Fig. 2.3*).

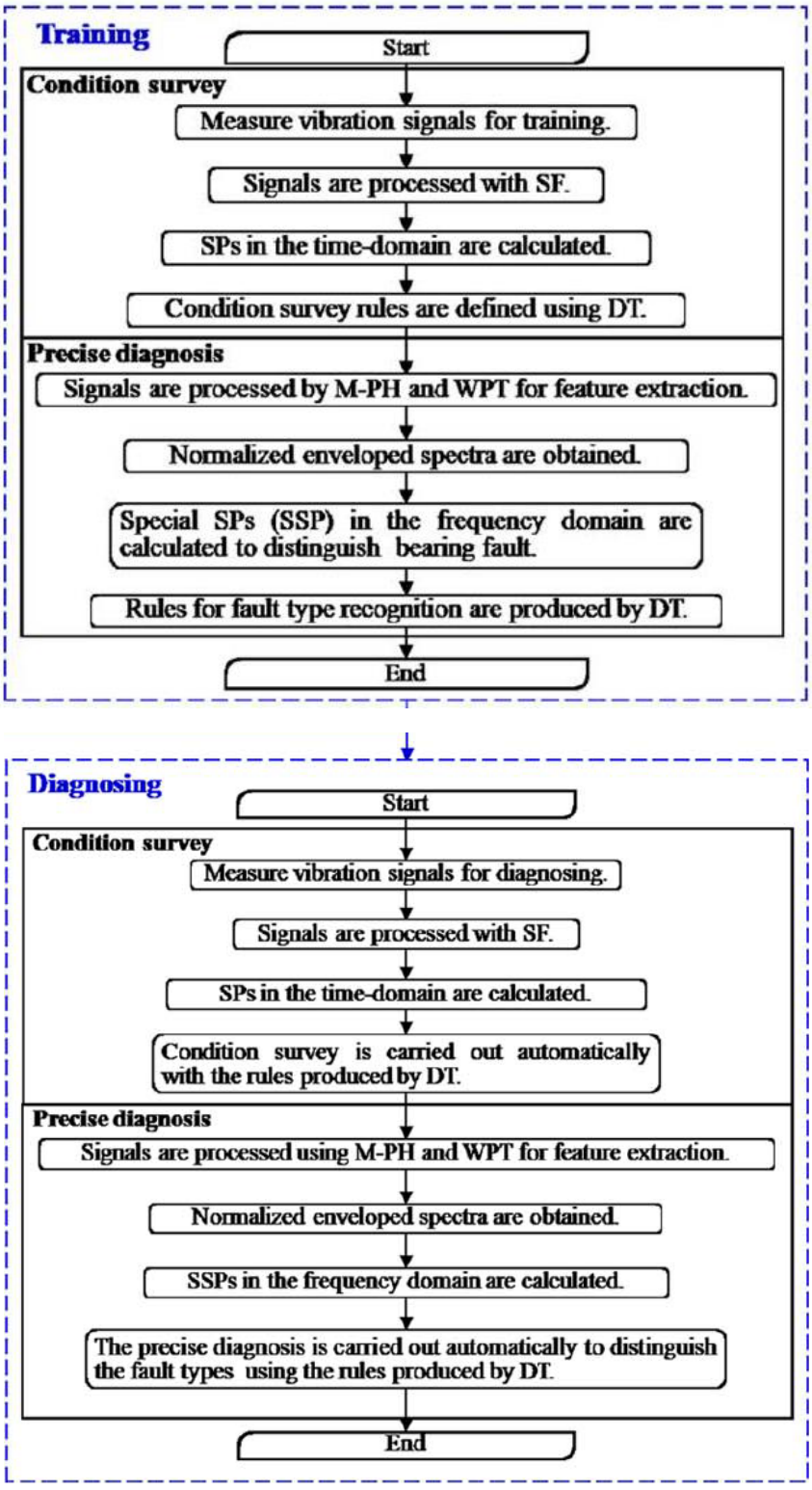

Fig. 2.3 Diagram of bearing diagnostics according to [5]

The diagnostic rules ascertained from the test measurements are then used to determine the condition of the low-speed bearing. This diagnostic method has been verified at a shaft speed of 40 rpm.

Running diagnostics on an axially low-speed bearing based on the expected time until a bearing fails (RUL, remaining useful life) is discussed in article [6]. The author uses the signal intensity estimator (SIE) described in [7] to process the recorded acoustic signal. In order to predict the time to failure, accelerated axial bearing lifespan tests are used in [6]. This data is then used to evaluate the condition of the bearing using ANN's deep-learning network (*Fig. 2.4*).

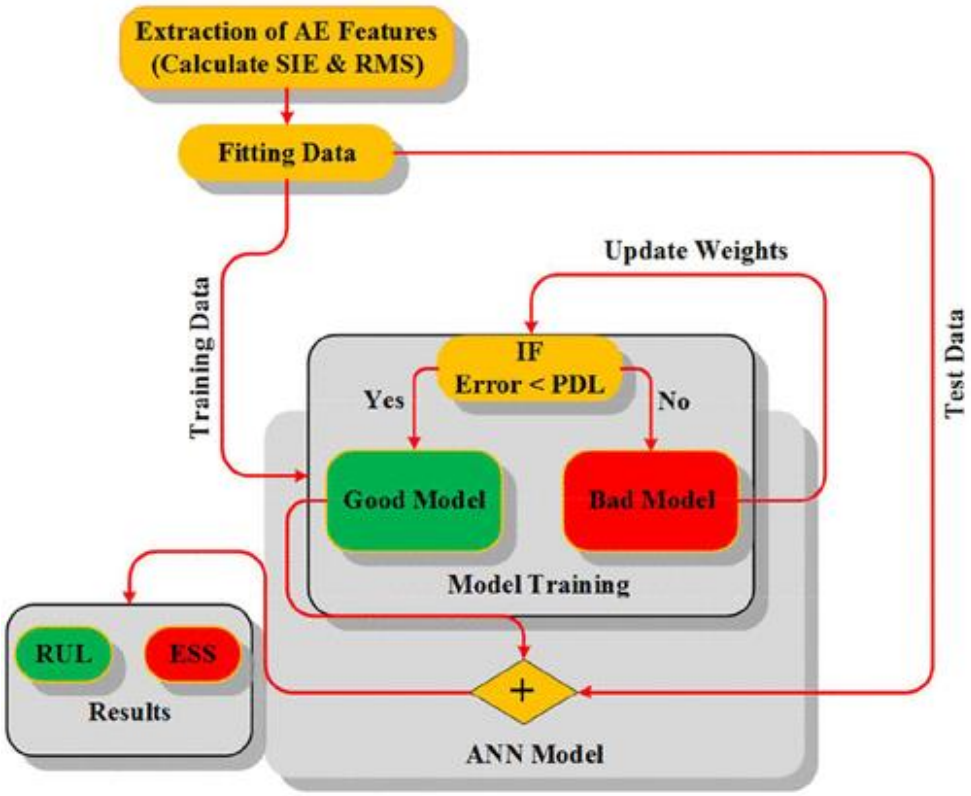

Fig. 2.4 Diagram of bearing diagnostics according to [6]

The predictions for the condition of the bearings were successfully realised under laboratory conditions at a shaft speed of 72 rpm.

According to the invention in [8], it is possible to run diagnostics on low-speed bearings by measuring the vibration acceleration signal. The recorded signal can then be processed using a weight filter that is applied to fast Fourier transform (FFT) signal analysis. The weight filter leads to a higher value for the operating frequency if the acceleration for other frequencies decreases accordingly. This increases the SNR. The solution described in application [8] was used for running diagnostics on low-speed lifts with an operating speed of 50 rpm.

The patent described in [9] addresses predicting the lifespan of a low-speed bearing. For this, an axial force is applied to a shaft. The resulting loads on the bearing are continuously measured under a constant load and subsequently converted into a calculation formula. The results then predict a theoretical bearing failure.

The patent described in [10] employs the measuring of the sound pressure signal to run diagnostics on low-speed bearings. For evaluation, this method compares a reference value of the sound pressure level or a reference value of the sound intensity level with the recorded signals.

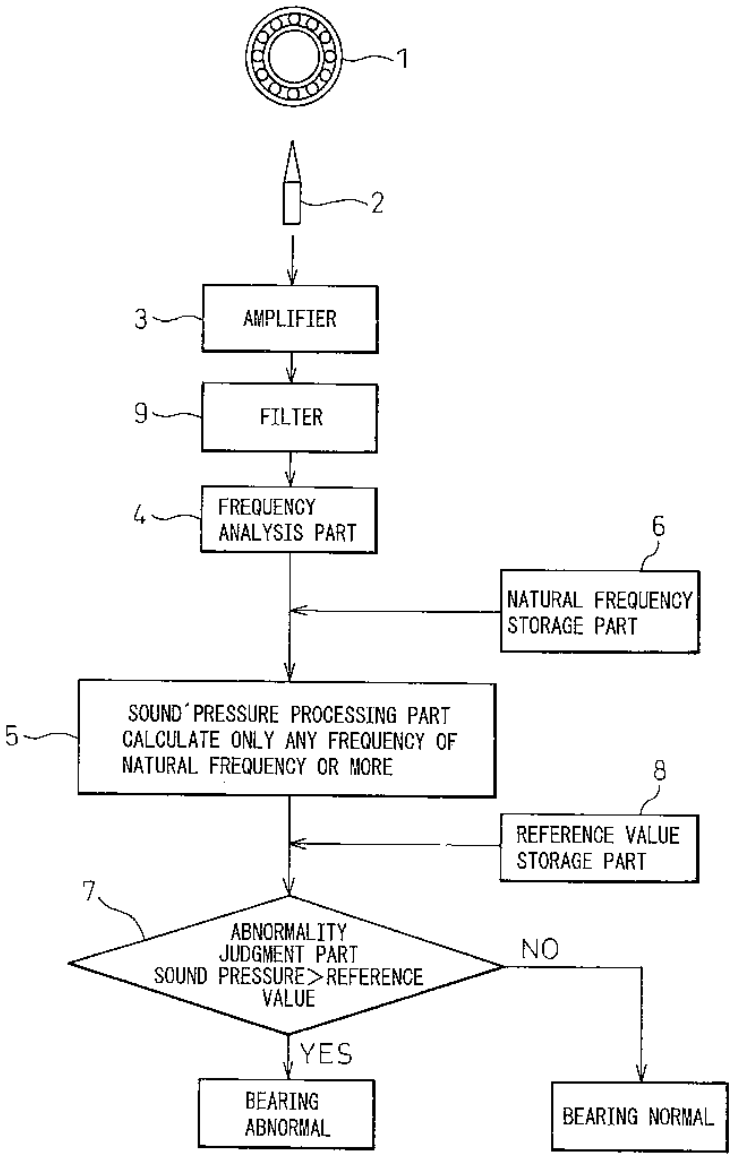

Fig. 2.5 Diagram of bearing diagnostics according to [10]

Fig. 2.5 is a diagram of how to run diagnostics on low-speed bearings according to [10], in particular running diagnostics on bearings at shaft speeds of less than 10 rpm. To actually measure the sound pressure signal as described in patent [11], it is pertinent to use a sensor that is equipped with a housing that reduces background noise and, at the same time, ensures that the sensor is protected from damage through the use of a flexible mounting.

3 Aim of thesis and processing methods

The aim of this thesis is to design and create a diagnostics system for low-speed ball and roller bearings, with a special focus on the sprocket shaft bearing assemblies in chain conveyors at the ŠKODA AUTO a.s. paint shop in Mladá Boleslav. Other outcomes of this thesis include stress analysis for the components of the sprocket shaft bearing assembly, prototype production, the verification of the diagnostics system's functionality under laboratory conditions, measurement of the load capacity as well as installation and series operation of the final prototype in a chain conveyor at the ŠKODA AUTO a.s. paint shop in Mladá Boleslav.

In order to design a diagnostics system for low-speed ball and roller bearings that accommodate the chain conveyor's sprockets, the current situation must be assessed. This is carried out based on a performance analysis of the conveyor's operating conditions and determination of the maximum load on the chain at the point at which the load is greatest. Depending on the actuating force acting on the chain, it is possible to determine the stress exerted on the shaft and bearings in the sprocket shaft bearing assembly.

These findings enable the conveyor's operating conditions to be simulated according to the finite element method, as well as the stress and deflection of the individual components present in the existing sprocket shaft bearing assembly to be calculated as a basis for designing the proposed solution as well as determining its required strength.

A diagnostics system for low-speed bearings can generally be designed based on the principle of measuring vibrations, the rolling resistance or the geometric accuracy of the shaft rotation.

The effective recording of vibrations requires a certain degree of measurable acceleration that cannot be achieved with low-speed shafts. To apply vibration diagnostic methods in the existing sprocket shaft bearing assembly, it would be necessary to regularly remove the chain from the sprocket in order to bring the sprocket shaft to a suitably high speed. It is not possible to apply such a method of running diagnostics on the bearings due to operational and financial reasons.

Another method of running diagnostics on bearings is by measuring rolling resistance. In this instance it is also necessary to remove the main conveyor chain.

Monitoring the geometric accuracy of the shaft rotation is demonstrably imprecise from an operational perspective and often not possible due to reasons of space.

As regards the permanent connection between the main conveyor chain and the sprocket, whose shaft is mounted in two low-speed bearings, this thesis proposes an alternative design solution that enables available diagnostic methods to be used whilst the chain conveyor is in operation.

The design of the proposed system takes into account the high requirements with regards to the chain conveyors' reliability and the speed of replacing the sprocket shafts. The main aspect of the design is the use of one pair of roller bearings on the shaft and one pair in the frame, which are connected by a component called the reference element which has a certain degree of rotational freedom. The shaft bearings ensure the shaft can rotate within the reference element, whilst the frame bearings enable the reference element to rotate within the frame.

By identifying a change in rolling resistance during a forced rotation of the reference element or by measuring any changes in vibration if a connected drive system rotates the reference element at a higher speed, this solution enables damage to any one of the bearings to be detected during operation.

As this was a new design solution, it was patented in the Czech Republic in April 2017 and at a European level in December 2018.

This thesis proposes a design solution that establishes a kinematic and frictional connection between the shaft and the reference element as well as between the reference element and the frame. This system allows the decomposition of the dynamic load on the shaft bearing and the frame bearing, which is advantageous from an operational perspective.

As a result of these connections, not only is the shaft forced to rotate in relation to the reference element during operation, but also the reference element in relation to the frame.

The kinematic and frictional connection between the shaft, reference element and frame led to further modifications in the design of the system, whereby a planetary mechanism involving spur gears or bevel gears was integrated. Applications were also filed to have this solution patented in the Czech Republic and at a European level.

Once the design and strength had been tested, the first prototype was produced and the deflection of the shaft bearing construction at nominal and peak loads was then measured. Following evaluation of the load tests and functional safety, the second prototype of the sprocket shaft bearing assembly including the complete diagnostics system was incorporated into the production line at the ŠKODA AUTO a.s. paint shop in Mladá Boleslav and integrated into series operation in the summer of 2018.

4 Low-speed bearings in conveyor systems

As already mentioned, low-speed ball and roller bearings are used in the construction of conveyor systems that allow for objects to be conveyed in a relatively low-speed rotary or translatory motion.

The running of diagnostics on ball and roller bearings specifically applies to a typical chain conveyor system at the paint shop in Mladá Boleslav. It relates to the main conveyor chains used in the production line for the chemical pretreatment of bodies in white prior to applying the paint finish, in operations referred to as the PT line. Here, the initial stages of the car body painting process such as cleaning, activating, phosphating and passivating are carried out.

To develop an effective diagnostics system for bearings, the kinematic ratios as well as the load ratios on the chain conveyor need to be known.

4.1 Kinematic diagram of the conveyor

The kinematic diagram of the PT line's conveyor system shown in *Fig. 4.1* includes the drive units at the entry and exit sides of the pretreatment tanks for the car bodies. With regard to the further course of action, it is important to clarify the ratios of loads and moments on the side where the car bodies exit the line, as this is where the chain conveyor system is under the most critical load.

The drive units are always in duplicate so that power can be transferred to the countershaft from the left or the right. This arrangement enables alternative use of the drive units and at the same time creates scope for availability and maintenance.

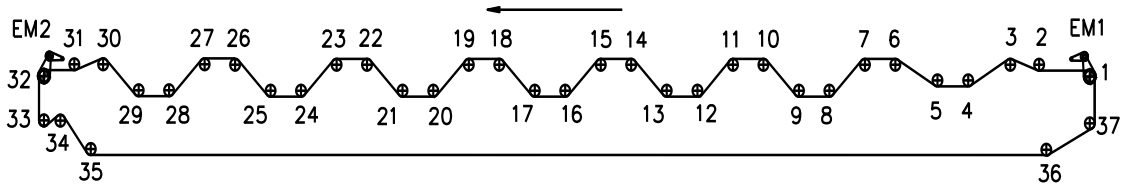

Fig. 4.1 Diagram of the PT line

The kinematic diagram of the conveyor system shown in *Fig. 4.1* includes drive unit EM1 where the car bodies enter the line and drive unit EM2 where they exit. The units drive two parallel 528-metre-long conveyor chains that are guided on both sides by sprockets in positions 1 to 37. Together with its shaft, each sprocket is mounted in two identical, double-row spherical roller bearings. Each bearing has a housing that is bolted to a welded installation frame made of thick sheet metal.

Each drive unit at the end where the car bodies exit the line consists of an electric motor with an integrated spur-gear system. The sprocket for the first chain drive is located on the gear system's output shaft. Here, the power is transferred to the countershaft and

then from there to the driven conveyor-chain sprocket. The latter is located on a shaft where sprockets from the left and the right side are also mounted; these are guided in sync via a sprocket unit. In this process, the car bodies suspended from pendulums pass through the individual tanks and are prepared accordingly for the painting process.

Guiding tracks complement the conveyor chain's guidance; they are made of drawn L-sections or thick strip steel. These provide support for the conveyor chain, especially in locations where excessive sagging may occur.

Both conveyor chains are also guided by castors integrated into the guide tracks, which are fixed to the walls of the conveyor system's frame. The conveyor chain's guidance makes it possible for the car body to be prepared for its transfer to the subsequent procedure, cathodic dip coating, after its exit from the pretreatment tank.

4.2 Drive units and gear systems

The chain conveyor system's drive units and gear systems are located where the car bodies enter and exit the line.

The primary, integrated drive unit is located where the car bodies exit the conveyor system and consists of an electric motor, which is controlled by a frequency converter, and a spur-gear system, which is flange-mounted onto the motor's output shaft. The gear system's output shaft actuates an upstream chain drive, and the drive sprockets for the PT line's main conveyor chain are located on the output of this chain drive.

The two drive units EM1 and EM2 are protected and their transmission mechanisms are either located on the left- or right-hand side of the conveyor system.

Drive unit EM1 is located at the entrance of the conveyor and has the following parameters, as listed in *Table 4.1*.

Table 4.1 Parameters of drive unit EM1

EM1	
Weight	290 kg
Length of the retaining spring lever	492 mm
Electric motor	
Nominal power output	9.5 kW
Nominal rotational speed	1470 rpm
Nominal voltage	AC Y 400 V
Power factor	0.79
Frequency	50 Hz
Gear system	
Transmission ratio	43.02
Torque at the output	2600 Nm
Rotational speed at the output	34.5 rpm
Brake	
Nominal braking torque	85 Nm
Nominal voltage	DC 180 V
Nominal current	0.33 A
Frequency converter	
Frequency	55.1 Hz
Current	9.63 A
Usage of torque	27.75 %

Table 4.2 Parameters of drive unit EM2

EM2	
Weight	357.8 kg
Length of the retaining spring lever	492 mm
Electric motor	
Nominal power output	18.5 kW
Nominal rotational speed	1470 rpm
Nominal voltage	AC Y 400 V
Power factor	0.79
Frequency	50 Hz
Gear system	
Transmission ratio	47.82
Torque at the output	5600 Nm
Rotational speed at the output	31 rpm
Brake	
Nominal braking torque	160 Nm
Nominal voltage	DC 180 V
Nominal current	0.43 A
Frequency converter	
Frequency of the electric motor	61.67 Hz
Rotational speed at the gear system's output	39.4 rpm
Torque at the output	3600 Nm

4.2.1 Right-hand side EM2 drive unit

Fig. 4.2 shows a kinematic diagram of the right-hand side EM2 drive unit. The drive unit consists of an electric motor, which has a spur-gear system flange-mounted onto its output shaft, as well as an upstream chain drive. The entire gear system, including the electric motor, is mounted on an assembly frame and can pivot on the axis of the gear system's output shaft. The gear system's driving torque is absorbed by a spring-mounted connected lever. The spring suspension consists of two cylindrical compression springs (1 and 2) that are connected in series. The springs provide a relatively high level of damping of the vibrations generated by the gear system for the output shaft's axis.

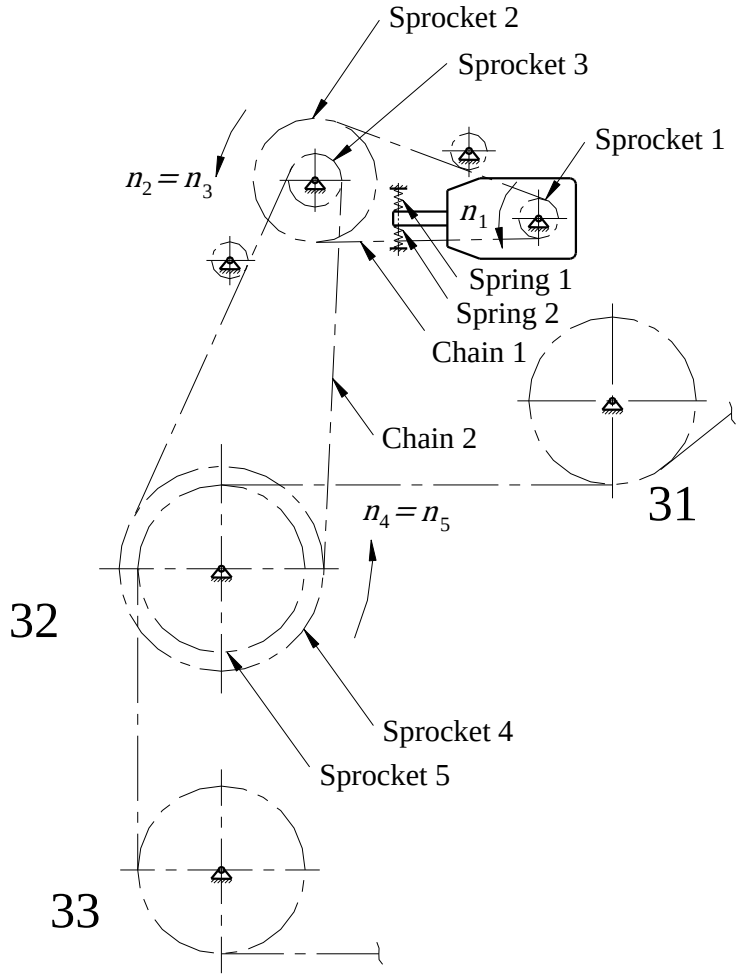

Fig. 4.2 Diagram of the PT line's right-hand side EM2 drive unit

4.2.2 Left-hand side EM2 drive unit

Fig. 4.3 shows a kinematic diagram of the left-hand side EM2 drive unit, which also consists of a gear system with an integrated electric motor and an upstream chain drive. The entire gear system, including the electric motor, is mounted on an assembly frame and can pivot on the axis of the gear system's output shaft. The gear system's driving torque is absorbed by a spring-mounted connected lever. In comparison to the right-hand side EM2 drive unit, the position of the spring suspension on the left-hand side EM2 drive unit has been rotated horizontally by 180 degrees. Again, the spring suspension consists of two cylindrical compression springs (1 and 2) that are connected in series. The springs provide a relatively high level of damping of the vibrations generated by the gear system for the output shaft's axis.

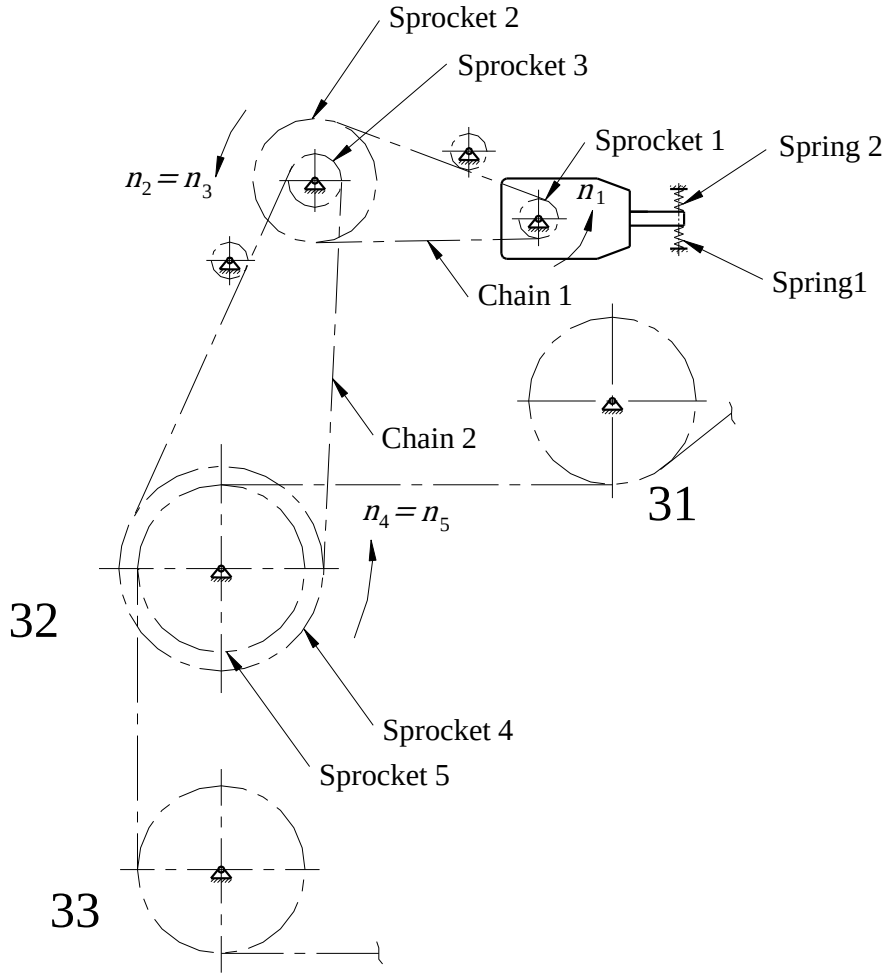

Fig. 4.3 Diagram of the PT line's left-hand side EM2 drive unit

4.2.3 The drive units' chain drive

The entire chain drive system consists of two individual reduction stages. The first stage is formed by the transmission from sprocket 1, which is located on the gear system's output shaft, to sprocket 2, which is located on the countershaft. The chain drive's second stage is formed by the transmission from sprocket 3, which is located on the countershaft, to sprocket 4, which is located on the chain conveyor's drive shaft.

Chain drive 1-2 is shown in *Fig. 4.4*. The respective parameters are outlined in *Table 4.3*.

Table 4.3 Chain drive 1-2

Transmission ratio	$i_{12} = 3.105$
Type of chain	RS 24B
Pitch of the chain links	$p_{12} = 38.1$ mm
Number of teeth on sprocket 1	$z_1 = 19$
Rotational speed of sprocket 1	$n_1 = 39.4$ rpm
Pitch diameter of sprocket 1	$d_1 = 231.5$ mm
Number of teeth on sprocket 2	$z_2 = 59$
Rotational speed of sprocket 2	$n_2 = 12.7$ rpm
Pitch diameter of sprocket 2	$d_2 = 716$ mm

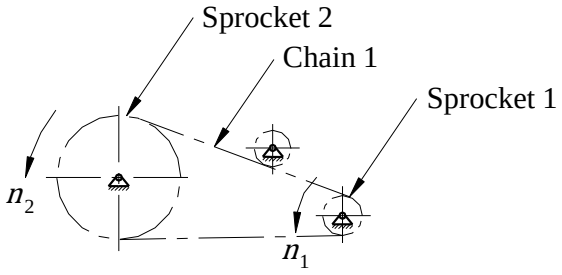

Fig. 4.4 Chain drive 1-2

Chain drive 3-4 is shown in *Fig. 4.5*. The respective parameters are outlined in *Table 4.4*.

Table 4.4 Chain drive 3-4

Transmission ratio	$i_{34} = 3.842$
Type of chain	RS 32B
Pitch of the chain links	$p_{34} = 50.8$ mm
Number of teeth on sprocket 3	$z_3 = 19$
Rotational speed of sprocket 3	$n_3 = 12.7$ rpm
Pitch diameter of sprocket 3	$d_3 = 307.5$ mm
Number of teeth on sprocket 4	$z_4 = 73$
Rotational speed of sprocket 4	$n_4 = 3.3$ rpm
Pitch diameter of sprocket 4	$d_4 = 1181$ mm

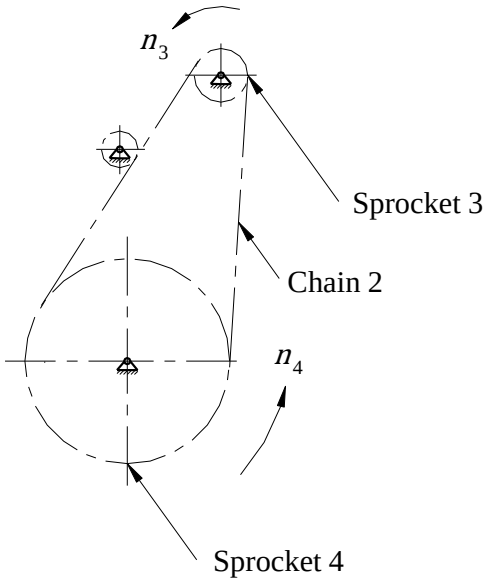

Fig. 4.5 Chain drive 3-4

4.2.4 The gear system's spring suspension

The gear system, including the electric motor, is mounted on an assembly frame and can pivot on the axis of the gear system's output shaft. The springs located in the gear system's suspension limit the movement of the gear system. Spring 1 has a damping effect and thereby limits the gear system's unwanted vibrational movements.

Spring 1 is shown in *Fig. 4.6* and the respective parameters are outlined in *Table 4.5*.

The load characteristics for spring 1, which exhibits a relatively large degree of hysteresis, are shown in *Fig. 4.7*.

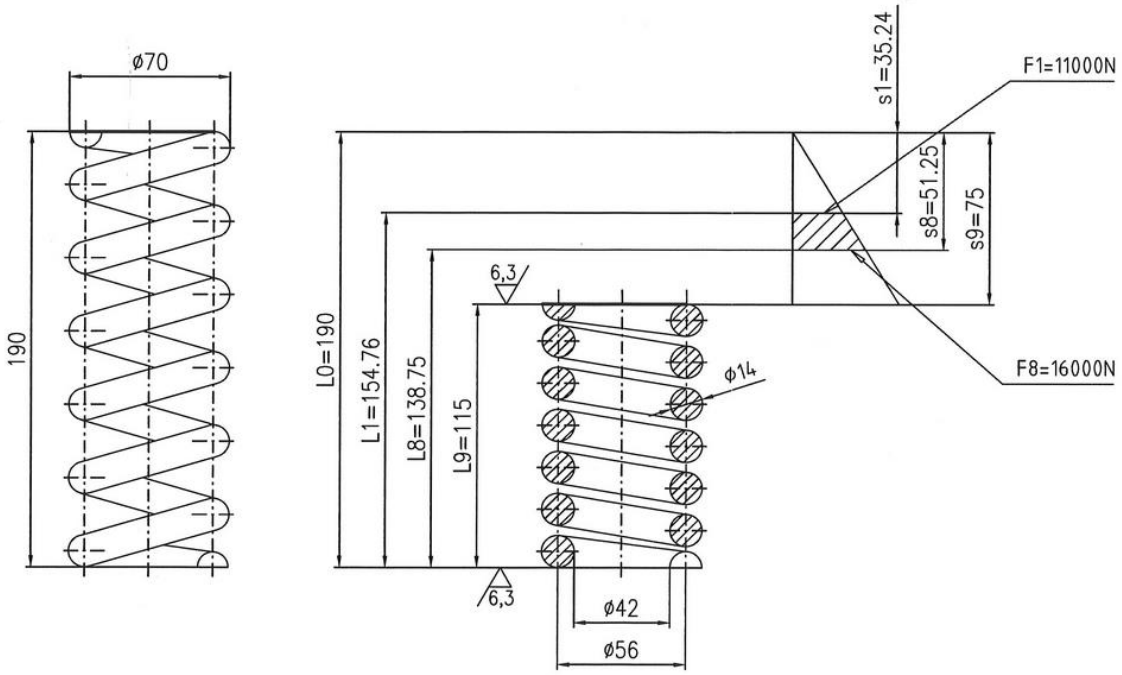

Fig. 4.6 Spring 1

Table 4.5 Parameters of spring 1

Number of effective coils	6
Total number of coils	8
Coil direction	right hand
Uncoiled length	1523.2 mm
Spring rate	312 $\mathrm{Nmm^{-1}}$

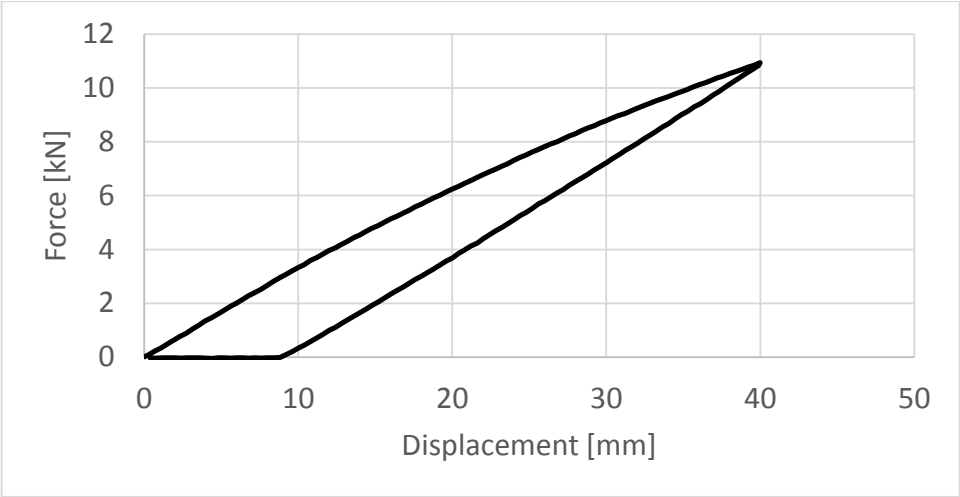

Fig. 4.7 Load characteristics of spring 1

Spring 2 is shown in *Fig. 4.8* and the respective parameters are outlined in *Table 4.6*

The load characteristics for spring 2 are shown in *Fig. 4.9.*

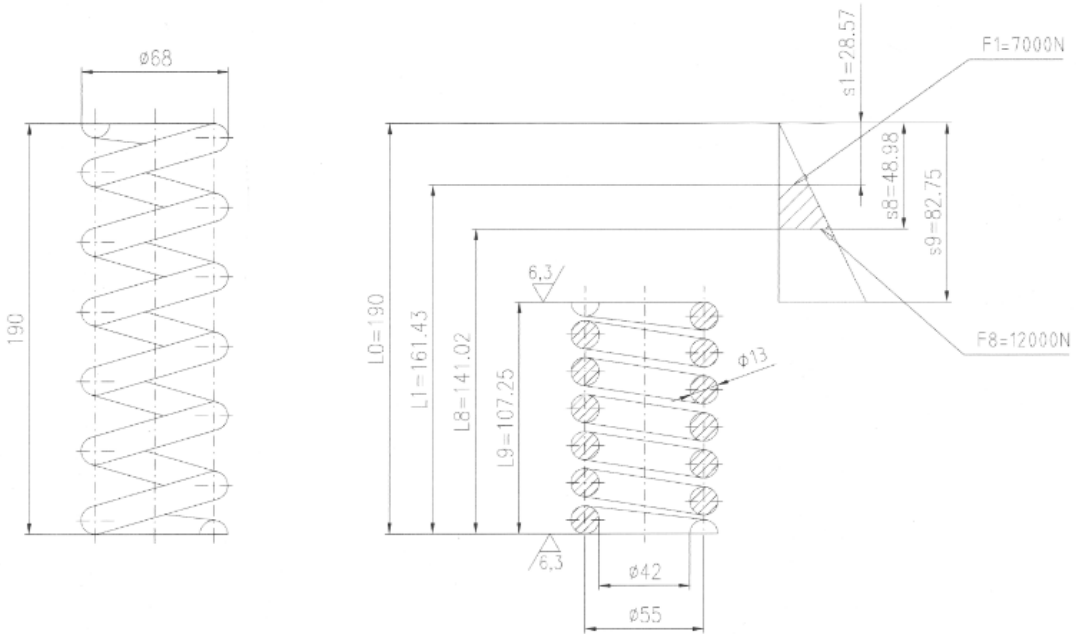

Fig. 4.8 Spring 2

Table 4.6 Parameters of spring 2

Number of effective coils	6
Total number of coils	8
Coil direction	right hand
Uncoiled length	1523.2 mm
Spring rate	245 $\mathrm{Nmm^{-1}}$

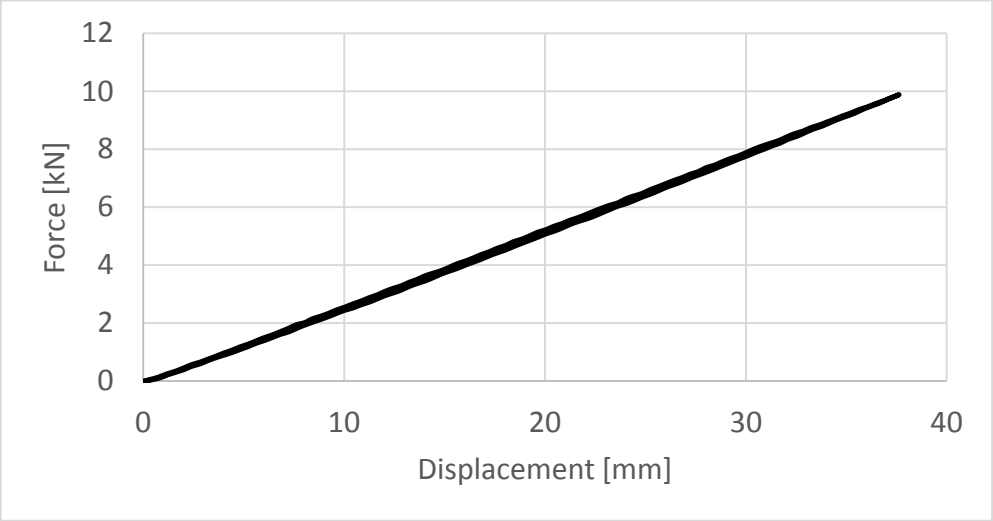

Fig. 4.9 Load characteristics of spring 2

4.3 Sprocket shaft bearing assembly

The sprocket shaft is mounted using two roller bearings that are fixed to a baseplate. This baseplate is firmly welded to the installation frame of the sprocket shaft bearing assembly. The installation frame in turn is firmly bolted into a window in the PT line's side wall and seals the technological area of the conveyor system. The sprocket, which is located in the chemical environment of the PT conveyor, is isolated from the bearings in the installation frame, which are located outside of the line, by seals. The bearings themselves are thereby not exposed to any chemical ingress. Due to the sealed bearing housings and one-point automated lubrication, the roller bearings operate in a dust-free environment with sufficient lubrication.

The current design of the sprocket shaft bearing assembly is shown in *Fig. 4.10*.

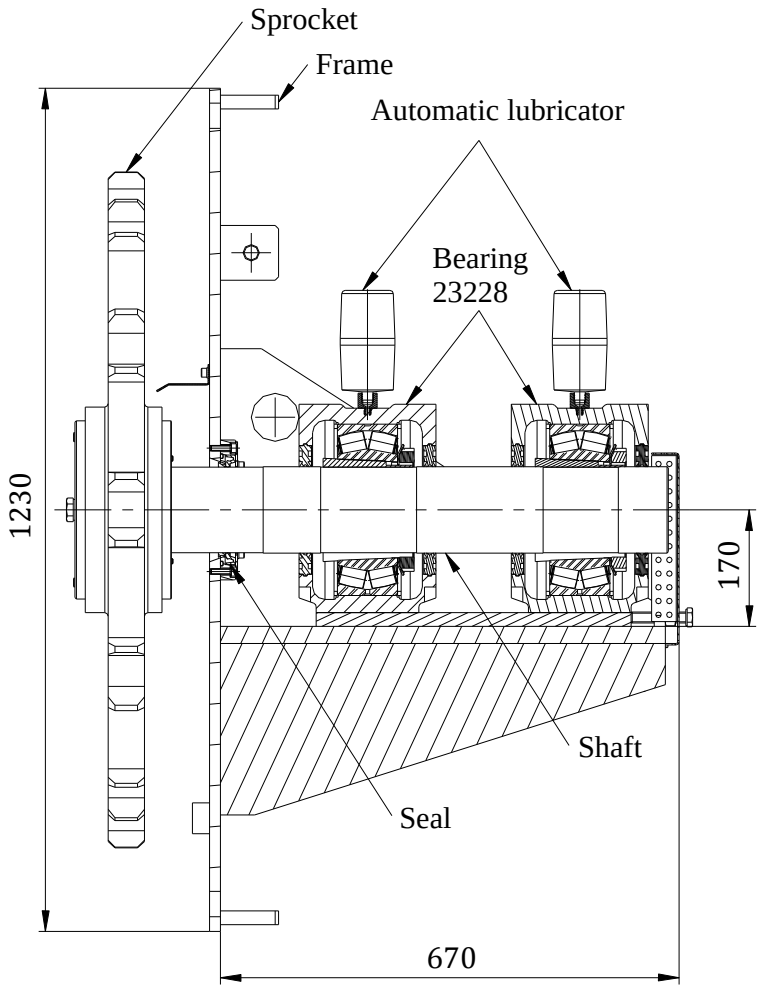

Fig. 4.10 Current assembly of the sprocket and the sprocket shaft including the spherical roller bearings

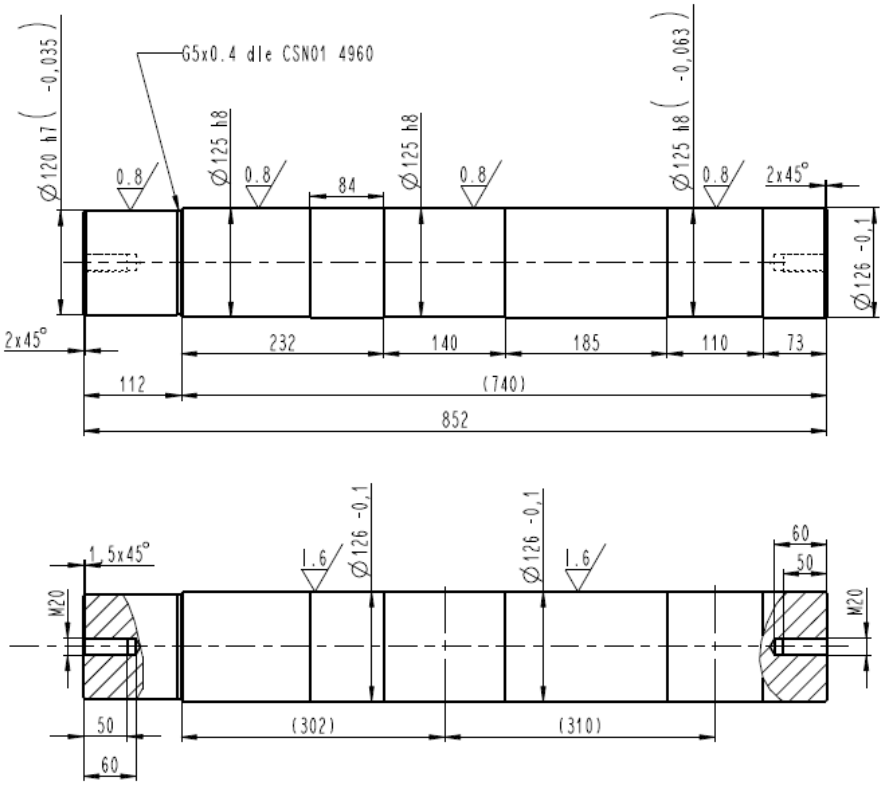

Fig. 4.11 Extract from the production drawings for the sprocket shaft

4.3.1 Bearing parameters

Two FAG 23228 spherical roller bearings with a tapered bore and H2328 adapter sleeves are used in the sprocket shaft bearing assembly. These roller bearings are mounted in FAG SNV250-F-L bearing housings. The parameters of the FAG bearings used and their bearing housings can be seen in *Fig. 4.12* and *Fig. 4.13* as well as in *Table 4.7* and *Table 4.8*.

Table 4.9 shows the fundamental material properties of the sprocket shaft.

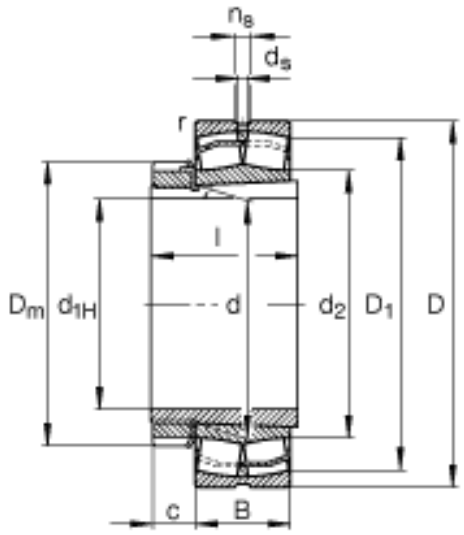

Fig. 4.12 Dimensions of the FAG 23228 spherical roller bearing with an H2328 adapter sleeve

Table 4.7 Parameters of the FAG 23228 roller bearing

Outer diameter	$\mathrm{D} = 250$ mm
Inner diameter	$d_{1H} = 125$ mm
Width	$B = 88$ mm
Weight	17.1 kg
Dynamic load rating	$C = 1090000$ N
Static load rating	$C_0 = 14000000$ N
Calculation factors	$e = 0.33$
	$Y_1 = 2.04$
	$Y_2 = 3.04$
	$Y_0 = 2$

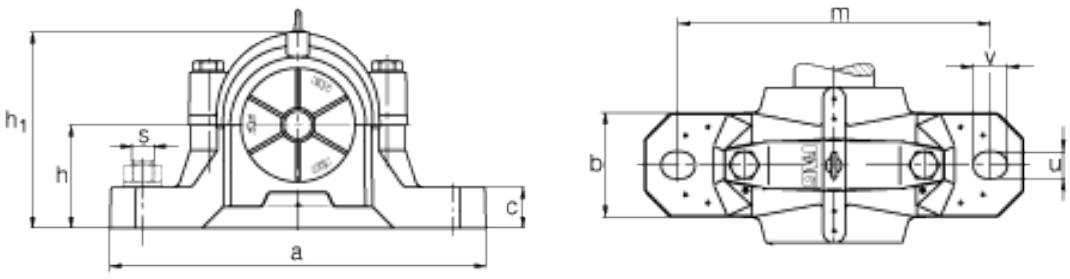

Fig. 4.13 Dimensions of the FAG SNV250-F-L bearing housing

Table 4.8 Parameters of the FAG SNV250-F-L bearing housing

Dimensions	h = 150 mm
	a = 500 mm
	b = 150 mm
Weight	38 kg

Table 4.9 Material properties of the sprocket shaft

Material	EN C55
Ultimate strength	R_m = 700 MPa
Yield strength	R_k = 345 MPa

4.3.2 Seal

A shaft seal (oil seal) is used to seal the shaft in the installation frame. To install a shaft seal, the entire sprocket shaft bearing assembly has to be dismantled. This form of seal can also be replaced with braided packing, which can be put in place without the sprocket shaft bearing assembly needing to be dismantled.

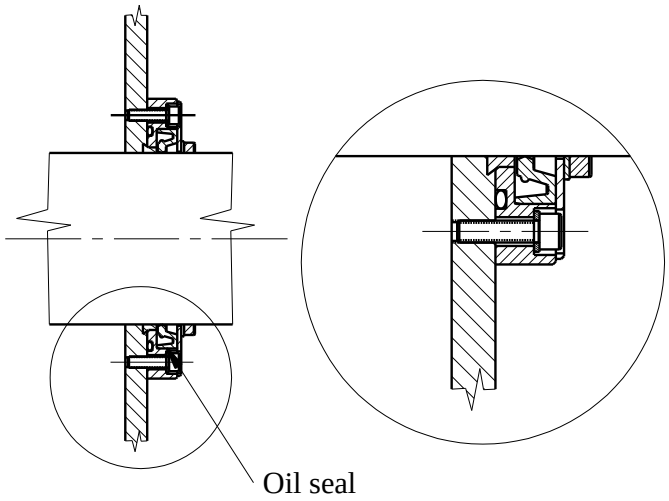

Fig. 4.14 Shaft seal in the installation frame

5 Strength of the current sprocket shaft bearing assembly

In order to design a diagnostic device for low-speed ball and roller bearings, it is necessary to calculate the strength ratios of the current sprocket shaft bearing assembly. The results obtained are used as a comparison for the new design, thereby assuring its reliability.

Substantial forces acting on the conveyor chain put a load on the sprocket shaft bearing assembly. The sprocket shaft and the two bearings are the crucial components that must be of sufficient strength.

5.1 Forces acting on the conveyor chain

During operation, the forces acting on the PT line's conveyor chain are clearly of a dynamic nature. For this reason, a mechanical model of the drive system is developed first. The force ratios and moment ratios have been defined using dynamic calculations.

Several methods were used for further defining the forces acting on the conveyor chain.

One method is based on the possibility of measuring the displacement that occurs in the springs located in the suspension of the drive unit's gear system. This method appears relatively simple, it does however not react quickly enough to the non-static, dynamic operation phases in the pretreatment line.

Another method for determining the forces and moments acting on the drive system is by using data from the electric motor's electronic frequency converter. This continuously supplies data relating to the torque of the drive unit. To determine the forces acting on the conveyor chain, the greatest and average values are to be used.

To establish the threshold for the force acting on the conveyor chain, it is sensible to base the calculations on the drive system's maximum torque. This would however only occur if the entire conveyor system had a serious technical malfunction.

5.1.1 Dynamic calculation of the conveyor's drive unit

The conveyor's drive unit is formed of an electric motor and a gear system. The dynamic calculation of the drive unit is derived from the mechanical model in *Fig. 5.1*. Here, the forces and moments acting on the mechanical model are adjusted so that the kinematic values correspond to real-life conditions.

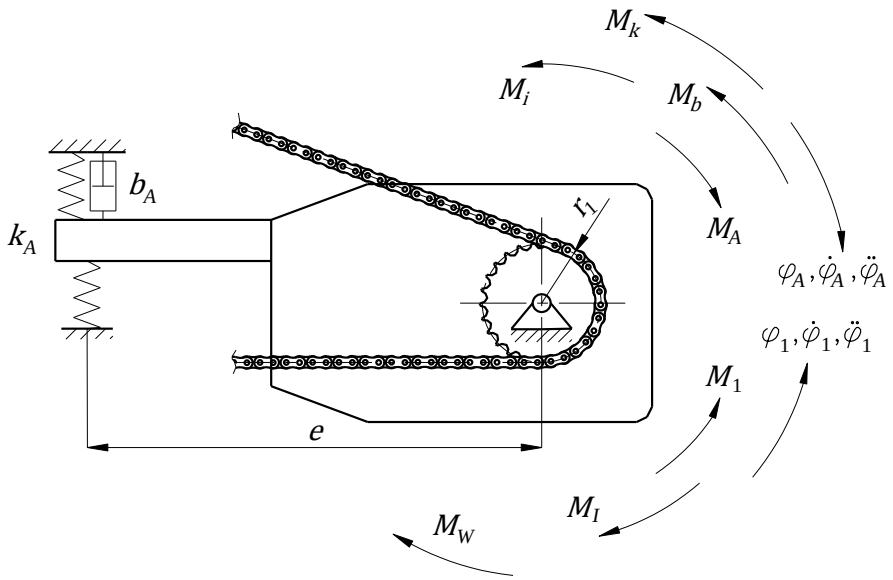

Fig. 5.1 Mechanical model of the conveyor's drive unit

The drive unit is mounted to the frame in a way that it can pivot on the axis of sprocket 1 and has a mass moment of inertia at this axis (J_A). Its movement is restricted by the suspension, which is formed of a lever and two springs working in series with the overall spring rate k_A and the distance e. One of the two springs exhibits a damping effect, which is characterised by the coefficient b_A.

The torque M_1, which is in equilibrium with the transformed moment M_W and the transformed moment of inertia M_I, drives the drive chain sprocket with the pitch radius r_1. These transformed moments are caused by the conveyed car bodies and other components attached to the conveyor (pendulums, sprockets etc.).

The dynamic equilibrium of the drive system can be described using the following equation of motion

$$M_i + M_b + M_k = M_A \,, \tag{5.1}$$

where M_i is the moment of the drive unit due to inertia, M_b is the damping moment and M_k is the reaction moment of the drive unit's spring suspension. The moment of acceleration on sprocket 1 is referred to as M_A in the equation (5.1).

The dynamic equilibrium on sprocket 1 of the drive unit can be expressed using the following equation

$$M_I + M_W = M_1 \,, \tag{5.2}$$

where M_I is the transformed moment of inertia due to the conveyed objects at the rotation axis of sprocket 1 and M_W is the transformed moment due to resistance of the conveyed objects at the rotation axis of sprocket 1.

The torque M_1 drives sprocket 1 and is in equilibrium with the moment of acceleration of the drive unit, meaning

$$M_A = M_1 \, . \tag{5.3}$$

The drive unit's moment due to inertia M_i is calculated using its mass moment of inertia J_A and the drive sprocket's angular acceleration $\ddot{\varphi}_A$, as follows

$$M_i = J_A \ddot{\varphi}_A \, . \tag{5.4}$$

The reaction moment M_k of the springs is

$$M_k = k_A e^2 \varphi_A \, , \tag{5.5}$$

where φ_A is the angular deviation of the actuating motion.

The damping moment M_b of one of the two springs is given from the damping coefficient b_1 and the angular velocity $\dot{\varphi}_A$ of the drive unit, such that

$$M_b = b_1 e^2 \dot{\varphi}_A \, . \tag{5.6}$$

The transformed moment of inertia due to the conveyed objects M_I at the rotation axis of sprocket 1 can be described as the product of the transformed mass moment of inertia J_I and the angular acceleration $\ddot{\varphi}_1$ of sprocket 1, so

$$M_I = J_I \ddot{\varphi}_1 \, . \tag{5.7}$$

The transformed moment due to resistance M_W of the conveyed objects at the rotation axis of sprocket 1 can be established using the transformed force due to resistance F_W in relation to the circumferential velocity v_1 and the transformed friction coefficient f_W. As such

$$M_W = F_W r_1 = f_W v_1 r_1 = f_W r_1^2 \dot{\varphi}_1 \, , \tag{5.8}$$

where $\dot{\varphi}_1$ is the angular velocity of sprocket 1.

The equations of motion (5.1) and (5.2) can be solved using the MAPLE calculator, provided that the relevant functional dependencies of the moment of acceleration M_A and the transformed moment due to resistance M_W are known. The results should match the real kinematic measurements taken from the drive system during operation of the PT line.

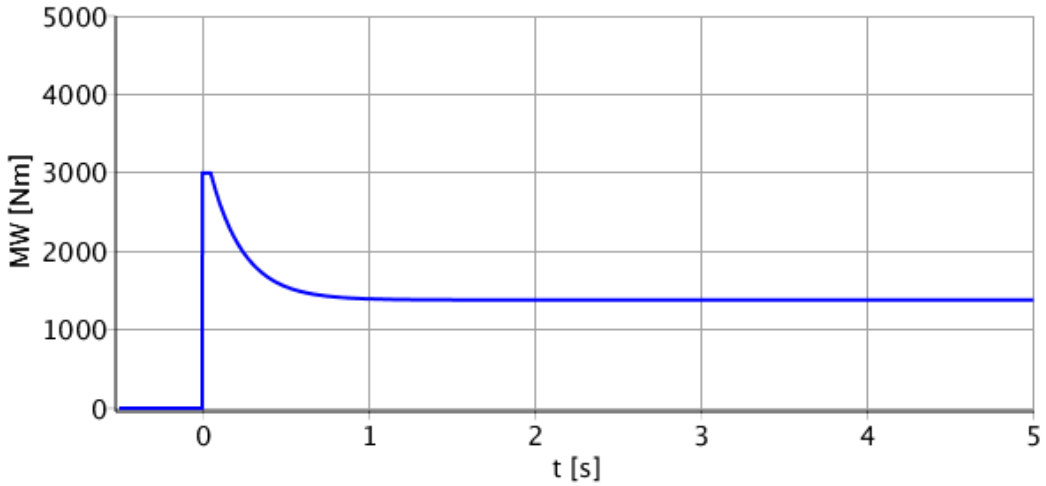

Fig. 5.2 Development of transformed moment due to resistance M_W over time

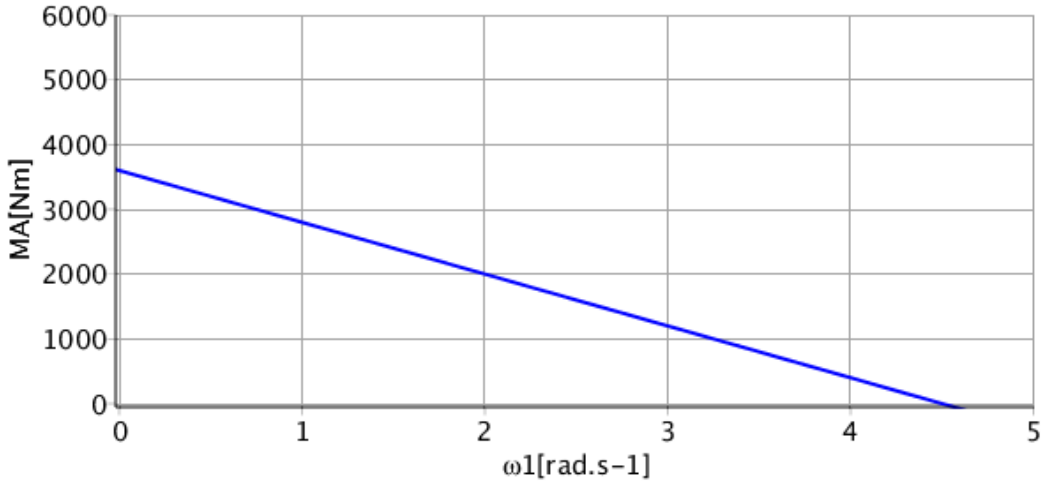

Fig. 5.3 Correlation between the moment of acceleration M_A and the angular velocity $\dot{\varphi}_1 = \omega_1$ of the driven sprocket 1

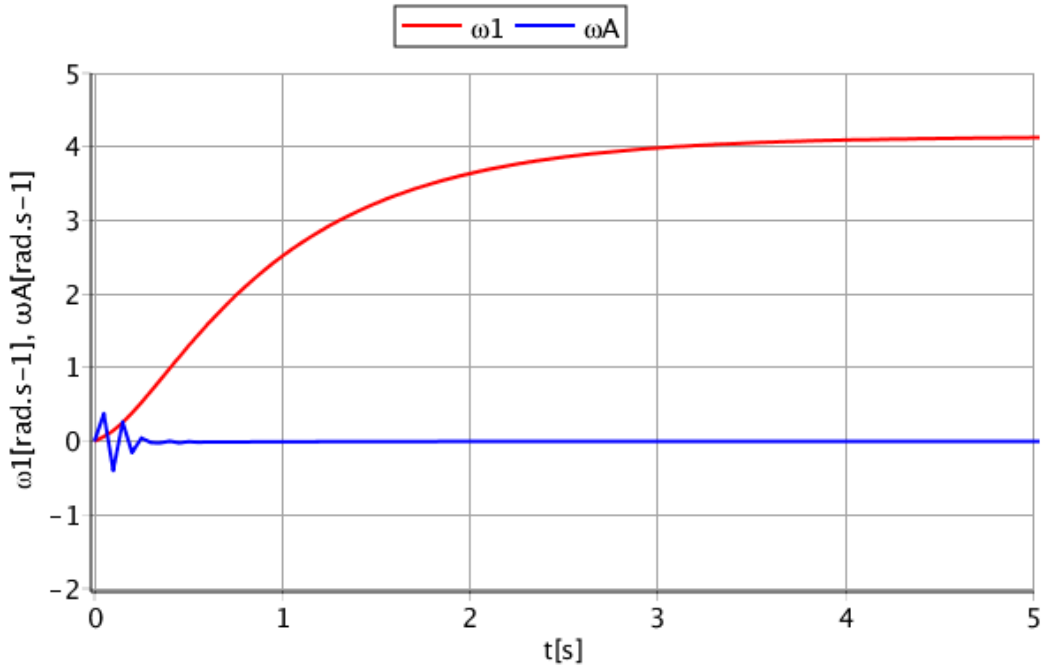

Fig. 5.4 *Development of the angular velocity $\dot{\varphi}_1 = \omega_1$ of the driven sprocket 1 and the angular velocity of the drive unit's vibrations $\dot{\varphi}_A = \omega_A$ over time*

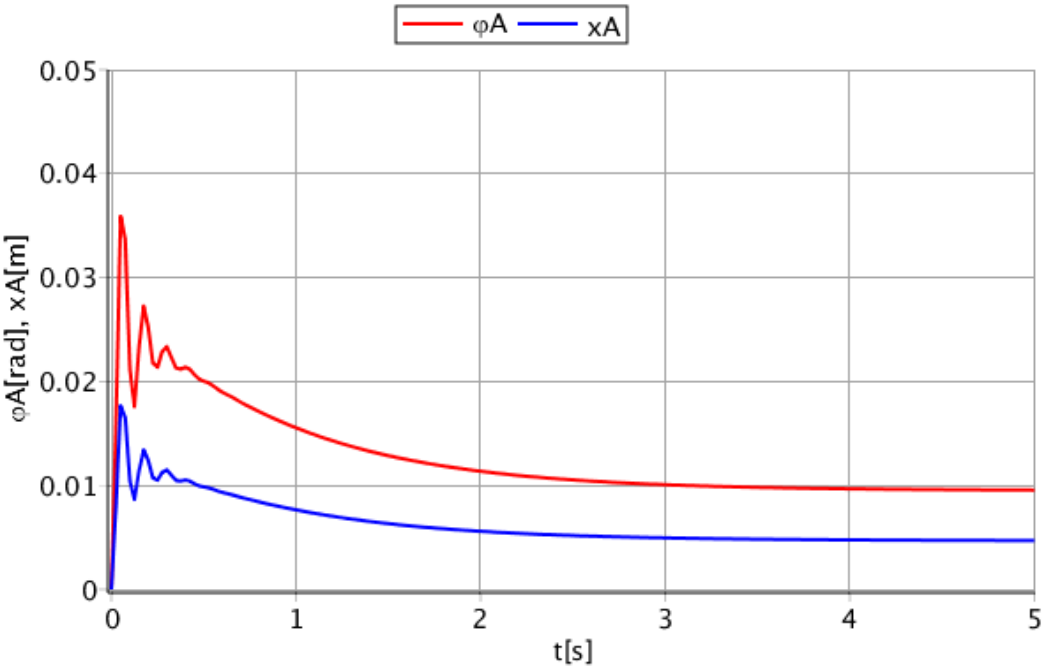

Fig. 5.5 *Development of the gear system's rotation φ_A and the final displacement of the lever x_A over time*

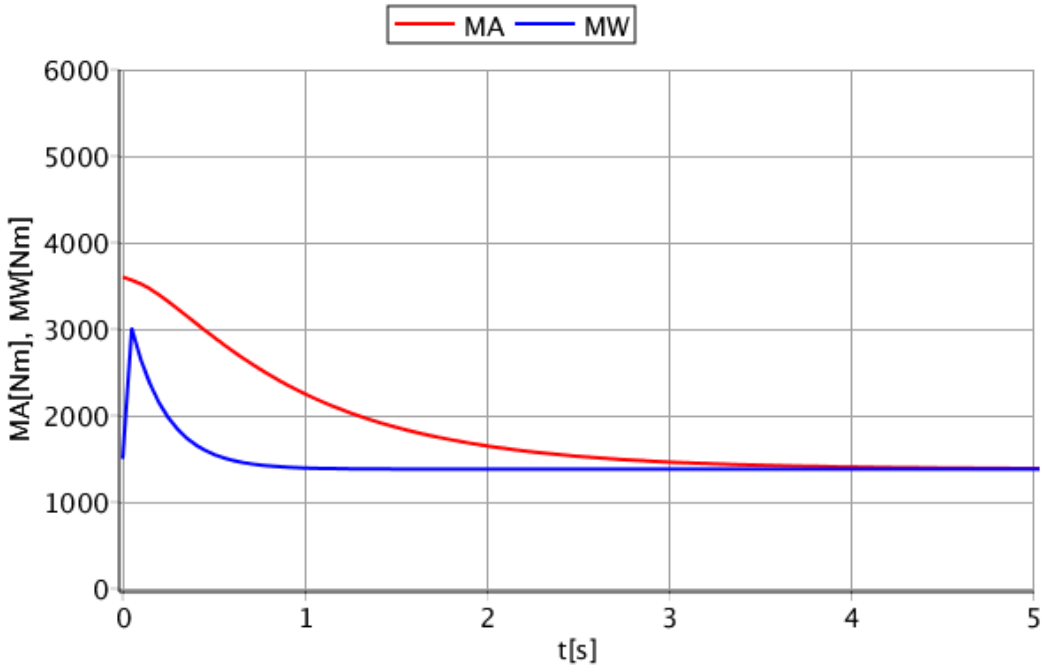

Fig. 5.6 Development of moment of acceleration M_A and transformed moment due to resistance M_W

5.1.2 Spring displacement in the suspension of the drive unit

Displacement of the springs located in the suspension of the drive unit was measured during start-up of the PT line as well as during stabilised operation of the line under different loads (with a gradual increase in the number of conveyed car bodies).

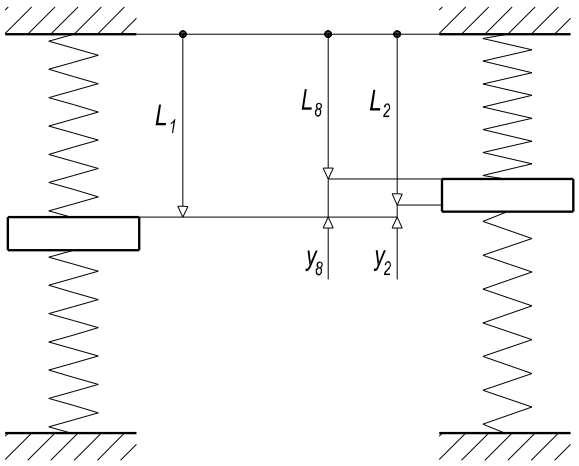

Fig. 5.7 Diagram showing the compression measured on the springs

Table 5.1 Measured spring lengths and calculated displacement of the springs

Measurement	Force	Free length of spring L_1	Length of spring during start-up L_8	Displacement of spring during start-up y_8	Length of spring during operation L_2	Displacement of spring during operation y_2
	[Number of car bodies]	[mm]	[mm]	[mm]	[mm]	[mm]
1	–	233.3	–	–	–	–
2	1	233.3	229.5	3.8	230.5	2.8
3	10	233.3	229.5	3.8	230.4	2.9
4	20	234.2	229.5	4.7	230.5	3.7
5	25	234.2	229.0	5.2	229.4	4.8
6	30	232.9	228.7	4.2	229.3	3.6
7	45	233.3	228.5	4.8	229.3	4

The maximum displacement y_8 of the springs during stabilised operation of the PT line is 4.8 mm.

Fig. 5.8 shows the amount of displacement of the spring system for springs 1 and 2 as measured in the lab.

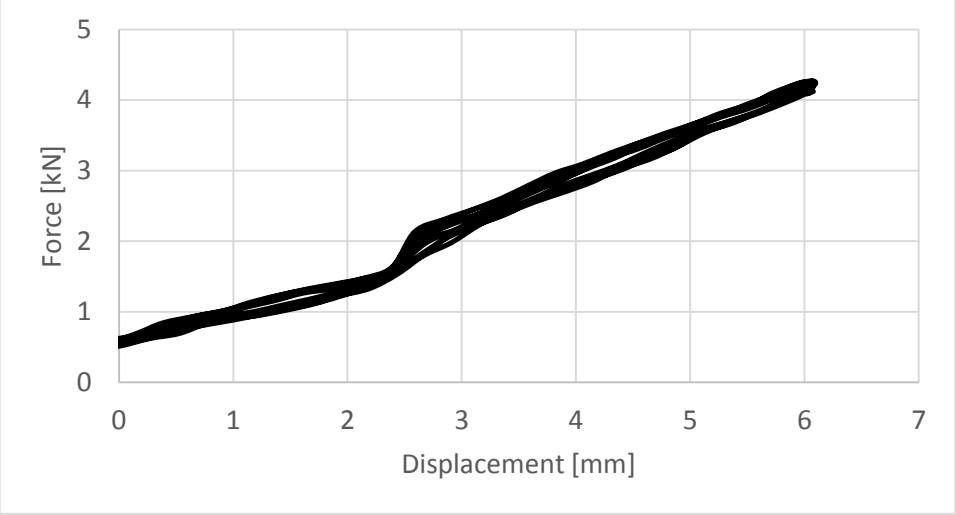

Fig. 5.8 Diagram showing force as a function of the displacement of springs 1 and 2 connected in series

According to the measurements from *Table 5.1* and *Fig. 5.8*, force F_8 of the spring system is to be calculated at maximum displacement y_8

$$F_8 = k_g y_8 = 602\ \text{Nmm}^{-1} \times 4.8\ \text{mm} = 2976\ \text{N}, \tag{5.9}$$

where the overall spring rate of the spring system from *Fig. 5.8* is

$$k_g = 602\ \text{Nmm}^{-1}. \tag{5.10}$$

The following applies for the equilibrium of the drive unit assembly

$$M_1 = F_8 \times e = 2976\ \text{N} \times 492\ \text{mm} = 1464\ \text{Nm}\ . \tag{5.11}$$

If the reduction ratio i_{14} is equivalent to

$$i_{14} = \frac{z_2}{z_1}\frac{z_4}{z_3} = \frac{59}{19} \times \frac{73}{19} = 11.93\ , \tag{5.12}$$

the following will be true for the torque $M_4 = M_5$

$$M_5 = M_1 i_{14} = 1464\ \text{Nm} \times 11.93 = 17466\ \text{Nm}\ . \tag{5.13}$$

The corresponding overall force driving the sprockets on the right- and left-hand sides of the conveyor system, i.e. the total force acting on both chains, is

$$F_{gK} = \frac{2M_4}{d_5} = \frac{2 \times 17466\ \text{Nm}}{0.966\ \text{m}} = 36161\ \text{N} \tag{5.14}$$

and the force acting on one chain is

$$F_K = \frac{F_{gK}}{2} = \frac{36161\ \text{N}}{2} = 18081\ \text{N}. \tag{5.15}$$

The force acting on the conveyor chain as per (5.15) is referred to as F_{K1}.

5.1.3 Data from the frequency converter

The frequency converter makes it possible to set the desired rotational speed of the electric motor and thus also the speed of the conveyor chain for conveying the car bodies. The electronic control unit also continuously provides data on frequency, current and the percentage of nominal torque used by the drive system.

The nominal torque of the drive unit is

$$M_N = 3600\ \text{Nm} \tag{5.16}$$

and, according to *Fig. 5.9*, the percentage of the nominal torque used is 63.45%. Using the data from the frequency converter, the torque M_1 can therefore be calculated as follows

$$M_1 = M_N \times 63.45\% = 3600\ \text{Nm} \times 63.45\% = 2284\ \text{Nm}\ . \tag{5.17}$$

Fig. 5.9 Current data from the frequency converter on frequency, current and the percentage of nominal torque used by the drive system

The torque on drive sprocket 5 is

$$M_5 = M_1 i_{14} = 2284\ \text{Nm} \times 11.93 = 27248\ \text{Nm}\,. \tag{5.18}$$

The corresponding overall force driving the sprockets on the right- and left-hand sides of the conveyor system, i.e. the overall force acting on both chains, is

$$F_{gK} = \frac{2M_5}{d_5} = \frac{2 \times 27248\ \text{Nm}}{0.966\ \text{m}} = 56414\ \text{N} \tag{5.19}$$

and the force acting on one chain is

$$F_K = \frac{F_{gK}}{2} = \frac{57996\ \text{N}}{2} = 28207\ \text{N}. \tag{5.20}$$

The force acting on the conveyor chain as per (5.20) is referred to as F_{K2}.

5.1.4 Malfunction

In the event of a malfunction, failure of the drive unit's control can be assumed. In this case, torque is expected to reach the maximum M_{1max} of 5600 Nm (index plate value).

Thus, raising the force acting on the conveyor chain to

$$F_K = \frac{M_{1max} i_{14}}{d_5} = \frac{5600\ \text{Nm} \times 11.93}{0.966\ \text{m}} \cong 69200\ \text{N}. \tag{5.21}$$

The force acting on the conveyor chain as per (5.21) is referred to as F_{K3}.

5.2 Sprocket shaft

In order to proceed with this thesis on running diagnostics on low-speed ball and roller bearings, it is important to know the strength ratios of the shaft. The forces acting on the conveyor chain were identified in the previous section. To define the representative values of the forces acting on the conveyor chain, the dynamic calculation can be used.

The lowest value F_{K1} (5.15) corresponds to the PT line being in continuous motion. The higher value F_{K2} (5.20) emerges during start-up of the pretreatment line or when the resistance is increased whilst the line is in motion. The maximum value for the force acting on the conveyor chain F_{K3} may emerge in the event of a malfunction and is given by the maximum torque available at the drive unit's output sprocket (5.21).

5.2.1 Load on the sprocket shaft

The load on the sprocket shaft bearing assembly occurs due to the force acting on the conveyor chain. The individual shafts of the sprockets in the PT line are exposed to different loads. The load depends on the position of the sprocket in the conveyor system. The greatest load acts on the shaft of sprocket 30 (*Fig. 4.1*).

The force acting on the chain causes the bending force F_{Bi} to act on the shaft at this position as per *Fig. 5.10*. The resulting force F_{Bi} comes from the vector sum of forces F_{Ki} acting on the two sections of the conveyor chain that are intermeshed with the sprocket.

The bending force F_{Bi} can be calculated as follows

$$F_{Bi} = 2F_{Ki}\cos\beta\ . \tag{5.22}$$

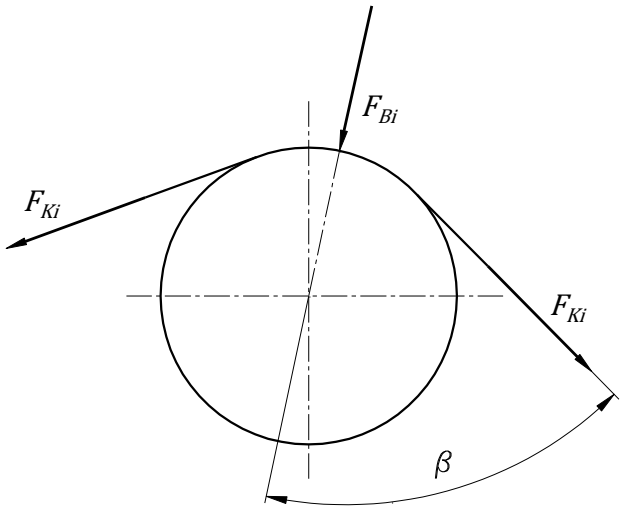

Fig. 5.10 Force ratios acting on sprocket 30

For the individual forces F_{Ki} acting on the conveyor chain, the following values emerge for the bending forces acting on the shaft

$$F_{B1} = 2F_{K1}\cos\beta = 2 \times 18081\ \text{N} \times \cos 58^{\circ} \cong 20\ \text{kN}\ , \tag{5.23}$$

$$F_{B2} = 2F_{K2}\cos\beta = 2 \times 28207\ \text{N} \times \cos 58^{\circ} \cong 30\ \text{kN} \tag{5.24}$$

and

$$F_{B3} = 2F_{K3}\cos\beta = 2 \times 69200\ \text{N} \times \cos 58^{\circ} \cong 75\ \text{kN}\ . \tag{5.25}$$

The force F_{B1}, calculated using the spring suspension in the drive unit, is based on the displacement of the springs used in the design.

Peak forces acting on the chain conveyor are evidently not captured in these measurements of spring displacement, unlike with the values obtained from the frequency converter. Thus, the force F_{B1} can be considered to be an average of the force acting on the chain. With these operational forces, the conveyor's components are

exposed to dynamic vibration stress and therefore their strength must be calculated for fatigue in the critical cross sections.

The force F_{B2}, calculated using data from the frequency converter, is based on the higher value of torque delivered by the motor during operation.

Despite the minimal probability of a malfunction occurring, these force components must be taken into consideration when designing and calculating the strength required for the structural parts. For this, the stress placed on the structural parts generated by force F_{B3} must not exceed the yield strength of the material.

The maximum bending moment can be expected at bearing position A, with the maximum bending stress and the corresponding strain on the shaft axis in the upper outer fibre of the cross section directly above A.

Force ratios acting on the sprocket shaft are shown in *Fig. 5.11*.

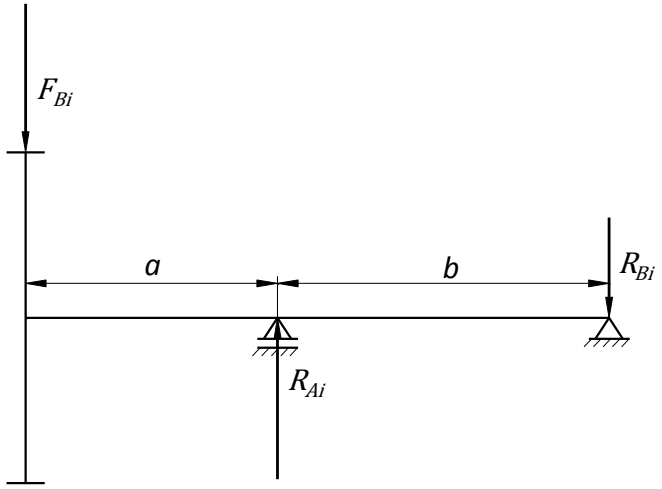

Fig. 5.11 Forces acting on the sprocket shaft

Equilibrium equations for the shaft are as follows

$$-F_{Bi} + R_{Ai} - R_{Bi} = 0\,, \tag{5.26}$$

$$R_{Ai}b - F_{Bi}(a+b) = 0\,. \tag{5.27}$$

Here

$$R_{Ai} = \frac{F_{Bi}(a+b)}{b} \tag{5.28}$$

and

$$R_{Bi} = \frac{F_{Bi}a}{b}\,. \tag{5.29}$$

The maximum bending moment is thus

$$M_{Bi} = |-F_{Bi}a| \,. \tag{5.30}$$

5.2.2 Calculating stress and strain

The maximum bending stress is calculated analytically using the following formula

$$\sigma_{Bi} = \frac{M_{Bi}}{W_B}, \tag{5.31}$$

where W_B is the section modulus for bending

$$W_B = \frac{\pi d^3}{32}. \tag{5.32}$$

The bending stress when exposed to force F_{B2} is

$$\sigma_{B2} = \frac{M_{B2}}{W_B} \cong 50 \text{ MPa} \,. \tag{5.33}$$

Stress and strain can be determined much more precisely using FEM analysis. The ANSYS Workbench program integrates the geometric and modelling material from Creo 2.0 and constructs a finite element mesh (*Fig. 5.12*).

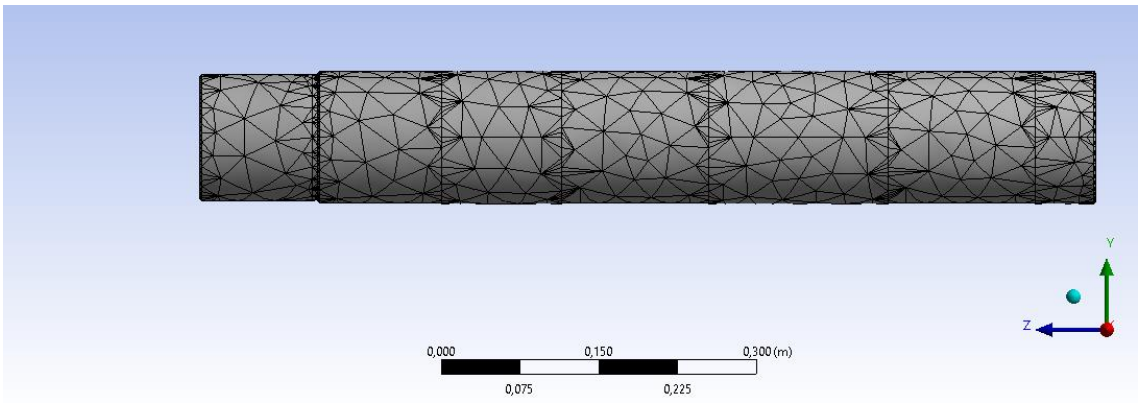

Fig. 5.12 Creation of a FEM mesh on the shaft

Boundary values and loads are then introduced. The boundary values are chosen to reflect the usual shaft bearing assembly, i.e. at position *B* axial displacement of the shaft is possible in the floating bearing and at position *A* displacement is not permitted in any direction in the fixed bearing. At the connection point between the sprocket and the shaft, the force acting on the shaft F_{Bi} is set as the force acting along the y axis (*Fig. 5.13*). The value of the bending force F_{Bi} was introduced as $F_{B2} = 30$ kN for the following FEM analysis, and the critical bending stress placed on the shaft's material in the event of a malfunction was taken into account with regards to the yield strength.

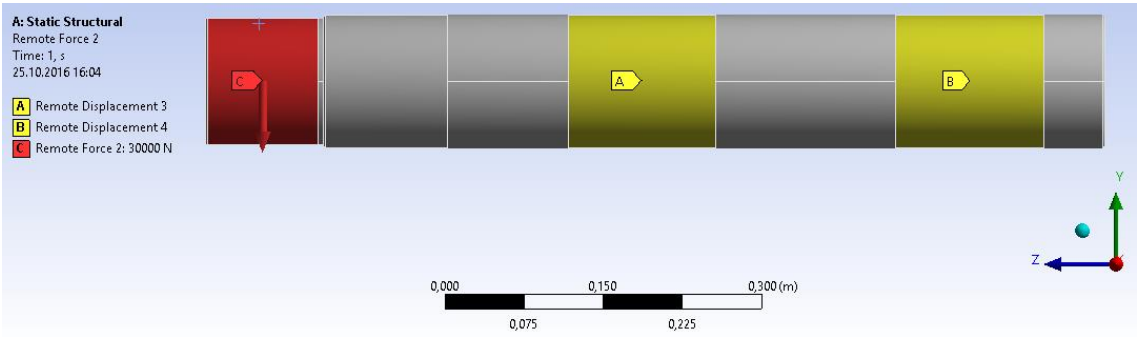

Fig. 5.13 Boundary values and load for the FEM analysis

Once the boundary values and load have been determined, the calculations can be executed. As a result, the directions of the most important elastic relative strain vectors can be shown (*Fig. 5.14*).

These directions (along the shaft axis) correspond to the normal stress (*Fig. 5.15*) and the normal strain (*Fig. 5.16*).

Fig. 5.17 and *Fig. 5.18* show the equivalent stress and equivalent strain including slight shear. These values differ only marginally from the normal values. *Fig. 5.19* shows the deflection of the shaft.

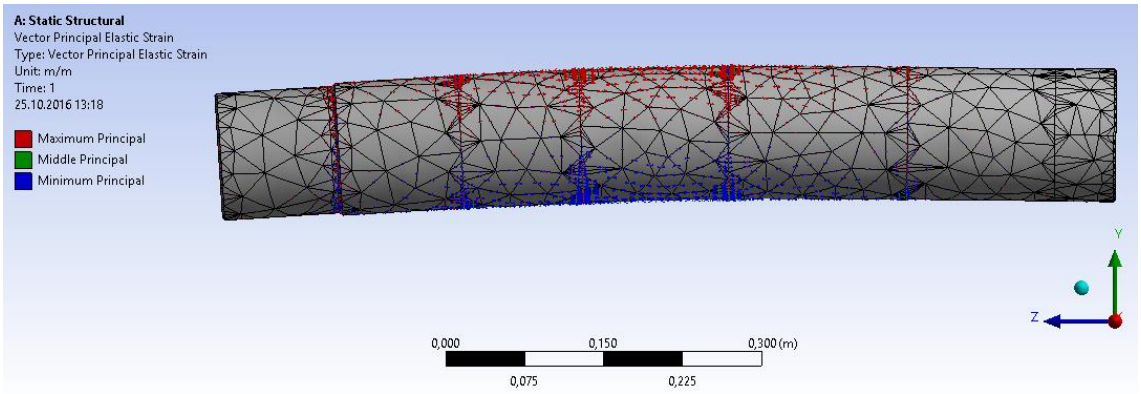

Fig. 5.14 Directions of elastic relative strain vectors

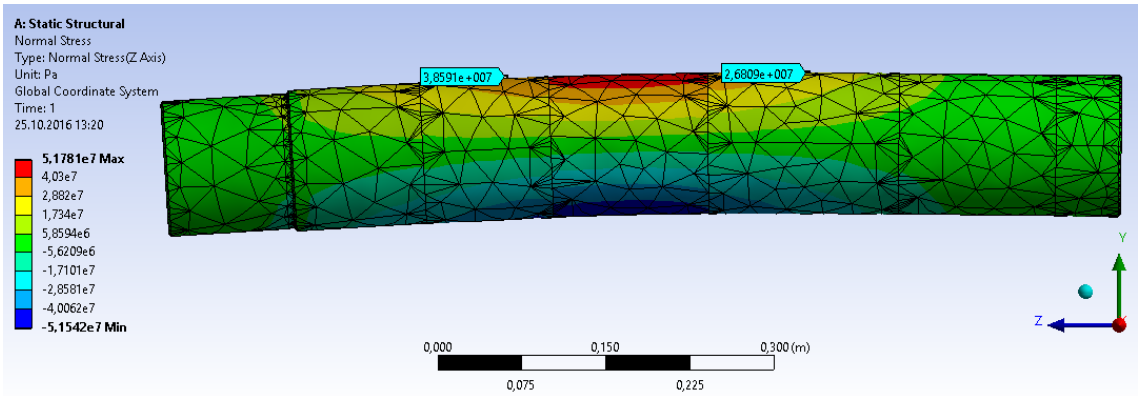

Fig. 5.15 Normal stress (along the z axis)

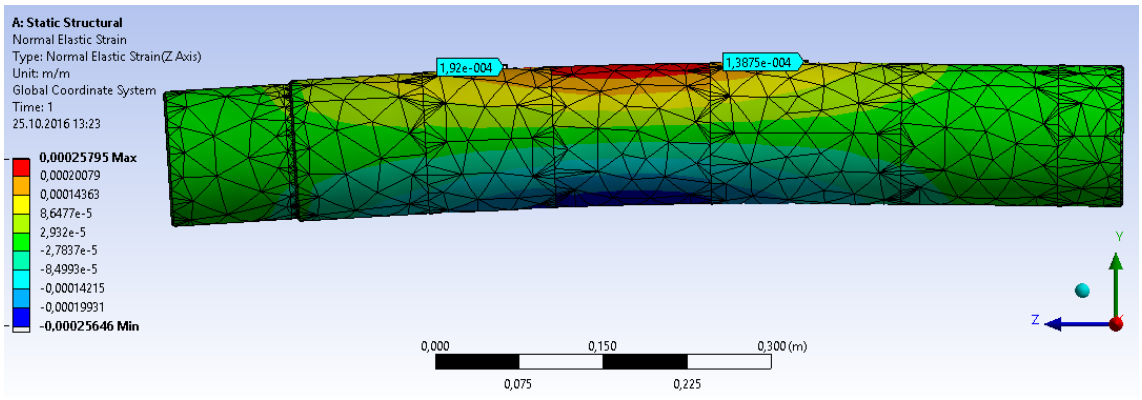

Fig. 5.16 Normal strain (along the z axis)

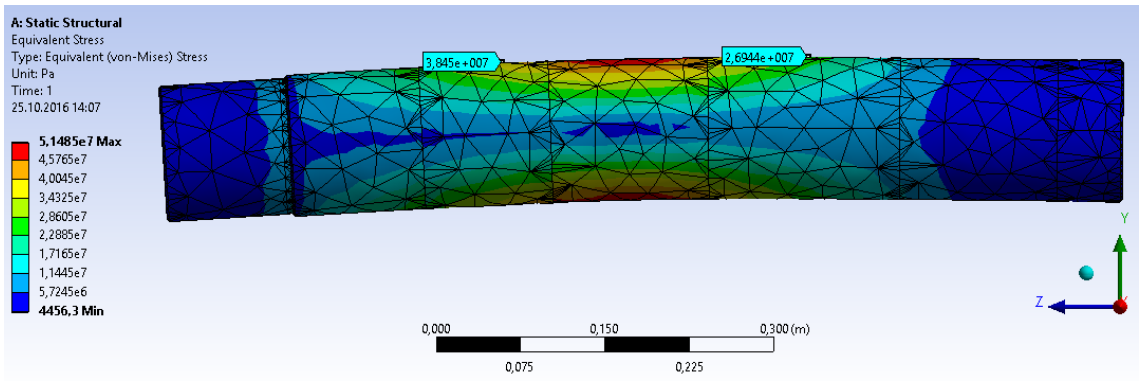

Fig. 5.17 Equivalent stress

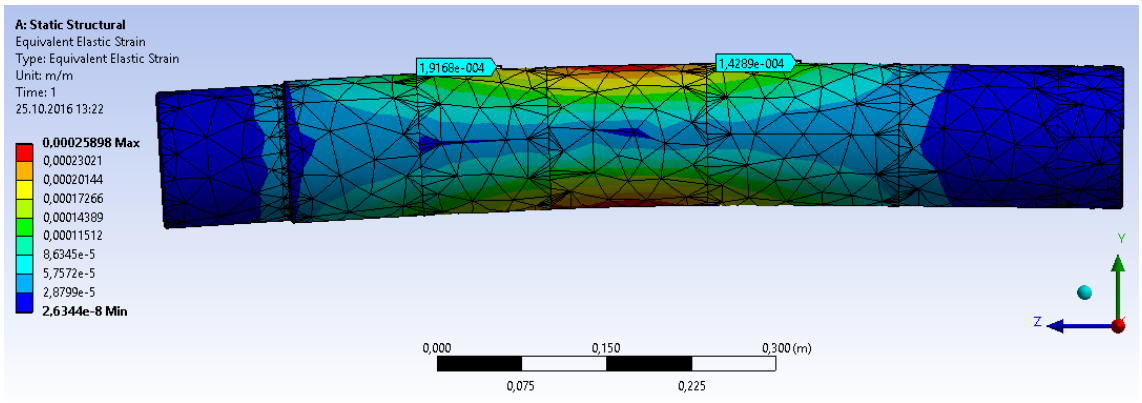

Fig. 5.18 Equivalent strain

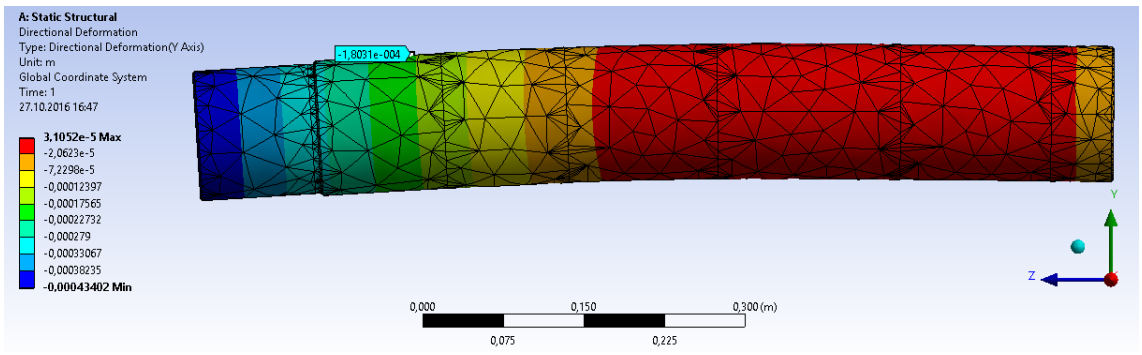

Fig. 5.19 Deflection of the shaft (along the y axis)

5.2.3 Measuring the strain on the sprocket shaft

The strain on the sprocket shaft was measured under laboratory conditions at the Technical University of Liberec (*Fig. 5.20* and *Fig. 5.21*). Two strain gauges were attached to the shaft in the direction of the main strain vectors. One sensor was placed between bearings *A* and *B* and the other between bearing *A* and the sprocket. In addition, the deflection of the shaft close to the sprocket was measured using a laser sensor.

The measurements are shown in *Fig. 5.22* to *Fig. 5.24*.

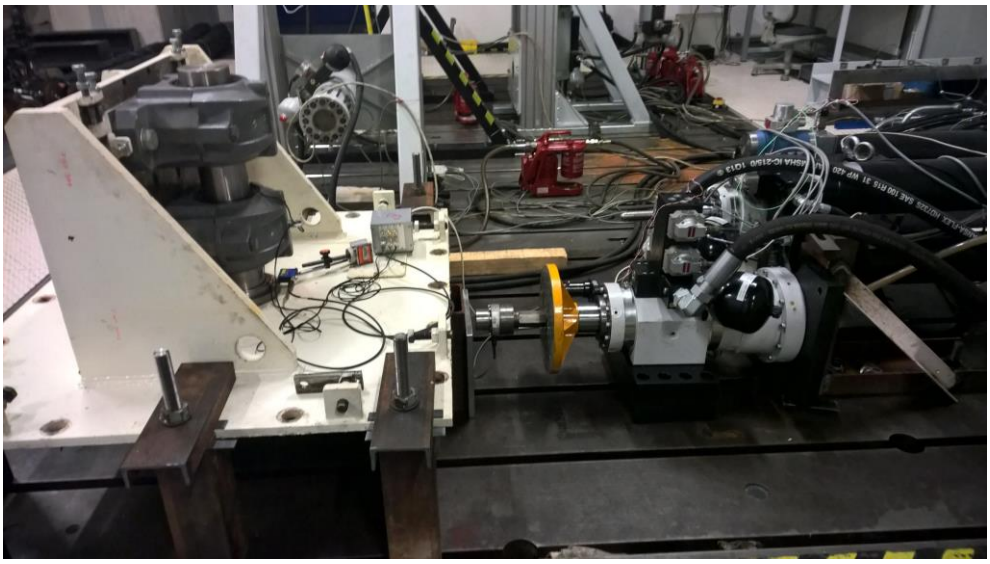

Fig. 5.20 Measurement of the strain and deflection of the sprocket shaft

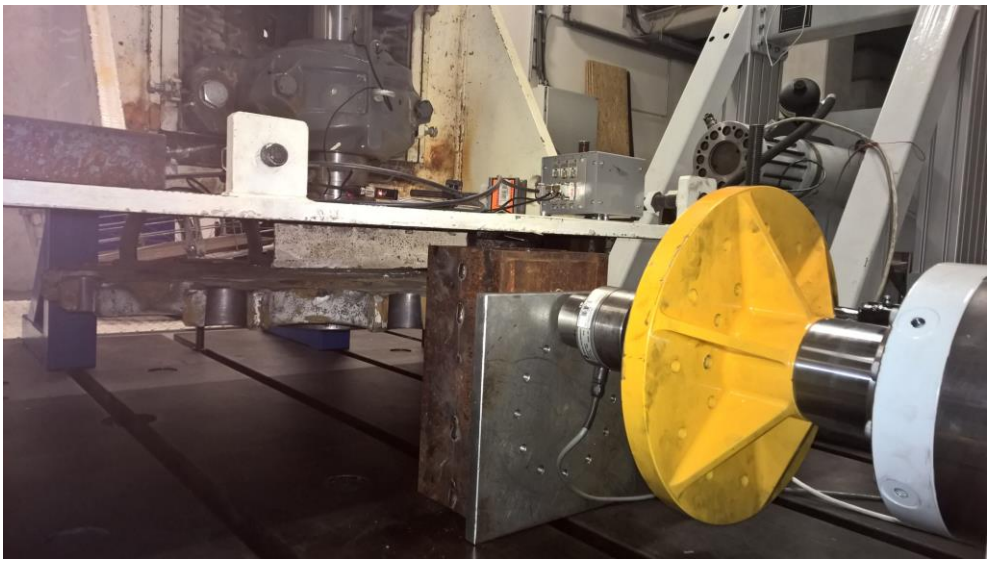

Fig. 5.21 Measurement of the strain and deflection of the sprocket shaft

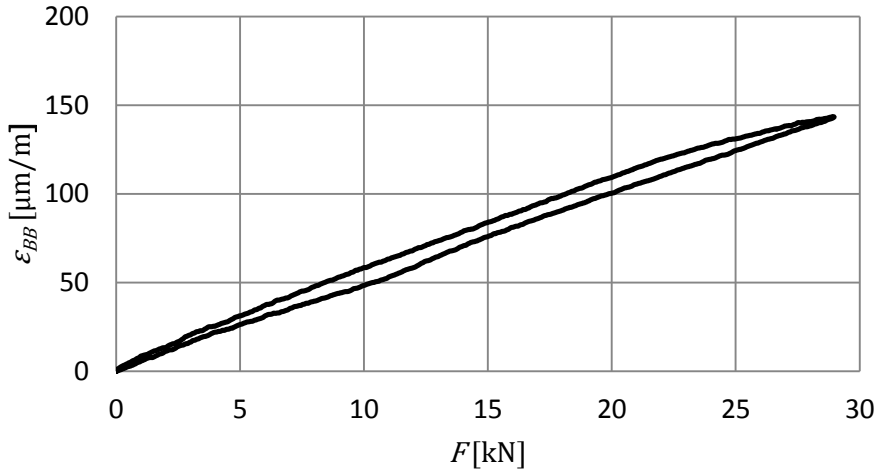

Fig. 5.22 Measurements of the relative strain of the shaft between the bearings

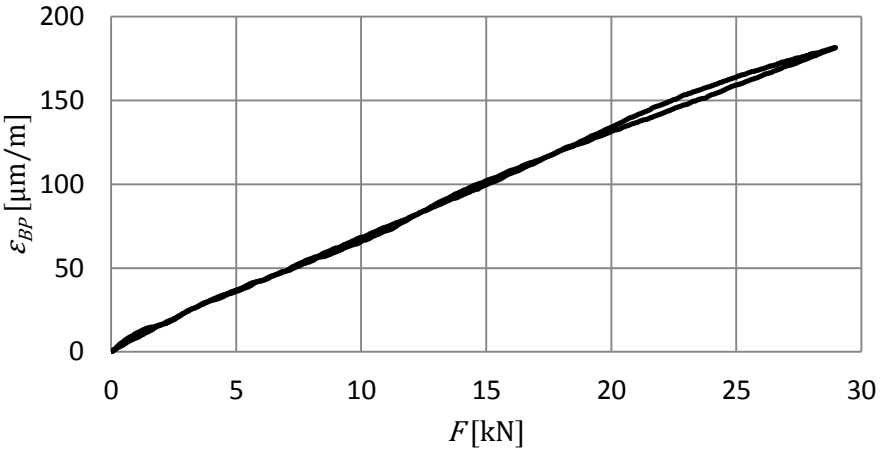

Fig. 5.23 Measurements of the relative strain of the shaft between bearing A and the sprocket

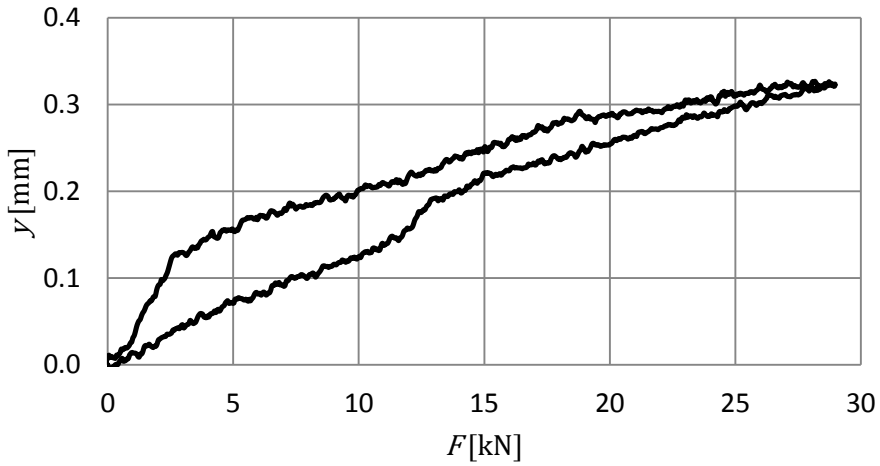

Fig. 5.24 Measurements of the shaft deflection between bearing A and the sprocket

5.2.4 Comparison of calculations and measurements

It is crucial to compare the FEM analysis results with the measurements from the laboratory. In doing so, the chosen boundary values in the FEM method and the accuracy of the method used in ANSYS can be checked.

In *Table 5.2* there are very slight differences in the values for the strain acting on the sprocket shaft. The difference in deflection is caused by other components of the sprocket shaft bearing assembly affecting the measurement. These components were primarily the spherical roller bearings, the bearing housings and the baseplate of the installation frame.

Table 5.2 Comparison of measured and calculated values

		Analytical calculation	**FEM analysis**	**Laboratory measurements**
Strain ε_{BB}	[µm/m]	–	138	145
Strain ε_{BP}	[µm/m]	–	192	180
Deflection y	[mm]	0.21	0.18	0.33

5.3 Bearings

To examine the strength of the bearings, the load rating is calculated under defined loads in line with the manufacturer's guidelines for ensuring the required bearing life. As a considerably greater load is placed on bearing A from the two roller bearings at positions A and B, further calculation is limited to bearing A.

5.3.1 Load on the bearing

The load on roller bearing A during its projected life is to be considered using three different load scenarios that, depending on the load, correspond to the different values relating to the forces acting on the conveyor chain. These scenarios were defined in the previous paragraph.

The force R_{A1} acting on bearing A, calculated using the spring displacement of the spring suspension in the drive unit, and the force R_{A2}, calculated using the upper torque

of the motor as per the data from the frequency converter, are each determined with the same proportions to calculate the lifespan of the bearing.

The force R_{A3} acting on bearing A only emerges in the event of a malfunction when the frequency converter, controlling the drive unit motor, and other conveyor safety features fail. In this emergency situation, the drive unit generates the maximum torque possible and the chain conveyor reaches its maximum operating capacity.

The operational proportion q_i of the three forces R_{Ai} across the required lifespan for bearing A is determined in the following values.

The load scenarios for bearing A are

$$R_{A1} = \frac{F_{B1}(a+b)}{b} = \frac{19\ \text{kN} \times (318\ \text{mm} + 352\ \text{mm})}{352\ \text{mm}} \cong 36\ \text{kN} \tag{5.34}$$

and

$$q_1 = 49.999\%\,, \tag{5.35}$$

$$R_{A2} = \frac{F_{B2}(a+b)}{b} = \frac{30\ \text{kN} \times (318\ \text{mm} + 352\ \text{mm})}{352\ \text{mm}} \cong 57\ \text{kN} \tag{5.36}$$

and

$$q_2 = 49.999\%\,, \tag{5.37}$$

$$R_{A3} = \frac{F_{B3}(a+b)}{b} = \frac{47\ \text{kN} \times (318\ \text{mm} + 352\ \text{mm})}{352\ \text{mm}} \cong 89\ \text{kN} \tag{5.38}$$

and

$$q_3 = 0.002\%\,. \tag{5.39}$$

5.3.2 Calculation of load rating

The roller bearings used to mount the sprocket shaft at positions A and B must have a bearing life of $L = 72000$ hours, which is equivalent to approximately 10 years.

Each roller bearing must satisfy the lifespan equation.

$$L = \frac{10^6}{60n}\left(\frac{C}{P}\right)^m\,, \tag{5.40}$$

where C is the dynamic load rating, P is the equivalent load, m is the exponent of the lifespan equation and n is the rotational speed of the shaft.

For roller bearing *A*

$$m = \frac{10}{3} \tag{5.41}$$

and

$$P = \left(\sum_{i=1}^{3} \left(R_{Ai}^{\frac{10}{3}} q_i \right) \right)^{\frac{3}{10}} = 49 \text{ kN} \tag{5.42}$$

The rotational speed of the shaft is

$$n = 3.3 \text{ min}^{-1} . \tag{5.43}$$

The required dynamic load rating of roller bearing *A* is thus

$$C = P \left(\frac{60n}{10^6} L \right)^{\frac{3}{10}} = 108 \text{ kN} . \tag{5.44}$$

As per *Table 4.7* it can be determined that the dynamic load rating of the bearing is ten times greater than it needs to be.

6 Diagnosing damage in ball and roller bearings

The principle of ball and roller bearing diagnosis is based on the definition of the individual bearing components' kinematic conditions.

6.1 Kinematic conditions of ball and roller bearings

The kinematics of ball and roller bearings (*Fig. 6.1*) fall within the scope of simultaneous movements of bodies in the plane.

Fig. 6.1 Ball and roller bearings [12]

In their elementary form, simultaneous movements of bodies are generated by the guide movement and the relative movement. The guide movement is the movement of the carrier 2 relative to the frame 1, and the relative movement is the movement of the object 3 that is to be observed in relation to the carrier 2 (*Fig. 6.2*).

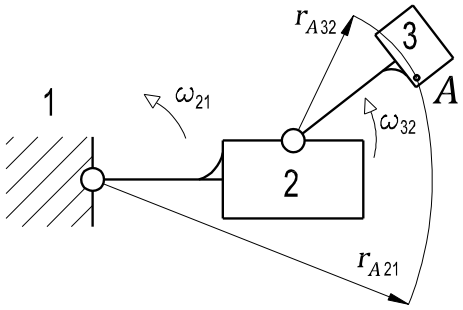

Fig. 6.2 Two simultaneous rotations of a body

The examination of the general values for the kinematic variables of the object 3 in the fixed coordinate system of the frame 1 is performed by a basic decomposition. In the case of three bodies (including the frame 1), the movement φ_{31} of the body 3 in relation to the frame 1 is

$$\varphi_{31} = \varphi_{32} + \varphi_{21}\,, \tag{6.1}$$

whereby φ_{21} is the relative rotation of the body 2 in relation to the frame 1, φ_{32} is the relative rotation of the body 3 in relation to the body 2, and ω_{31} is the angular velocity of the body 3 in relation to the frame 1.

$$\omega_{31} = \omega_{32} + \omega_{21} \,. \tag{6.2}$$

The same relationship is used for the angular acceleration ε_{31}

$$\varepsilon_{31} = \varepsilon_{32} + \varepsilon_{21} \,, \tag{6.3}$$

but only if the rotation axes of both bodies are in parallel. If the rotation axes intersect, the acceleration of Résal ε_R, must be added to the equation, whereby

$$\varepsilon_R = \omega_{21} \times \omega_{32} \,. \tag{6.4}$$

The acceleration ε_R is generated by the change in direction of the rotation axis for relative movement 32.

Regarding issues with ball and roller bearings, it is assumed that the axes of the rolling elements' synchronous rotations are in parallel and that no acceleration of Résal occurs.

Based on the kinematic values for the object to be examined calculated as per the relationships in (6.1) to (6.3), the kinematic values s, v, and a for any point *A* of the body 3 can be determined by the basic decomposition of the movements 21 and 32. It therefore applies that

$$s_{A31} = s_{A32} + s_{A21} = r_{A32}\varphi_{32} + r_{A21}\varphi_{21} \,, \tag{6.5}$$

$$v_{A31} = v_{A32} + v_{A21} = r_{A32}\omega_{32} + r_{A21}\omega_{21} \tag{6.6}$$

and

$$a_{A31} = a_{A32} + a_{A21} = r_{A32}\varepsilon_{32} + r_{A21}\varepsilon_{21} \,, \tag{6.7}$$

whereby r_{A21} and r_{A32} are position vectors from point *A* of the body 3 to the respective rotation axes.

Using the body 3, another body such as the outer ring *O* or the inner ring *I* (*Fig. 6.3*) can be connected, thus creating a kinematic diagram of a rolling-element bearing or of a simple planetary gear system.

The calculation of the kinematic values for the bodies in the system according to *Fig. 6.3* enables damage to the bearing's rolling element to be detected, for example.

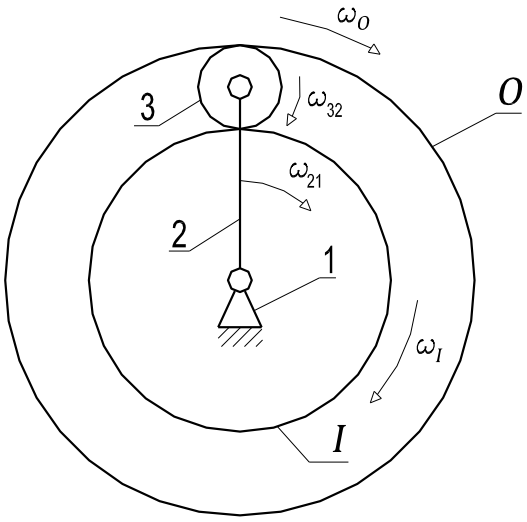

Fig. 6.3 Planetary gear system

6.2 Kinematic analogy of rolling-element bearings and planetary gear systems

Ball and roller bearings (*Fig. 6.4*) are mechanical systems in which at least one component performs two simultaneous rotations on both the shaft axis and its own axis. These characteristics also apply to planetary gear systems.

Fig. 6.4 Ball and roller bearings [12]

Ball and roller bearings are kinematically similar to planetary gear systems where the carrier 2 is the same as a cage C and the simple planet gears 3 are rolling elements R (*Fig. 6.5*). This analogy allows for a kinematic solution which is known from planetary gear theory. In this case it is necessary to define a replacement planetary gear system with simple planet gears which correspond to the bearing's rolling elements (*Fig. 6.5*).

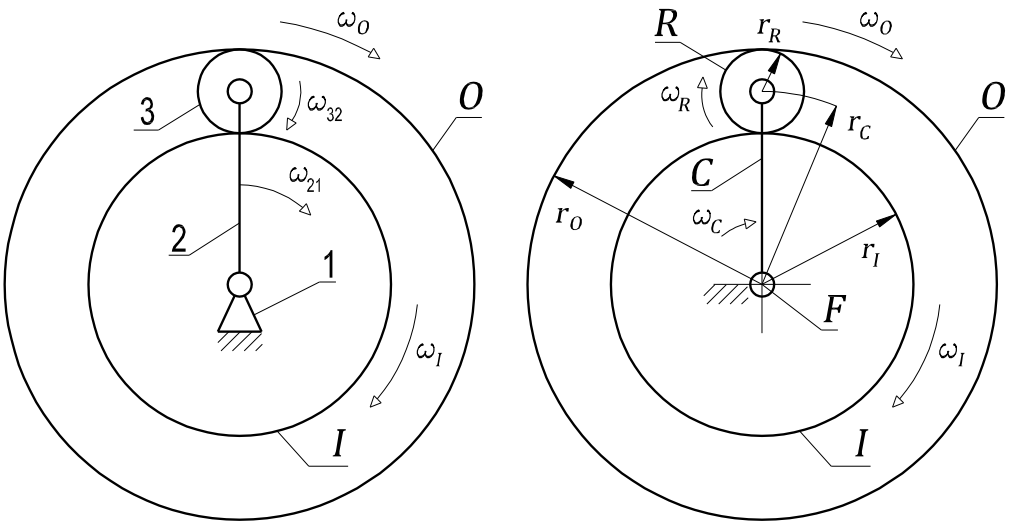

Fig. 6.5 Replacement planetary gear system with simple planet gears

While the carrier C and the rings O and I rotate on the central rotation axis, the rolling element R makes two simultaneous rotations, one on its own axis and one together with the carrier C on the central rotation axis (*Fig. 6.5*).

To describe the kinematics of the individual bearing components, two methods can be used. These methods are also approaches used in describing the kinematics of planetary gear systems. The first approach is based on the prerequisite that the gears are rolling and that the circumferential speed is the same at the respective contact points, which are the poles of the relative movements.

The second approach (*Willis method*) is based on replacing the planetary gear system with a standard primary reduction transmission. In this case, the observer sees the gears rotating at relative speeds in relation to the carrier C. The gear ratio can then be expressed as the ratio of the relative angular velocities, which defines the kinematic relationship of the gear system. From this relationship, the angular velocities of any element can be determined.

This calculation for the angular velocities of the parts of a planetary gear system is much shorter and ultimately more efficient, especially in more complex cases where planetary gear systems are combined. The principle behind this method is shown using the example of a simple planetary gear system (*Fig. 6.6*).

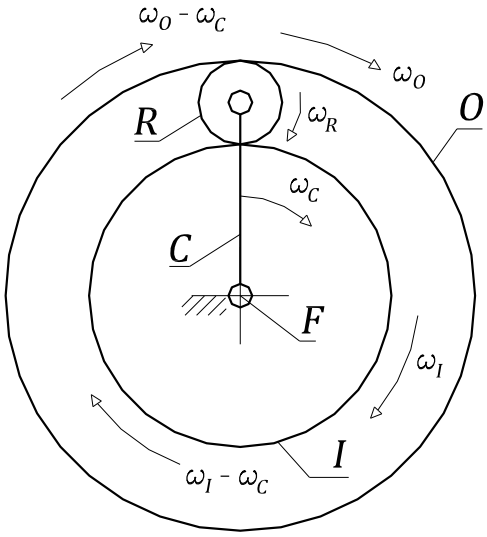

Fig. 6.6 Solution of the kinematics of a planetary gear system according to Willis

After introducing the clockwise rotational direction for the angular velocities of the gears I, R and O as well as carrier C, the planetary gear system is replaced by a reduction transmission. The relative movement of gears I and O in relation to carrier C is now observed.

For the ratio of the relative angular velocities of any two elements, it can be assumed that the ratio of the relative angular velocities between gears I and O is as follows

$$\frac{\omega_I - \omega_C}{\omega_O - \omega_C} = -\frac{r_R}{r_I}\frac{r_O}{r_R} = -\frac{r_O}{r_I}, \tag{6.8}$$

For $\omega_O = 0$, it follows that

$$\omega_C = \frac{r_I}{r_I + r_O}\,\omega_I\,, \tag{6.9}$$

which means the ratio between gears I and R is

$$\frac{\omega_I - \omega_C}{\omega_R} = -\frac{r_R}{r_I}, \tag{6.10}$$

and finally, this results in a relationship between the gears O and R which is

$$\frac{\omega_R}{\omega_O - \omega_C} = \frac{r_O}{r_R}. \tag{6.11}$$

It should be noted that the angular velocity ω_R of the rolling element R is introduced relative to the carrier C because the rolling element R has a different rotation axis than the carrier C and the other gears O and I.

Thus, if the above relationship $\omega_O = 0$ is assumed, it is possible to calculate the angular velocity ω_C of the cage C and the angular velocity ω_R of the rolling element R.

6.3 Vibration frequencies caused by bearing damage

The vibration frequency caused by bearing damage can be determined based on kinematic bearing ratios. From these calculations it can also be determined whether the damage is on the outer ring, inner ring or the rolling element.

Relations to determine the respective excitation frequencies in the vibration spectra can be found in the relevant literature (*Table 6.1*).

Table 6.1 Table of damaged rolling bearing excitation frequencies [13]

Ursache	Erregerfrequenz
Überrollfrequenz Außenring (Außenringschaden)	$f_a = \frac{1}{2} f_n z \left[1 - (D_w/D_T)\cos\alpha\right]$ (1)
Überrollfrequenz Innenring (Innenringschaden)	$f_i = \frac{1}{2} f_n z \left[1 + (D_w/D_T)\cos\alpha\right]$ (2)
Rotationsfrequenz Käfig (Käfigschaden)	$f_k = \frac{1}{2} f_n \left[1 - (D_w/D_T)\cos\alpha\right]$ (3)
Rotationsfrequenz Wälzkörper (Wälzkörperschaden)	$f_w = \frac{1}{2} f_n (D_T/D_w) \left[1 - ((D_w/D_T)\cos\alpha)^2\right]$ (4)
Überrollfrequenz eines Wälzkörperbereichs	$f_ü = f_n (D_T/D_w) \left[1 - \left((D_w/D_T)\cos\alpha\right)^2\right]$ (5)

Die in diesen Gleichungen vorkommenden Größen sind in Bild 3.9 eingetragen und haben folgende Bedeutung:

f_n Wellendrehfrequenz (Drehfrequenz des Innenringes $f_n = n(\text{min}^{-1})/60$),
z Anzahl der Wälzkörper,
D_w Wälzkörperdurchmesser,
D_T Teilkreis- oder Rollkreisdurchmesser
α Druckwinkel, vgl. Bild 3.9.

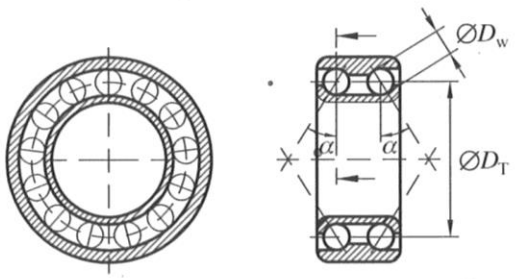

6.3.1 Damage to the outer ring

Fig. 6.7 shows a diagram of damage to the outer ring O. In the frequency spectrum of vibrations, this type of damage is identified through the frequency generated by the rotation of the cage C (multiplied by the number m of rolling elements).

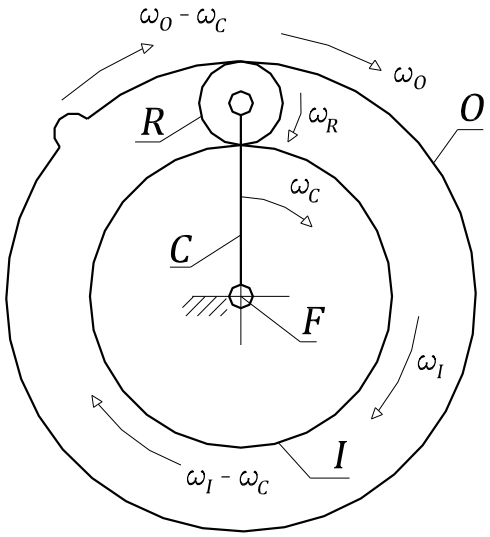

Fig. 6.7 Damage to the outer ring

From the relationship in (6.9), the angular velocity ω_C of the cage C can be determined if the outer ring O is stationary and it applies that

$$r_I = r_C - r_R \tag{6.12}$$

and

$$r_O = r_C + r_R\,, \tag{6.13}$$

then, the angular velocity of the cage C is

$$\omega_C = \frac{r_I}{r_O + r_I}\omega_I = \frac{1}{2}\left(1 - \frac{r_R}{r_C}\right)\omega_I\,. \tag{6.14}$$

If the number of rolling elements m and the general relationship of the frequency f of the shaft rotation and the angular velocity ω are used

$$f = \frac{\omega}{2\pi}\,, \tag{6.15}$$

the following formula applies for the frequency f_{DO} of the vibrations, which are associated with damage to the outer ring

$$f_{DO} = \frac{1}{2}\left(1 - \frac{r_R}{r_C}\right) f_I m\,. \tag{6.16}$$

6.3.2 Damage to the inner ring

Fig. 6.8 shows a diagram of damage to the inner ring I. In the frequency spectrum of vibrations, this type of damage is shown in the frequency of the relative rotation of the cage C in relation to the inner ring I multiplied by the number of rolling elements m.

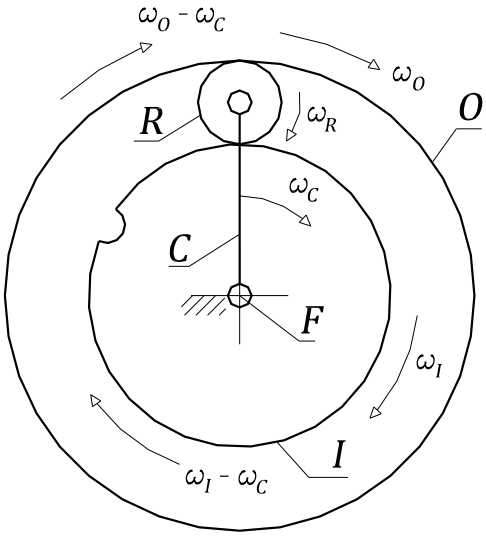

Fig. 6.8 Damage to the inner ring

From the relationship in (6.8), the relative angular velocity of the inner ring I and the carrier C can be determined if the outer ring O is stopped. It then applies that

$$\omega_I - \omega_C = \frac{r_O}{r_I}\omega_C \,, \tag{6.17}$$

(6.9) can also be inserted, resulting in

$$\omega_I - \omega_C = \frac{r_O}{r_I}\frac{r_I}{r_O + r_I}\omega_I = \frac{r_O}{r_O + r_I}\omega_I = \frac{1}{2}\left(1 + \frac{r_R}{r_C}\right)\omega_I \,. \tag{6.18}$$

Furthermore, the number of rolling elements m and equation (6.15) can be assumed. This results in frequency f_{DI} of the vibration due to damage to the inner ring I

$$f_{DI} = \frac{1}{2}\left(1 + \frac{r_R}{r_C}\right) f_I m \,. \tag{6.19}$$

6.3.3 Damage to the rolling element

Fig. 6.9 shows a diagram of damage to the rolling element R. In the frequency spectrum of vibrations, this type of damage is shown when the frequency of the rotation of the rolling element R is doubled.

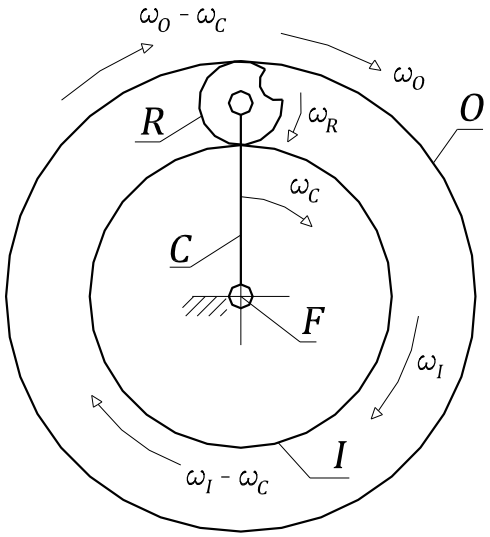

Fig. 6.9 Damage to the rolling element

From the relationship in (6.9) after inserting (6.11) and further adaptation, the angular velocity ω_R of the rolling element R becomes

$$\omega_R = -\frac{r_O}{r_R}\omega_C = -\frac{r_O}{r_R}\frac{r_I}{r_I + r_O}\omega_I = -\frac{r_C + r_R}{r_R}\ \frac{r_C - r_R}{2r_C}\omega_I$$
$$= -\frac{r_C^2 - r_R^2}{2r_C r_R}\omega_I = -\frac{1}{2}\frac{r_C}{r_R}\ \frac{r_C^2 - r_R^2}{r_C^2}\omega_I = -\frac{1}{2}\frac{r_C}{r_R}\left(1 - \frac{r_R^2}{r_C^2}\right)\ \omega_I. \tag{6.20}$$

The minus sign expresses the opposite rotational direction as assumed in the calculation. Thus, the frequency of vibration f_{DR}, which is linked to damage to the rolling element R is

$$f_{DR} = 2\frac{\omega_R}{2\pi} = \frac{r_C}{r_R}\left(1 - \frac{r_R^2}{r_C^2}\right) f_I\ . \tag{6.21}$$

7 Diagnostic device for low-speed ball and roller bearings

Over the course of this thesis, two principles behind the devices for running diagnostics on low-speed ball and roller bearings were developed and realised. In both cases, the devices make use of a reference element and two pairs of bearings for mounting the sprocket shaft in the frame.

In the first case, any damage to a bearing or bearing component is detected by measuring vibrations and in the second case, by identifying increased rolling resistance.

7.1 Running diagnostics based on measuring vibrations

The principle behind the device that detects damage to a bearing or its components by measuring vibrations is shown in *Fig. 7.1* (as per patent application [13]).

In this particular case, the low-speed sprocket shaft 1 is mounted using two pairs of roller bearings 2 and 4. The two shaft bearings 2 are seated within a reference element 3 and the reference element itself is mounted in the frame 5 using a further two frame bearings 4.

When the reference element 3 is brought to the necessary angular velocity using a driven pulley 11 with a v-belt 12, damage to the roller bearings 2 and 4 can be detected by measuring the vibrations using sensors 13a and 13b.

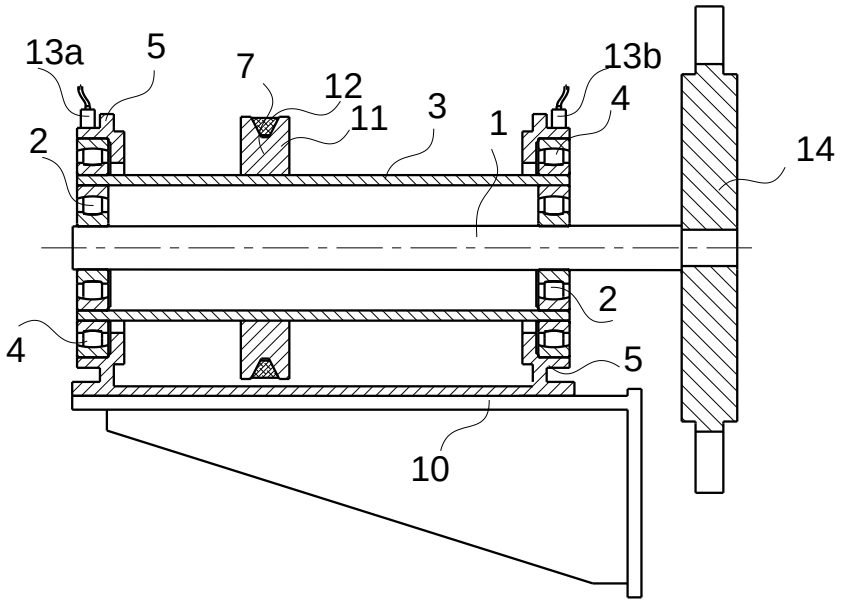

Fig. 7.1 Principle behind the diagnostic device for low-speed ball and roller bearings based on measuring vibrations

A kinematic diagram of the device for running diagnostics on low-speed ball and roller bearings based on measuring vibrations is shown in *Fig. 7.2*.

The sizes of the inner ring IS, outer ring OS, rolling element RS and cage CS of the shaft bearing for shaft S are identified by the indices IS, OS, RS and CS.

The sizes of the inner ring IF, outer ring OF, rolling element RF and cage CF of the frame bearing for frame F are identified by the indices IF, OF, RF and CF.

By examining the kinematic relationships of the entire diagnostics system, the excitation frequency, which occurs as a result of damage to individual bearing components, can be ascertained. Thereby, it evidently applies that

$$\omega_{OS} = \omega_{IF} = \omega_{RE}\,, \tag{7.1}$$

where ω_{RE} is the known angular velocity of the reference element RE.

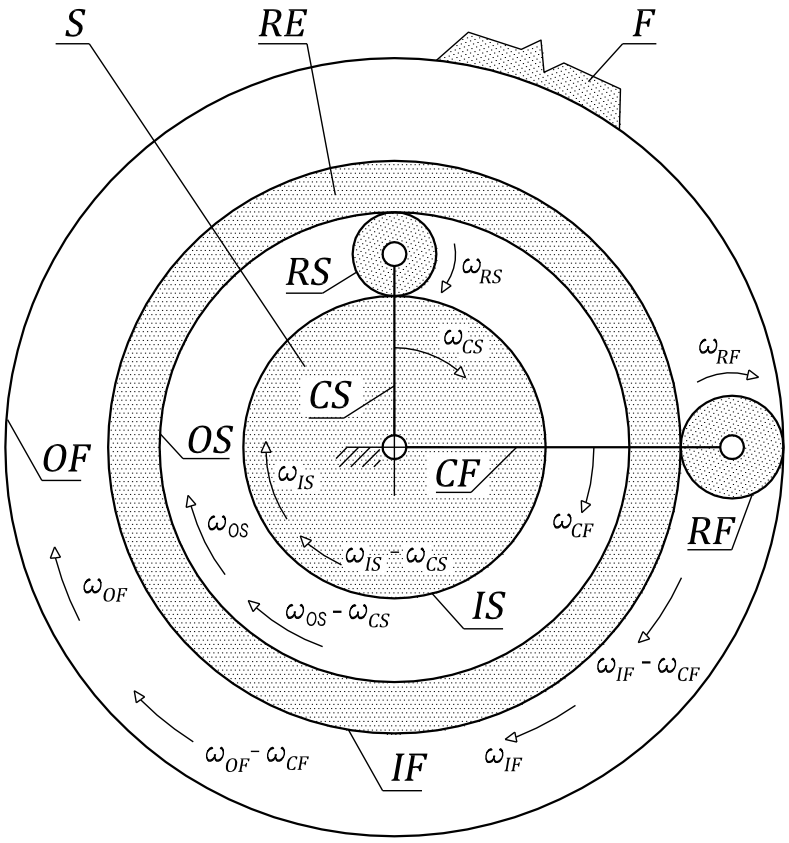

Fig. 7.2 Kinematic diagram of the diagnostic device for low-speed ball and roller bearings

For the shaft bearing S it applies that

$$\frac{\omega_{IS}-\omega_{CS}}{\omega_{OS}-\omega_{CS}}=-\frac{r_{RS}}{r_{IS}}\frac{r_{OS}}{r_{RS}}=-\frac{r_{OS}}{r_{IS}} \tag{7.2}$$

and

$$\frac{\omega_{IS}-\omega_{CS}}{\omega_{RS}}=-\frac{r_{RS}}{r_{IS}} \tag{7.3}$$

and equally that

$$\frac{\omega_{RS}}{\omega_{OS}-\omega_{CS}}=\frac{r_{OS}}{r_{RS}}. \tag{7.4}$$

The relationships (7.2) to (7.4) allow the angular velocities ω_{CS} and ω_{RS} to be determined if the angular velocity ω_{IS} of the shaft and the angular velocity ω_{OS} of the outer ring or the reference element are known.

By inserting (7.1) into (7.2) we can see that

$$\frac{\omega_{IS}-\omega_{CS}}{\omega_{RE}-\omega_{CS}}=-\frac{r_{OS}}{r_{IS}} \tag{7.5}$$

and from which it follows that

$$\omega_{CS}=\frac{1}{r_{IS}+r_{OS}}\left(r_{IS}\omega_{IS}+r_{OS}\omega_{RE}\right). \tag{7.6}$$

For the relative angular velocity $\omega_{IS}-\omega_{CS}$ we see that

$$\omega_{IS}-\omega_{CS}=\omega_{IS}-\frac{1}{r_{IS}+r_{OS}}\left(r_{IS}\omega_{IS}+r_{OS}\omega_{RE}\right)=\frac{r_{OS}}{r_{IS}+r_{OS}}\left(\omega_{IS}-\omega_{RE}\right) \tag{7.7}$$

and that based on (7.3) the following applies for the angular velocity ω_{RS}

$$\omega_{RS}=\frac{r_{OS}}{r_{IS}+r_{OS}}\frac{r_{IS}}{r_{RS}}\left(\omega_{RE}-\omega_{IS}\right). \tag{7.8}$$

For the relative angular velocity $\omega_{OS}-\omega_{CS}$ we see that

$$\omega_{OS}-\omega_{CS}=\omega_{RE}-\omega_{CS}=\frac{r_{IS}}{r_{IS}+r_{OS}}\left(\omega_{RE}-\omega_{IS}\right). \tag{7.9}$$

The same applies for the frame bearing F

$$\frac{\omega_{IF}-\omega_{CF}}{\omega_{OF}-\omega_{CF}}=-\frac{r_{RF}}{r_{IF}}\frac{r_{OF}}{r_{RF}}=-\frac{r_{OF}}{r_{IF}} \tag{7.10}$$

and

$$\frac{\omega_{IF}-\omega_{CF}}{\omega_{RF}}=-\frac{r_{RF}}{r_{IF}} \tag{7.11}$$

as well as

$$\frac{\omega_{RF}}{\omega_{OF} - \omega_{CF}} = \frac{r_{OF}}{r_{RF}} . \tag{7.12}$$

The relationships (7.10) and (7.12) allow the angular velocities ω_{CF} and ω_{RF} to be determined if the angular velocity ω_{IF} of the reference element is known and (7.1) applies. The angular velocity ω_{OF} of the frame is generally zero.

By inserting (7.1) into (7.2), we can see that

$$\frac{\omega_{RE} - \omega_{CF}}{\omega_{OF} - \omega_{CF}} = -\frac{r_{OF}}{r_{IF}} \tag{7.13}$$

and from that

$$\omega_{CF} = \frac{r_{IF}}{r_{IF} + r_{OF}} \omega_{RE} . \tag{7.14}$$

For the relative angular velocity $\omega_{RE} - \omega_{CF}$ we see that

$$\omega_{RE} - \omega_{CF} = \omega_{RE} - \frac{r_{IF}}{r_{IF} + r_{OF}} \omega_{RE} = \frac{r_{OF}}{r_{IF} + r_{OF}} \omega_{RE} \tag{7.15}$$

and that based on (7.3) the following applies for the angular velocity ω_{RS}

$$\omega_{RF} = -\frac{r_{OF}}{r_{IF} + r_{OF}} \frac{r_{IF}}{r_{RF}} \omega_{RE} . \tag{7.16}$$

For the relative angular velocity, we see that

$$\omega_{OF} - \omega_{CF} = -\omega_{CF} = -\frac{r_{IF}}{r_{IF} + r_{OF}} \omega_{RE} . \tag{7.17}$$

If the values of the angular velocities of all rotating bearing components can be derived, the excitation frequencies, which occur due to each type of damage to the shaft or frame bearings, can be ascertained.

7.1.1 Damage to the shaft bearing's inner ring

Damage to the shaft bearing's inner ring IS (*Fig. 7.3*) exhibits a relative angular velocity ω_{DIS}, which determines the frequency of the damage, whereby

$$\omega_{DIS} = (\omega_{IS} - \omega_{CS})m_S \,. \tag{7.18}$$

By inserting (7.7), we can see that

$$\omega_{DIS} = \frac{r_{OS}}{r_{IS} + r_{OS}}(\omega_{IS} - \omega_{RE})m_S \tag{7.19}$$

and by further inserting (6.12) and (6.13) the following applies for the frequency f_{DIS}

$$f_{DIS} = \frac{\omega_{DIS}}{2\pi} = \frac{1}{2}\left(1 + \frac{r_{RS}}{r_{CS}}\right)(f_{IS} - f_{RE})m_S \,. \tag{7.20}$$

The frequency f_{DIS} is the frequency that, in the frequency spectrum of the vibrations measured at the sprocket shaft bearing assembly, corresponds to damage to the inner ring IS.

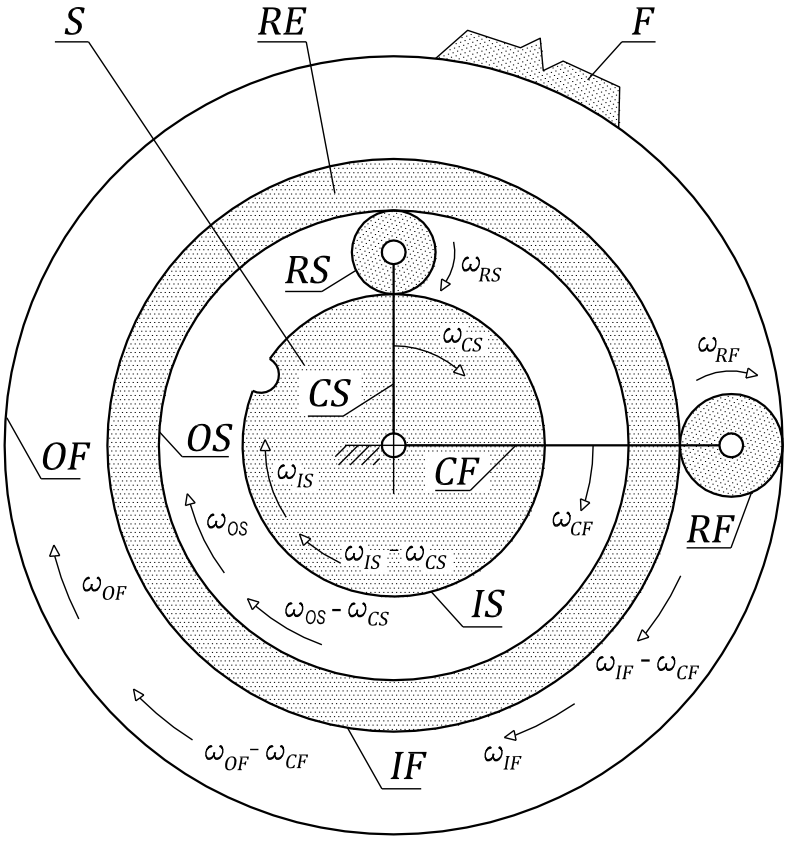

Fig. 7.3 Damage to the shaft bearing's inner ring

7.1.2 Damage to the shaft bearing's rolling element

Damage to the shaft bearing's rolling element *RS* (*Fig. 7.4*) exhibits a relative angular velocity ω_{DRS}, which determines the frequency of the damage, whereby

$$\omega_{DRS} = 2\omega_{RS}\,. \tag{7.21}$$

By inserting (7.8) and further (6.12) and (6.13), we can see that

$$\omega_{DRS} = 2\frac{r_{OS}}{r_{IS}+r_{OS}}\,\frac{r_{IS}}{r_{RS}}(\omega_{RE}-\omega_{IS}) = 2\frac{r_{CS}}{r_{RS}}\,\frac{r_{CS}^2-r_{RS}^2}{2r_{CS}^2}(\omega_{RE}-\omega_{IS})\,. \tag{7.22}$$

The frequency f_{DRS} is the frequency that, in the frequency spectrum of the vibrations measured at the sprocket shaft bearing assembly, corresponds to damage to the rolling element *RS* and which is

$$f_{DRS} = 2\frac{\omega_{BRS}}{2\pi} = \frac{r_{CS}}{r_{RS}}\left(1-\frac{r_{RS}^2}{r_{RS}^2}\right)(f_{RE}-f_{IS}). \tag{7.23}$$

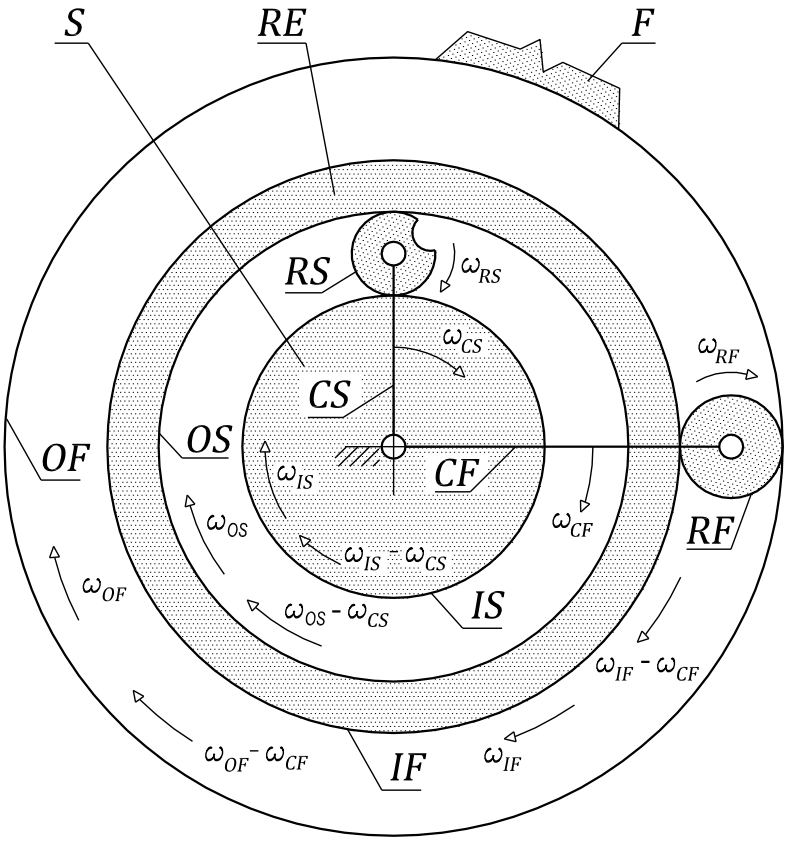

Fig. 7.4 Damage to the shaft bearing's rolling element

7.1.3 Damage to the shaft bearing's outer ring

Damage to the shaft bearing's outer ring OS (*Fig. 7.5*) exhibits a relative angular velocity ω_{DOS}, which determines the frequency of the damage and by inserting (7.1) the following applies

$$\omega_{DOS} = (\omega_{OS} - \omega_{CS})m_S = (\omega_{RE} - \omega_{CS})m_S. \tag{7.24}$$

By inserting (7.8) and further (6.12) and (6.13), we can see that

$$\omega_{OS} - \omega_{CS} = \omega_{RE} - \omega_{CS} = \frac{r_{IS}}{r_{IS} + r_{OS}}(\omega_{RE} - \omega_{IS}) \tag{7.25}$$

and

$$\omega_{DOS} = \frac{1}{2}\left(1 - \frac{r_{RS}}{r_{CS}}\right)(\omega_{RE} - \omega_{IS})\, m_S. \tag{7.26}$$

The damage frequency f_{DOS} is the frequency that, in the frequency spectrum of the vibrations measured at the sprocket shaft bearing assembly, corresponds to damage to the outer ring OS and which is

$$f_{DOS} = \frac{1}{2}\left(1 - \frac{r_{RS}}{r_{CS}}\right)(f_{RE} - f_{IS})m_S\,. \tag{7.27}$$

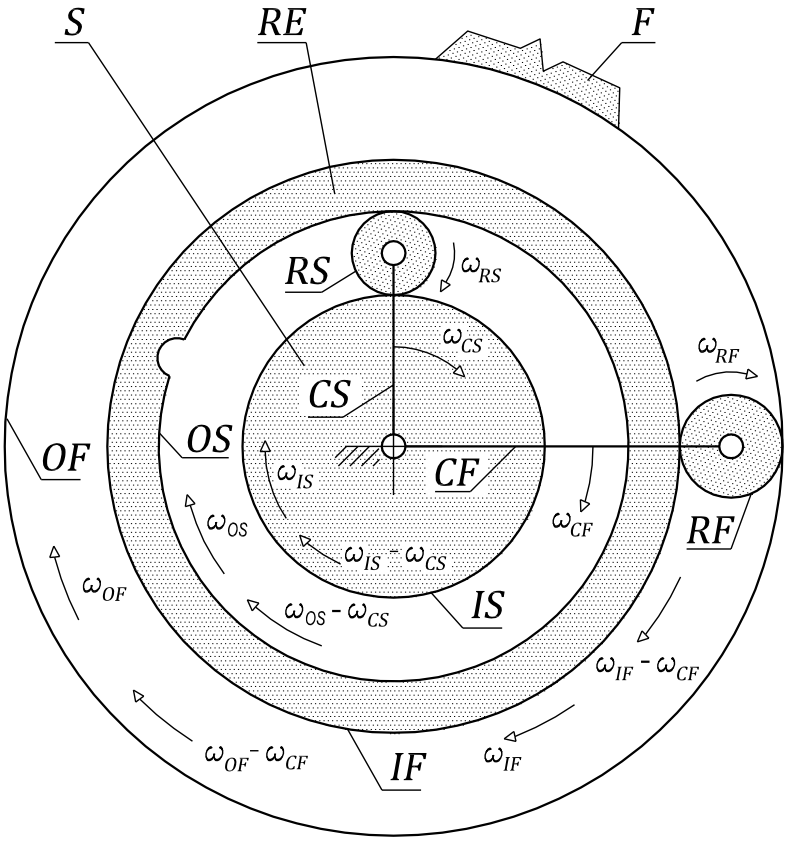

Fig. 7.5 Damage to the shaft bearing's outer ring

7.1.4 Damage to the frame bearing's inner ring

Damage to the frame bearing's inner ring IF (*Fig. 7.6*) exhibits a relative angular velocity ω_{DIF}, which determines the frequency of the damage, and by inserting (7.1) we see that

$$\omega_{DIF} = (\omega_{IF} - \omega_{CF})m_F = (\omega_{RE} - \omega_{CF})m_F \,. \tag{7.28}$$

By inserting (7.15) and further (6.12) and (6.13), we can see that

$$\omega_{DIF} = \frac{r_{OF}}{r_{IF} + r_{OF}}\omega_{RE} = \frac{1}{2}\left(1 + \frac{r_{RF}}{r_{CF}}\right)\omega_{RE} \,. \tag{7.29}$$

The frequency f_{DIF} is the frequency that, in the frequency spectrum of the vibrations measured at the sprocket shaft bearing assembly, corresponds to damage to the inner ring IF and which is

$$f_{DIF} = \frac{1}{2}\left(1 + \frac{r_{RF}}{r_{CF}}\right)f_{RE}m_F \,. \tag{7.30}$$

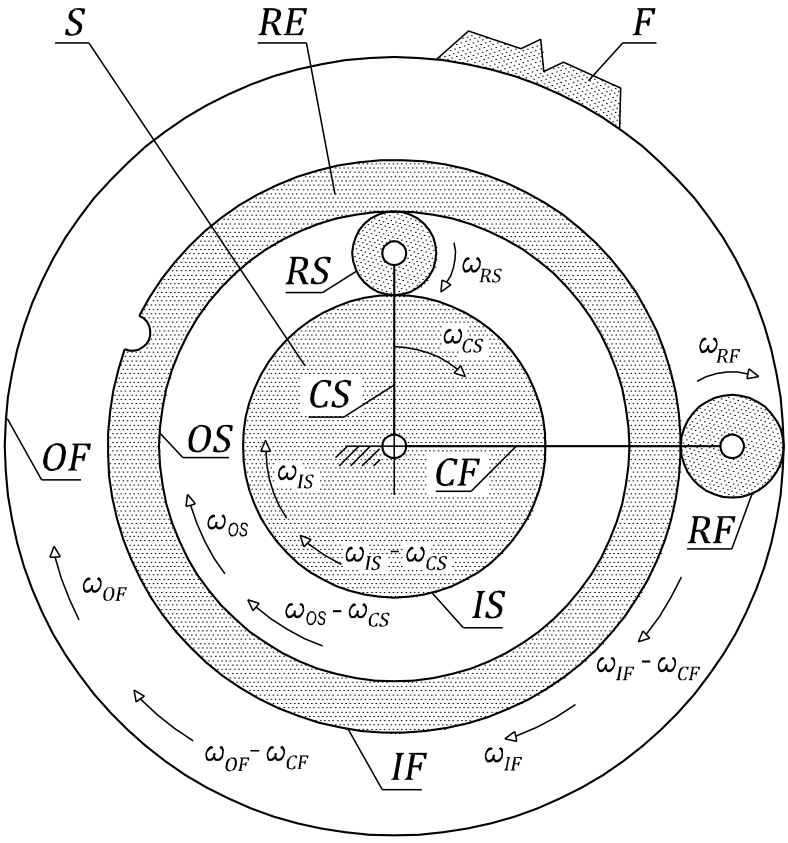

Fig. 7.6 Damage to the frame bearing's inner ring

7.1.5 Damage to the frame bearing's rolling element

Damage to the frame bearing's rolling RF (*Fig. 7.7*) exhibits a relative angular velocity ω_{DRF}, which determines the frequency of the damage, whereby

$$\omega_{DRF} = 2\omega_{RF} \,. \tag{7.31}$$

By inserting (7.16) and further (6.12) and (6.13), we see that

$$\omega_{DRF} = -2\frac{r_{OF}}{r_{IF}+r_{OF}}\frac{r_{IF}}{r_{RF}}\omega_{RE} = -\frac{r_{CF}}{r_{RF}}\left(1-\frac{r_{RF}^2}{r_{RF}^2}\right)\omega_{RE} \,. \tag{7.32}$$

The frequency f_{DRF} is the frequency that, in the frequency spectrum of the vibrations measured at the sprocket shaft bearing assembly, corresponds to damage to the rolling element RF and which is

$$f_{DRF} = \frac{r_{CF}}{r_{RF}}\left(1-\frac{r_{RF}^2}{r_{RF}^2}\right) f_{RE} \,. \tag{7.33}$$

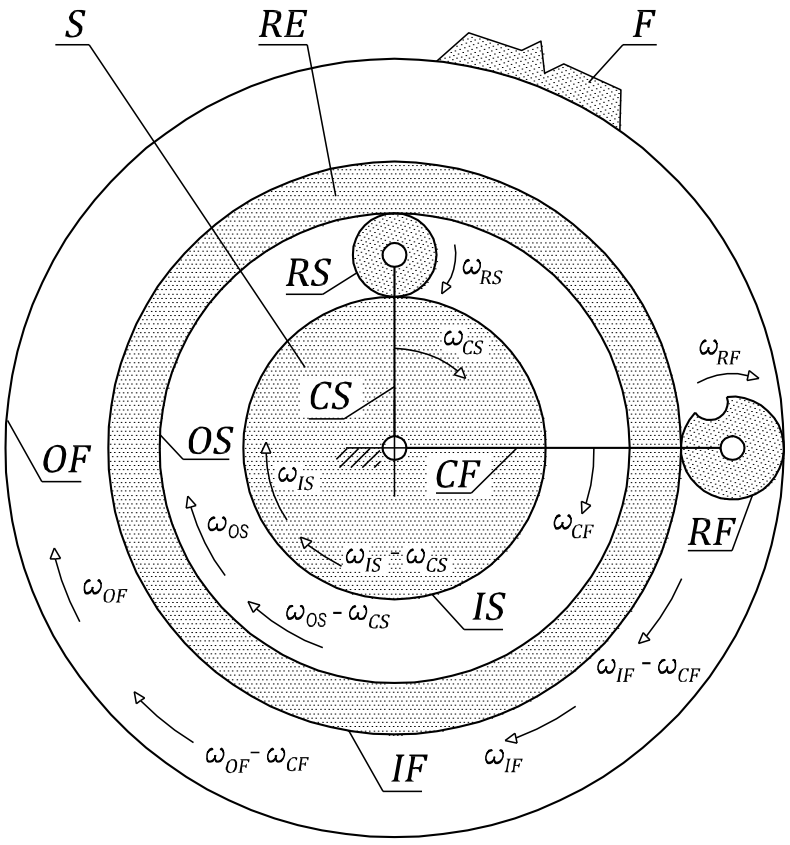

Fig. 7.7 Damage to the frame bearing's rolling element

7.1.6 Damage to the frame bearing's outer ring

Damage to the frame bearing's outer ring OF (*Fig. 7.8*) exhibits a relative angular velocity ω_{DOF}, which determines the frequency of the damage, whereby

$$\omega_{DOF} = (\omega_{CF} - \omega_{OF})m_F = \omega_{CF}m_F \,. \tag{7.34}$$

By inserting (7.17) and further (6.12) and (6.13), we can see that

$$\omega_{DOF} = \frac{r_{IF}}{r_{IF} + r_{OF}}\omega_{RE}m_F \tag{7.35}$$

The frequency f_{DOF} is the frequency that, in the frequency spectrum of the vibrations measured at the sprocket shaft bearing assembly, corresponds to damage to the outer ring OF and which is

$$f_{DOF} = \frac{1}{2}\left(1 - \frac{r_{RF}}{r_{CF}}\right) f_{RE}m_F. \tag{7.36}$$

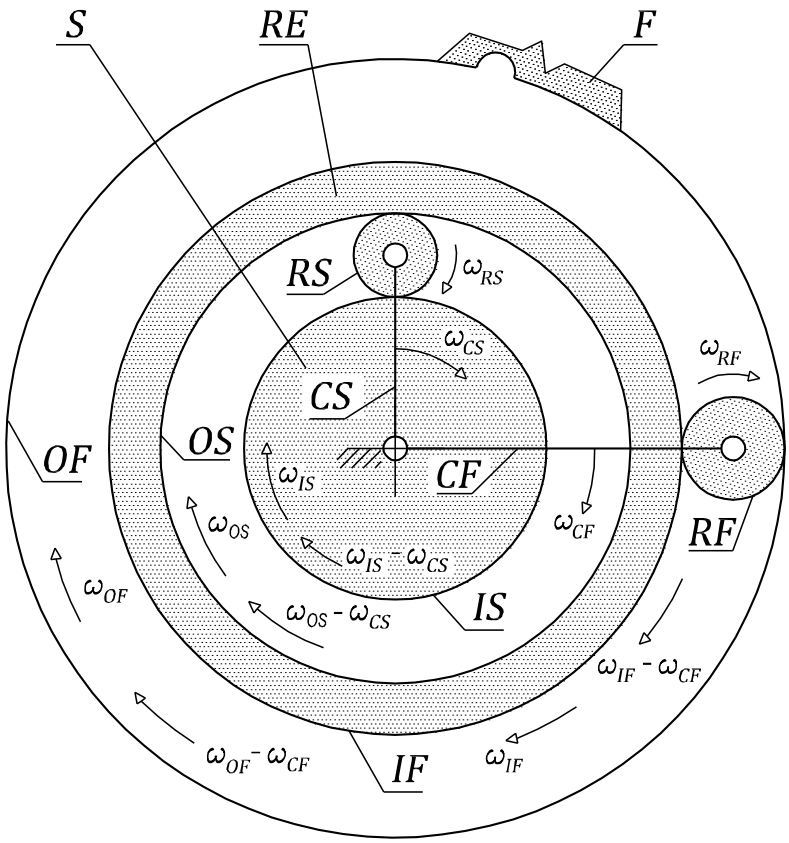

Fig. 7.8 Damage to the frame bearing's outer ring

7.2 Running diagnostics based on identifying increased rolling resistance

The principle behind the device that detects damage to a bearing or its components by identifying increased rolling resistance is shown in *Fig. 7.9*.

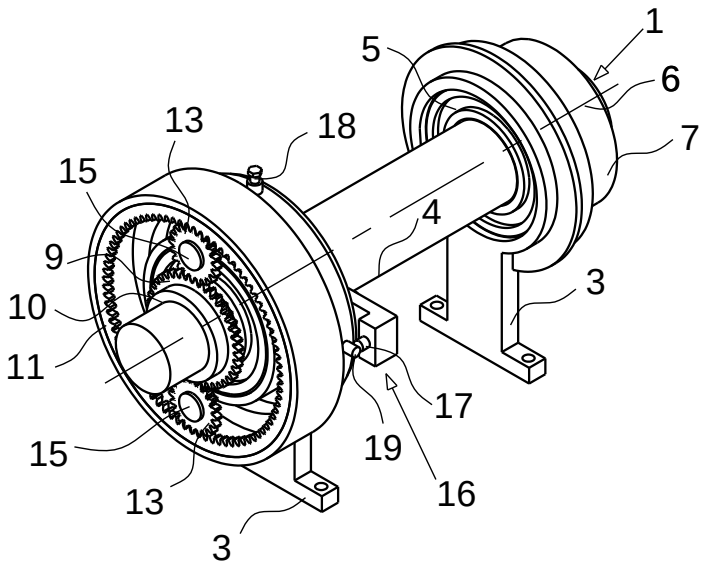

Fig. 7.9 *Principle behind the diagnostic device for low-speed ball and roller bearings based on identifying increased rolling resistance [15]*

With this device, diagnostics are run on the low-speed ball and roller bearings with regards to increased rolling resistance using a planetary gear system. Here, the sun gear 9 is firmly coupled to the shaft 10. The planet gears 13 are connected to the reference element 4 using the pins 15 and rotate in the ring gear 11, which is frictionally engaged with the frame 3.

The planetary gear system ensures the continuous motion of the reference element 4 and thus the consistent rotation of the two pairs of low-speed bearings.

Should rolling resistance increase or the shaft bearings be obstructed, the shaft 10 and reference element 4 will both pivot on the shaft axis at the same speed. The planet gears 13 will then force the ring gear 11 to rotate. As soon as the force of the frictional engagement with frame 3 is exceeded, the ring gear 11 will rotate. This rotational movement triggers the position sensor 16.

The simplified diagram in *Fig. 7.10* shows the frame F, the reference element RE, the frame bearing's shaft S, outer ring OF, inner ring IF, and rolling element RF, as well as the shaft bearing's outer ring OS, inner ring IS and rolling element RS.

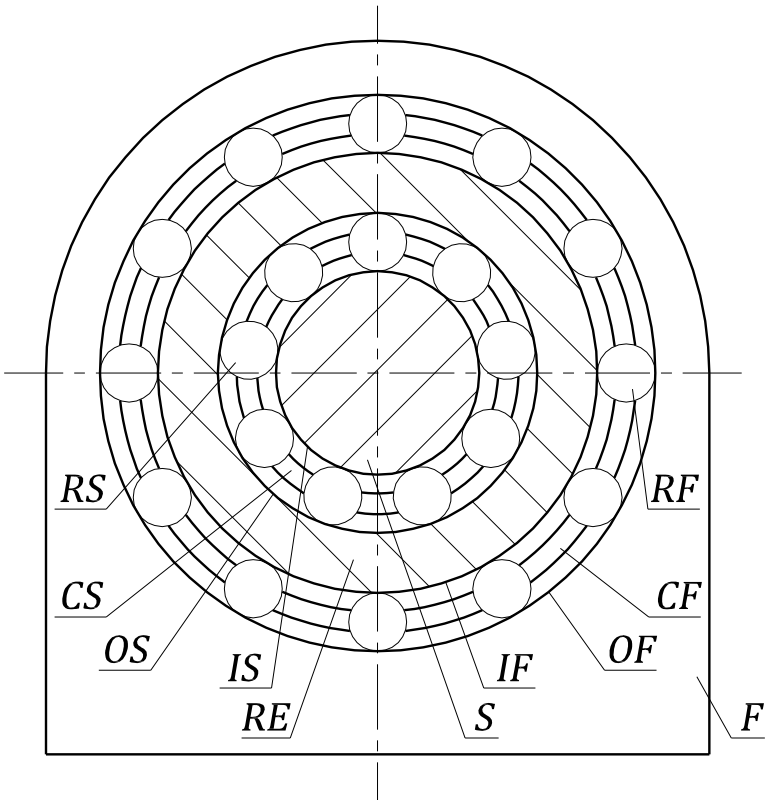

Fig. 7.10 Simplified diagram of the sprocket shaft bearing assembly

It is possible to couple the planetary gear system *Fig. 7.11* to the sprocket shaft bearing assembly shown in *Fig. 7.10*, with the sun gear SG coupled to the shaft S.

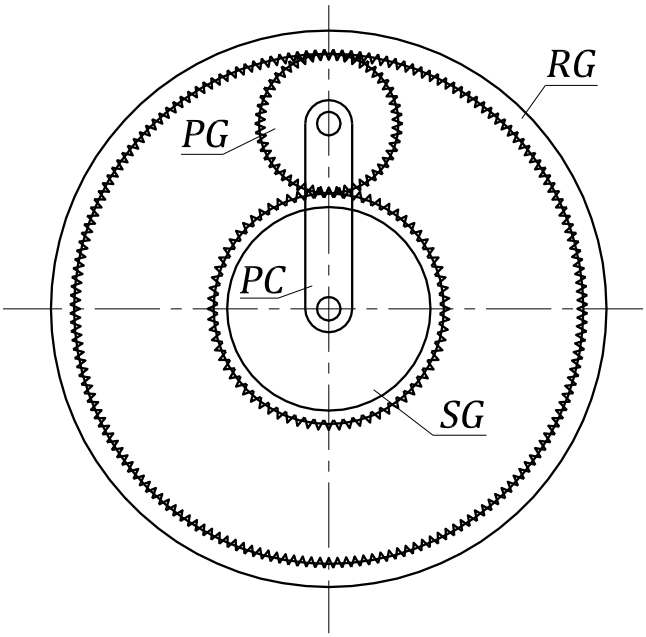

Fig. 7.11 Planetary gear system used for running diagnostics on low-speed ball and roller bearings

The pin in the carrier PC is connected to the reference element RE and the ring gear RG is frictionally engaged with the frame F using friction moment M_{Fr} (*Fig. 7.12*).

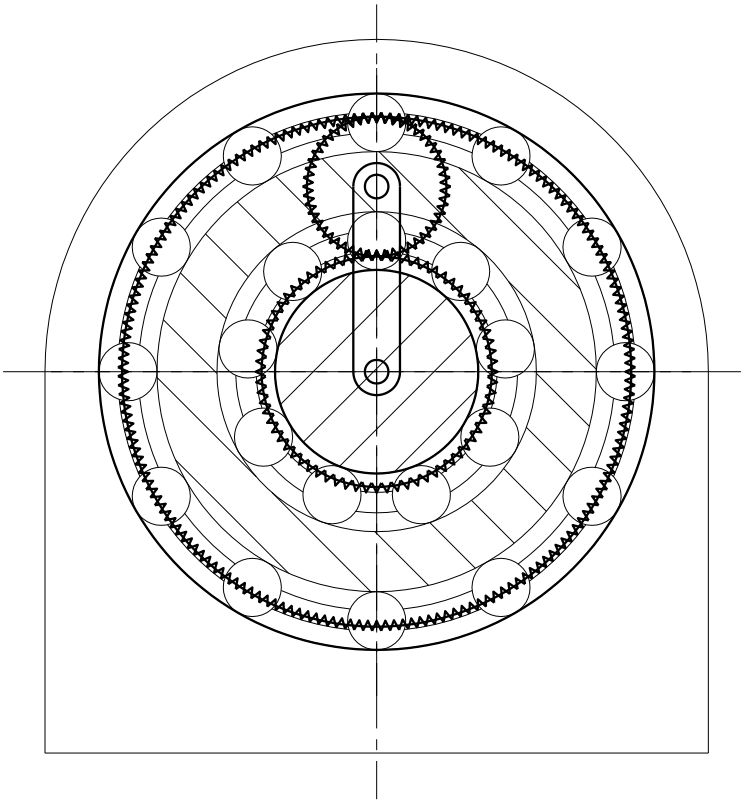

Fig. 7.12 Planetary gear system used for running diagnostics on shaft or frame bearings

Based on the solution relating to force and moment ratios, it is possible to determine the relationship between the friction moment M_{Fr} of the ring gear RG in the frame and the magnitude of the moment due to resistance of the damaged shaft or frame bearing.

7.2.1 Shaft bearing

If the rolling resistance of the shaft bearing increases, the moment M_{SB} from the shaft S acts on the reference element RE as a result of the damaged bearing.

This generates a circumferential force F_{PC} on the pins of the carrier PC, which also acts on the planet gear PG via the carrier PC. Due to the connection with the planet gear PG, this force is transferred to the sun gear SG and the ring gear RG in equal measure. Here, the following applies

$$M_{SB} = F_{PC} r_{PC} = M_{PC} \,. \tag{7.37}$$

If the frictional engagement that is provided by the moment M_{Fr} between the frame F and the ring gear RG should not be exceeded, it must apply that

$$M_{Fr} \geq M_{RG} = F_{PG} r_{RG} \,. \tag{7.38}$$

Furthermore, it applies that

$$M_{PC} = F_{PC} r_{PC} = 2\mathrm{F}_{PG} r_{PC} = F_{PG}(r_{SG} + r_{RG}). \tag{7.39}$$

The following conditions must be fulfilled for normal operation of the sprocket shaft bearing assembly

$$M_{Fr} \geq \frac{M_{PC}}{2r_{PC}} r_{RG} = \frac{M_{SB}}{r_{SG} + r_{RG}} r_{RG}\,, \tag{7.40}$$

meaning that for the shaft bearing's moment due to rolling resistance M_{SB}, the following must apply

$$M_{SB} \leq \frac{r_{SG} + r_{RG}}{r_{RG}} M_{Fr}\,. \tag{7.41}$$

If the set frictional engagement M_{Fr} is exceeded and the conditions (7.40) and (7.41) no longer apply, the ring gear RG will rotate in the direction of the force F_{PG}, i.e. in the direction the shaft S is rotating. In this instance, the carrier PC will rotate more quickly and the planet gear PG will rotate more slowly.

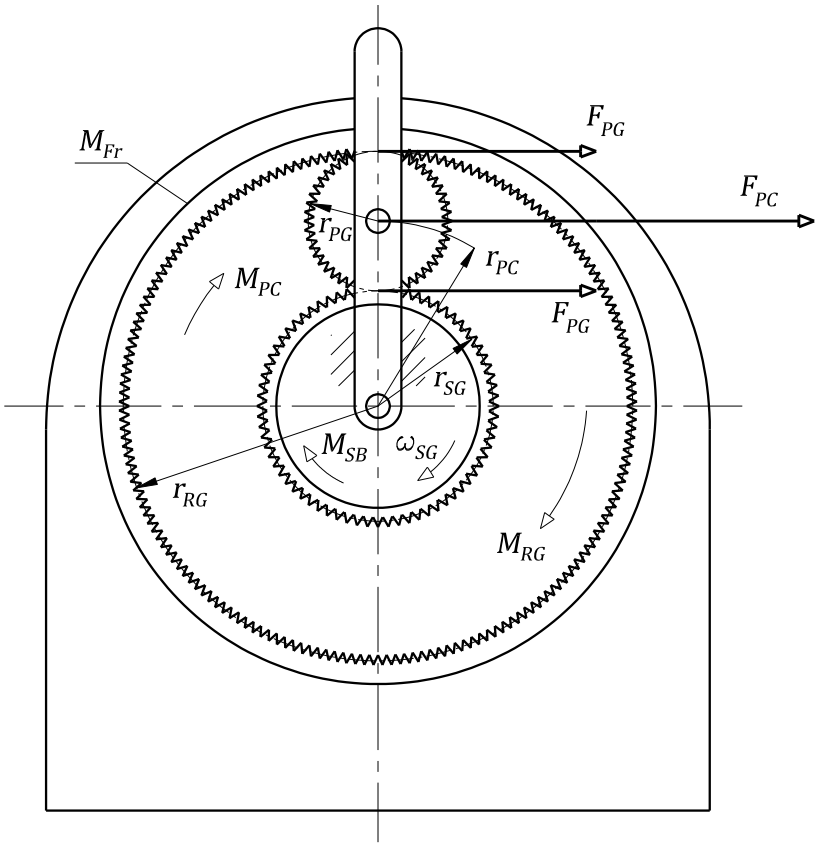

Fig. 7.13 Forces present in the event of damage to shaft bearing

7.2.2 Frame bearing

If the rolling resistance of the frame bearing increases, the moment M_{FB} from the frame F acts on the reference element RE. This generates a circumferential force F_{PC} on the pins of the carrier PC, which also acts on the planet gear PG via the carrier PC. Due to the connection with the planet gear PG, this force F_{PC} is transferred to the sun gear SG and the ring gear RG in equal measure. The force F_{PG}, which due to the current equilibrium of the planet gear PG is equal to the force F_{PG} arising from the connection between the planet gear PG and the sun gear SG, then acts on the ring gear RG via the planet gear PG.

If the frictional engagement that is provided by the moment M_{Fr} between the frame and the ring gear RG should not be exceeded, the following must apply

$$M_{Fr} \geq F_{PG} r_{RG} \, . \tag{7.42}$$

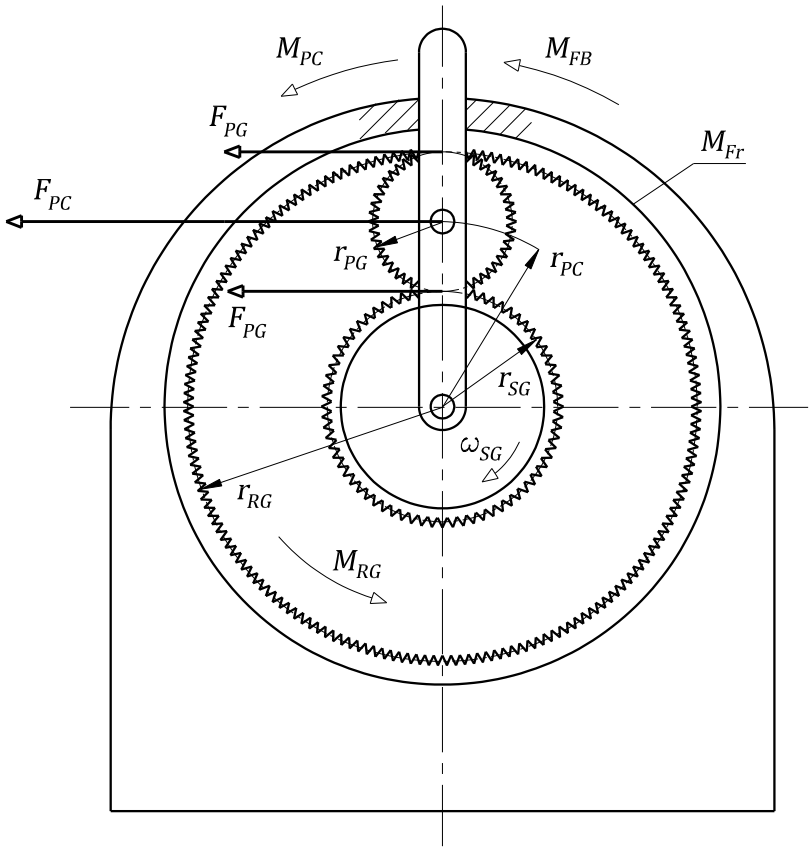

Fig. 7.14 Forces present in the event of damage to the frame bearing

Furthermore, it applies that

$$M_{FB} = F_{PC} r_{PC} = 2\mathrm{F}_{PG} r_{PC} \,. \tag{7.43}$$

For the faultless operation of the sprocket shaft bearing assembly, the following applies

$$M_{Fr} \geq \frac{M_{FB}}{2r_{PC}} r_{RG} = \frac{M_{FB}}{r_{SG} + r_{RG}} r_{RG} \,, \tag{7.44}$$

meaning that for the shaft bearing's moment due to rolling resistance M_{FB}, the following must apply

$$M_{FB} \leq \frac{r_{SG} + r_{RG}}{r_{RG}} M_{Fr} \,. \tag{7.45}$$

If the set frictional engagement M_{Fr} is exceeded and the conditions (7.44) and (7.45) no longer apply, the ring gear RG will rotate in the direction of the force F_{PG}. In this instance, the carrier PC will rotate more slowly and the planet gear PG will rotate more quickly.

8 Design of the diagnostic device for low-speed bearings

In order to prevent disruptions to production as much as possible, the sprocket shaft bearing assembly must be designed in a way that makes it completely reliable, always available and require minimal maintenance and servicing. The strength of the shafts and other bearing components is tested analytically in line with standard procedure as well as using the finite element method.

8.1 Design of a new sprocket shaft bearing assembly

The design of a new sprocket shaft bearing assembly is based on the principles outlined in the patent described in [14] and is also based on the documentation available for the current design of the sprocket shaft bearing assembly.

This technical documentation and the relevant stress analyses show that the current sprocket shaft bearing assembly is significantly overdesigned. The components have been designed to work under maximum load, i.e. when a malfunction occurs.

The shaft has been designed so that it has a safety factor of 2.6. The load rating of the bearings has been calculated with a relatively high degree of contamination and 96% reliability for the required bearing life.

Based on the operating load and other operating conditions, the shaft diameter can be optimised in the design. The load rating of the bearings can be calculated with the bearing life reliability at 90%. The higher value of the nominal bearing life with a reliability of 96% is compensated by detecting bearing damage early on using the proposed design of a diagnostic device for low-speed bearings.

Mounting the sprocket shaft in two bearings located within the so-called reference element is one design solution (*Fig. 8.1*) as per the patent described in [14]. The sprocket shaft is then mounted in the frame using two further bearings. The reference element has a degree of rotational freedom and, by measuring the moment of resistance during its rotation, it is possible to reliably diagnose the degree of damage to one of the bearings.

Another factor in the design of a new sprocket shaft bearing assembly is the ability to quickly and easily replace a damaged bearing if required.

The fundamental design of the sprocket shaft bearing assembly solves this problem by using a shaft coupling that enables the section of the shaft connected to the sprocket to be reliably connected and disconnected. This two-part sprocket shaft design ensures that parts are only replaced on site at the production line and that the assembly can be repaired in the maintenance workshop. This considerably shortens the time that the conveyor is out of use during repair. This solution reduces the time it takes to install the bearings after they have been replaced because the bearing housings are already pre-

installed on the removable section of the assembly. This design also makes the alignment of the bearings more accurate.

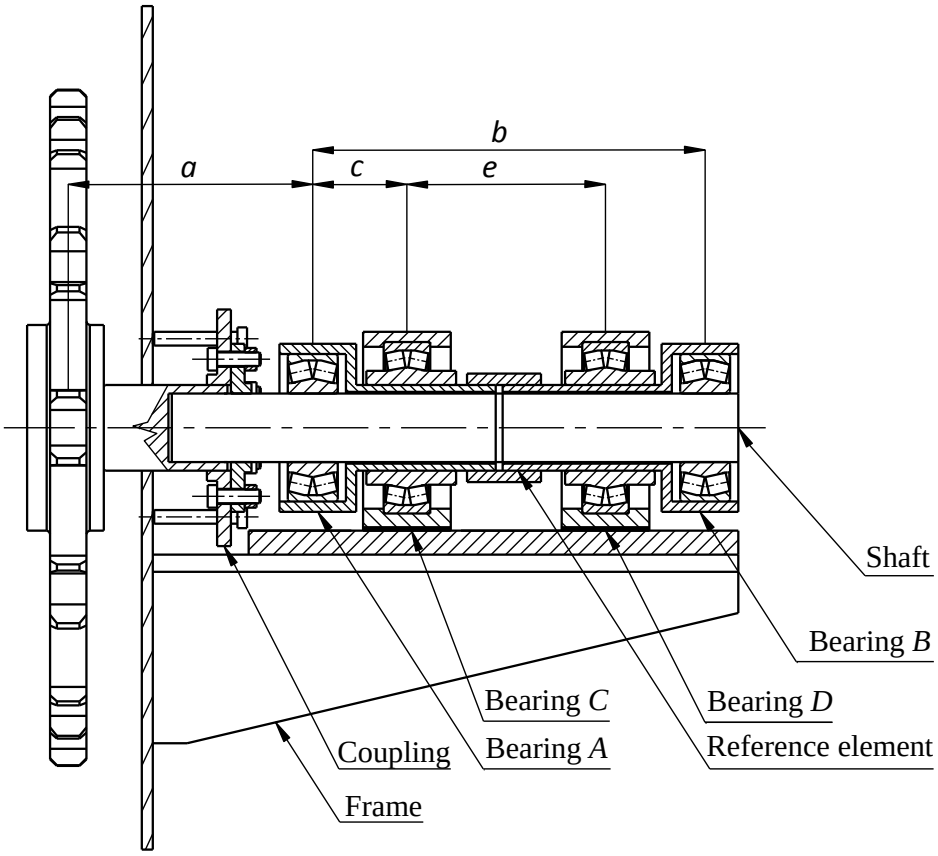

Fig. 8.1 Sprocket shaft bearing assembly

Fig. 8.1 shows the sprocket shaft bearing assembly. Bearings A and B connect the shaft and the reference element, which in this case is divided. Bearings C and D fix the reference element to the baseplate of the installation frame. Bearings C and D are always located between bearings A and B in each of the proposed solutions outlined below. The bearing distance e has been taken from the design currently in use due to the geometry in the pretreatment line. The outer diameter of the reference element in bearings C and D is equal to the shaft diameter from the current solution.

Three key design variants were derived from this design principle. In all three variants, the reference element is always a single piece, which is seen as advantageous in terms of production and strength.

8.2 Stress analyses for a new assembly

The stress analyses for the new design of the sprocket shaft bearing assembly are the same for all of the key design variants outlined below, thereby enabling the strength and load rating to be quantified. The required components that need to be calculated are the shaft, reference element and bearings. The strengths for the shaft and reference element were first determined by carrying out a stress analysis and then also by using FEM analysis. For the bearings, the dynamic load rating was calculated and then the type of bearing was chosen.

8.2.1 The shaft's load, stress and safety factor

The load ratios in the sprocket shaft are similar to those displayed in *Fig. 5.11*, thus making it possible to use the algorithms in (5.26) to (5.33) for calculating the bending stress. The force F_{B2}, which produces the forces R_{A2} and R_{B2} in the shaft bearings, is assumed. These forces R_{A2} and R_{B2} consequently put a load on the reference element.

The stress analysis for the shaft, in the proposed design of the assembly, is performed using the load caused by the force F_{B2}, which was ascertained at maximum torque of the drive unit under normal operating conditions.

The force F_{B2} causes a bending stress σ_{B2A} and a shearing stress in the critical cross section at position A. Both stresses alternate dynamically and symmetrically. In terms of strength, the bending stress σ_{B2A} has much greater significance than the shearing stress, which plays somewhat less of a role.

The safety factor for this case is

$$s_{B2A} = \frac{\sigma_{BA}^{*}}{\sigma_{B2A}}, \tag{8.1}$$

whereby σ_{BA}^{*} is the fatigue strength in bending and σ_{B2A} is the amplitude of the bending stress in the critical cross section at position A.

Furthermore, it is useful to determine the safety factor s_{B3A} for the shaft in the event of a malfunction. In this situation, the load only occurs for a short time and can therefore be considered static.

The safety factor for this case is

$$s_{B3A} = \frac{\sigma_{By}}{\sigma_{B3A}}, \tag{8.2}$$

whereby σ_{By} is the yield strength in bending and σ_{B3A} is the static bending stress in the critical cross section at position A.

8.2.2 The reference element's load, stress and safety factor

The load on the reference element caused by the forces R_{A2} and R_{B2} is shown in *Fig. 8.2*.

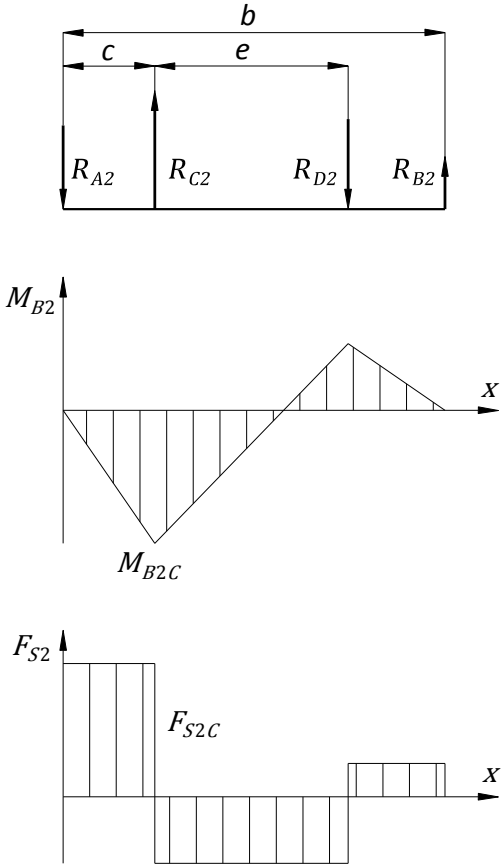

Fig. 8.2 Load on the reference element

Equilibrium equations for the reference element are

$$-R_{A2} + R_{C2} - R_{D2} + R_{B2} = 0\,, \tag{8.3}$$

and

$$R_{C2}c - R_{D2}(c + e) + R_{B2}b = 0\,, \tag{8.4}$$

whereby the forces R_{C2} and R_{D2} occur in the frame bearings.

The maximum bending moment M_{B2C} at position C on the reference element is as follows

$$M_{B2C} = |-R_{A2}c|\,. \tag{8.5}$$

The maximum bending stress is calculated analytically according to the following formula

$$\sigma_{B2C} = \frac{M_{B2C}}{W_{BC}}, \tag{8.6}$$

whereby W_{BC} is the section modulus at position C

$$W_{BC} = \frac{\pi(D_C^4 - d_C^4)}{32D_C}, \tag{8.7}$$

and D_C is the outer diameter and d_C the inner diameter of the reference element at position C.

The shear force at position C is referred to as F_{S2C} and the corresponding shearing stress τ_{S2C} is as follows

$$\tau_{S2C} = \frac{F_{S2C}}{S_C}, \tag{8.8}$$

whereby S_C is the critical cross-sectional area at position C

$$S_C = \frac{\pi(D_C^2 - d_C^2)}{4}. \tag{8.9}$$

In principle, the stress analysis for the reference element is the same as the stress analysis for the sprocket shaft. In this case, the critical cross section is at position C. Here, the critical stress is also the bending stress σ_{B2C} or σ_{B3C}. However, the shearing stress τ_{S2C} or τ_{S3C} cannot be neglected here as the distance c is relatively small.

For the safety factor relating to shearing stress τ_{S2C}, the following applies

$$s_{S2C} = \frac{\tau_{SC}^*}{\tau_{S2C}}, \tag{8.10}$$

whereby τ_{SC}^* is the fatigue strength in shear and τ_{B2A} is the amplitude of the shearing stress in the critical cross section at position C.

It is also useful to determine the safety factor s_{S3C} for the reference element in the event of a malfunction. As the load only occurs for a short time in this situation, it can be considered static.

The safety factor for this case is

$$s_{S3C} = \frac{\tau_{Sy}}{\tau_{S3C}}, \tag{8.11}$$

whereby τ_{Sy} is the yield strength in shear and τ_{B3C} is the static shearing stress in the critical cross section at position C.

If the shearing stress in the critical cross section at position C is not to be neglected, the safety factor for the reference element is calculated using the following formula

$$s_{2C} = \frac{s_{B2C} s_{S2C}}{\sqrt{s_{B2C}^2 + s_{S2C}^2}}, \tag{8.12}$$

or

$$s_{3C} = \frac{s_{B3C} s_{S3C}}{\sqrt{s_{B3C}^2 + s_{S3C}^2}}. \tag{8.13}$$

8.2.3 Stress analysis using FEM

The force F_{B3} and the maximum torque of the drive unit can be input into simplified 3D models of the three key design variants as per the patent described in [14]. The FEM analysis results can then be interpreted as meaning that this force does not occur during normal operation.

The FEM analyses for each of the three design variants are based on a simplified 3D model that has had loads and boundary values introduced. The deflections and equivalent stresses for the entire sprocket shaft bearing assembly and the normal stresses on the shaft and the reference element are then shown.

8.2.4 Load rating of the bearings

The load rating of the spherical roller bearings in the assembly at all positions A, B, C and D is calculated according to the methods in (5.40) to (5.44).

8.3 Design variants

Three different design variants for the sprocket shaft bearing assembly, based on the patent described in [14], are introduced below. In terms of ease of maintenance during disassembly, all three variants use a two-piece shaft design, i.e. a shaft that is joined to a coupling.

The stress analysis results for the individual design variants as well as the FEM analysis results were compiled in a table.

For each of the three design variants, the safety factors were analytically calculated and the optimal solution chosen as the basis for one design variant to be further optimised.

8.3.1 Design variant I

The first design variant uses a reference element in the form of a tube, which all bearings are mounted on. Two types of bearing pairs are used in this variant. Two identical outer roller bearings connect the shaft to the reference element and the inner pair of roller bearings mounts the reference element to the frame of the assembly.

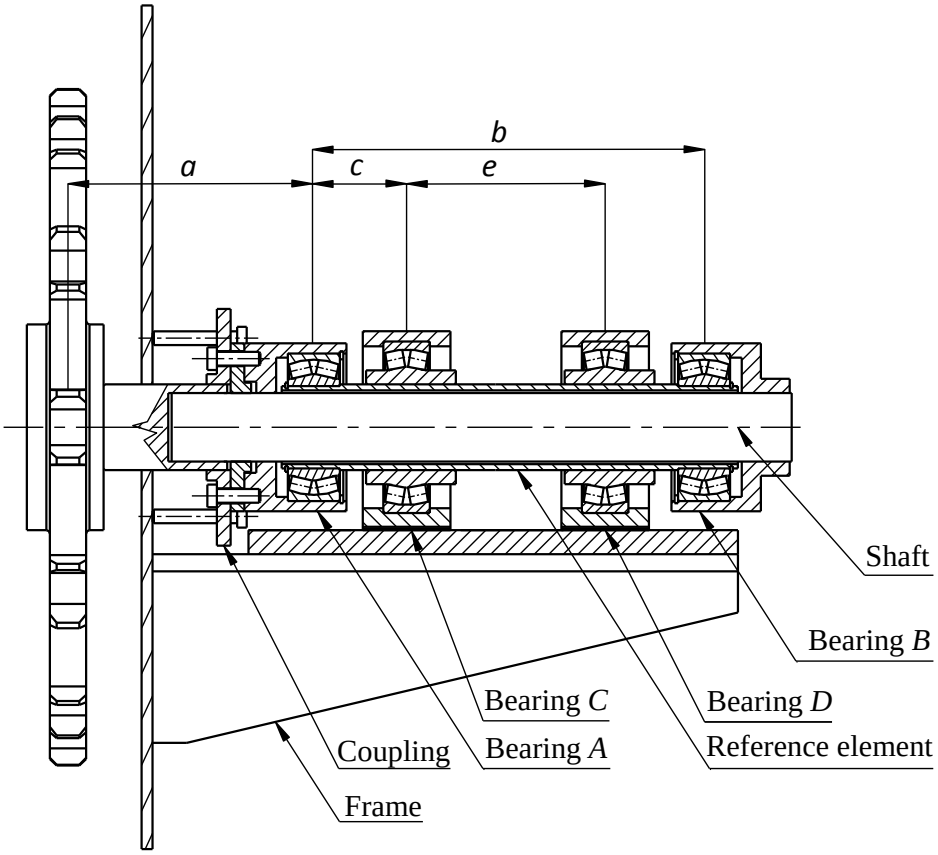

Fig. 8.3 Design variant I

The stress analysis results are summarised in *Table 8.1*.

Table 8.1 Design variant I – stress analysis results

Shaft		**Reference element**			
σ_{B2A} [MPa]	101	σ_{B2C} [MPa]	58	τ_{S2C} [MPa]	11.6
σ_{B3A} [MPa]	253	σ_{B3C} [MPa]	145	τ_{S3C} [MPa]	29
s_{B2A}	1.76	s_{B2C}	2.9	s_{S2C}	8.2
s_{B3A}	1.36	s_{B3C}	2.4	s_{S3C}	12.1

Roller bearings chosen based on calculations (5.40) to (5.44) from *TIMKEN*'s catalogue are recorded in *Table 8.2*.

Table 8.2 Design variant I – types of bearing

Bearing *A*	**Bearing *B***	**Bearing *C***	**Bearing *D***
23224 spherical roller bearing	23224 spherical roller bearing	22228 spherical roller bearing	22228 spherical roller bearing

FEM analysis

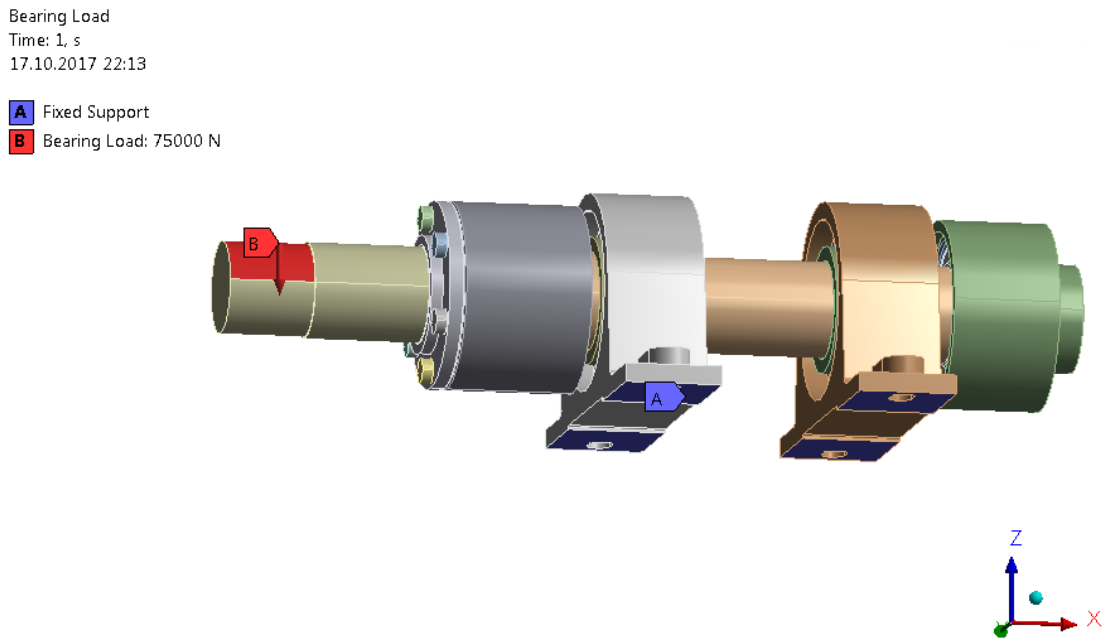

Fig. 8.4 Design variant I – load and boundary values

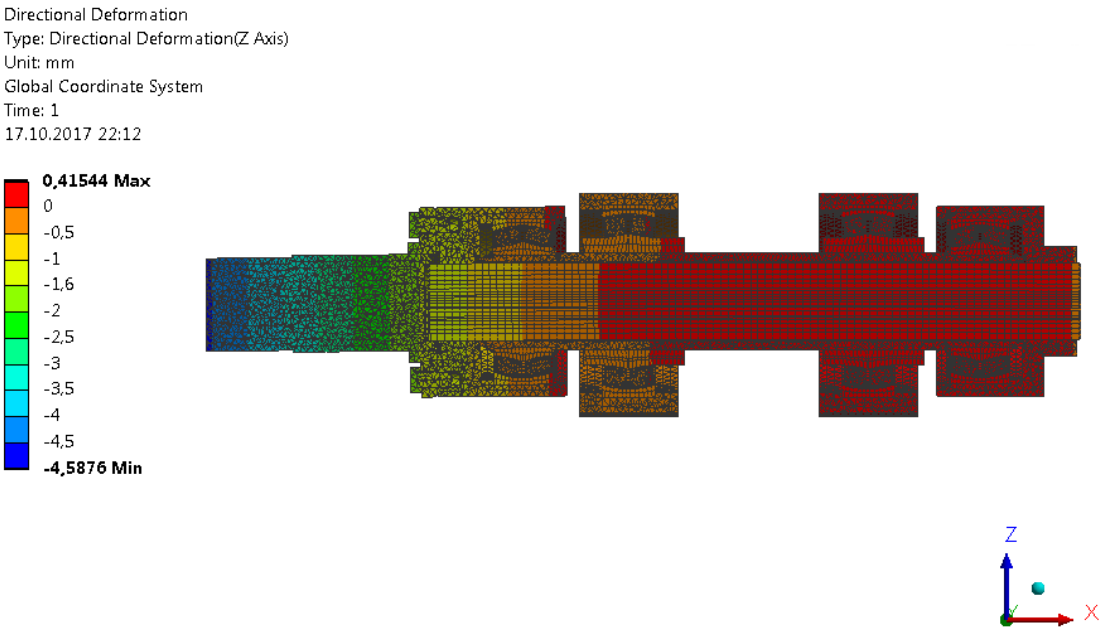

Fig. 8.5 Design variant I – deflection

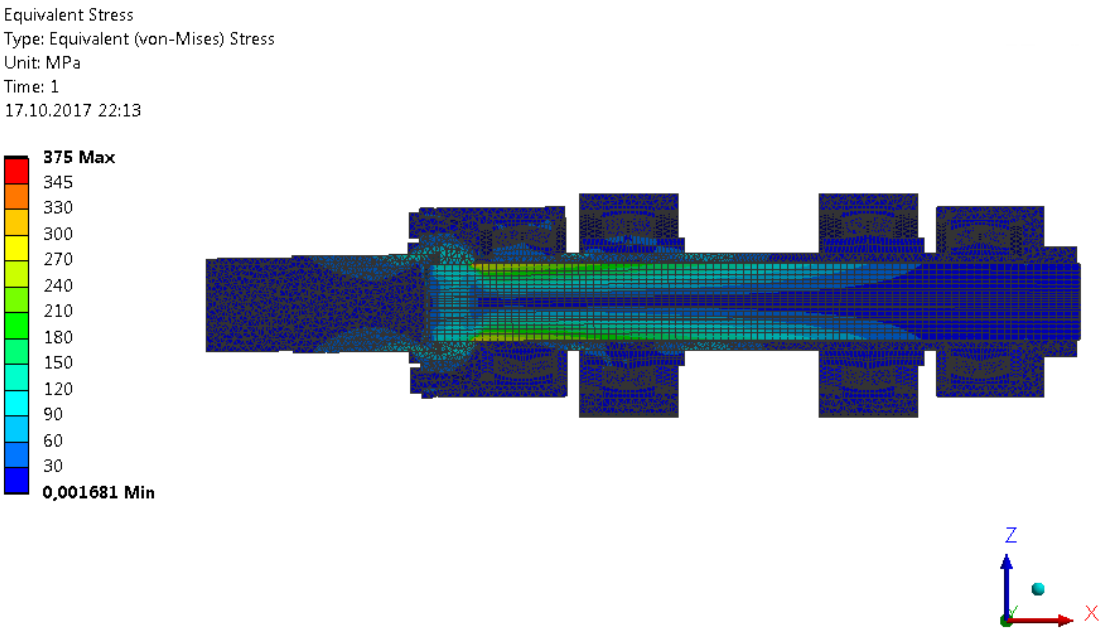

Fig. 8.6 Design variant I – equivalent stress (according to von Mises)

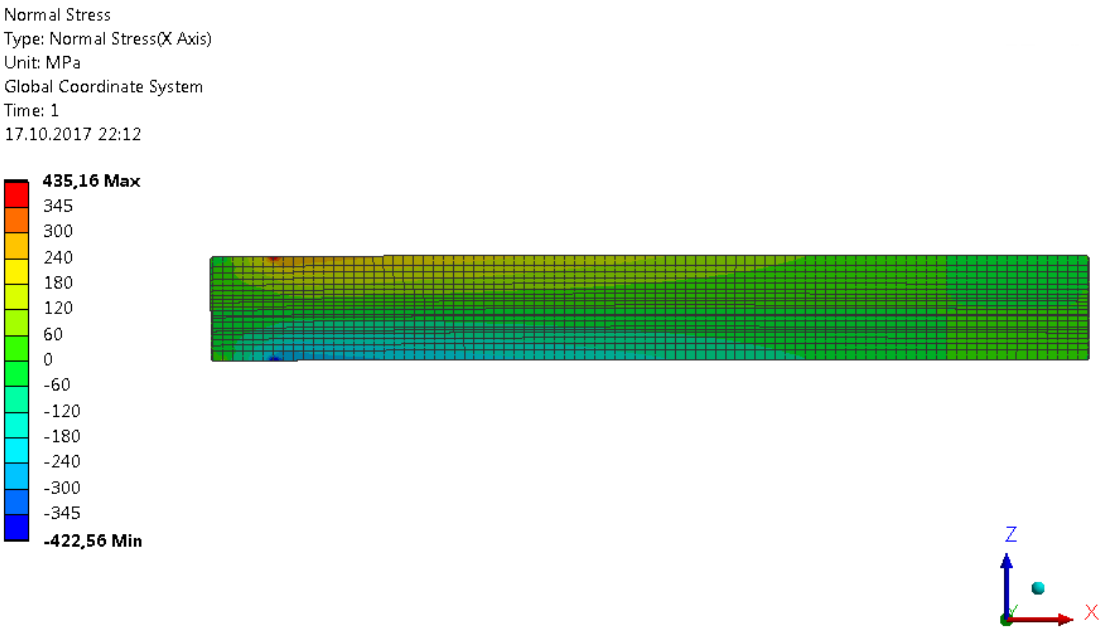

Fig. 8.7 Design variant I – normal stress along x axis – shaft

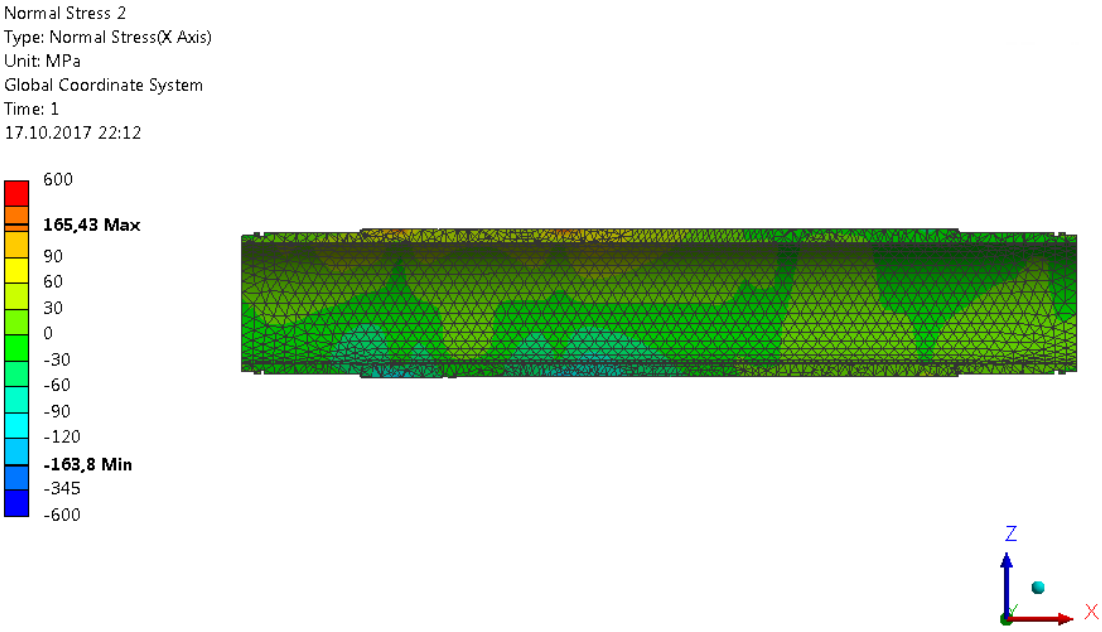

Fig. 8.8 Design variant I – normal stress along x axis – reference element

8.3.2 Design variant II

The second design variant has a one-piece reference element. The roller bearing at position *A* is mounted directly onto the sprocket shaft. In this case, the shaft coupling is designed as a separate unit. Three different types of bearing are used in this design variant. In this case, bearings *A* and *B* are not of the same type due to their different inner diameters.

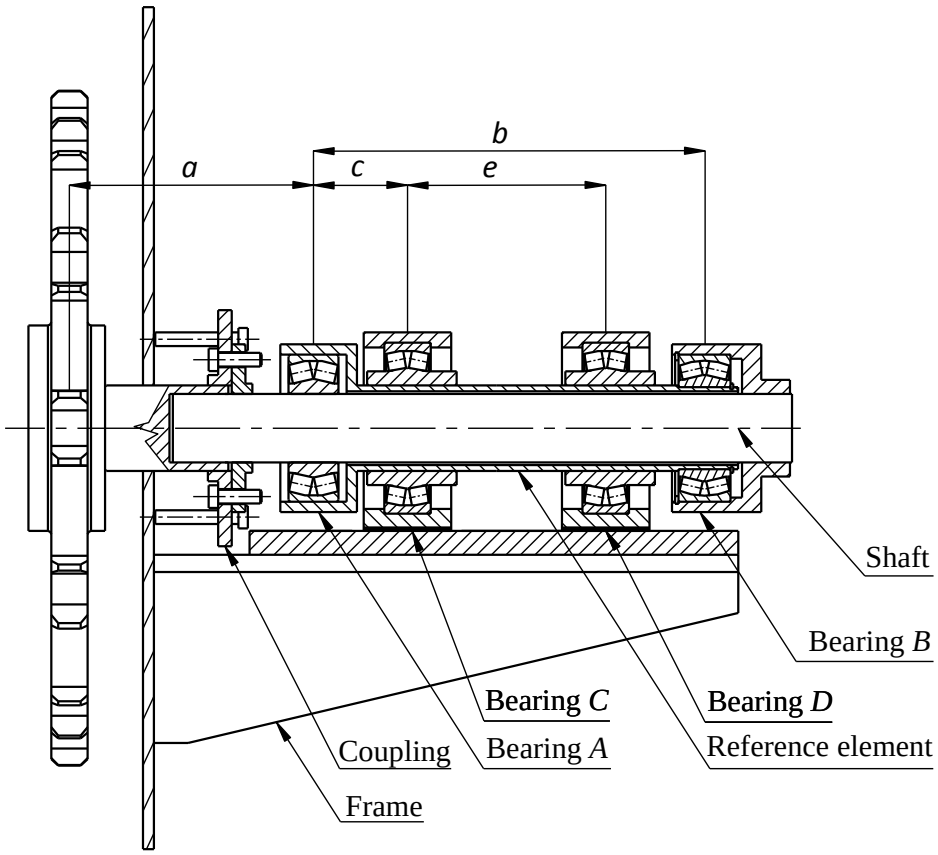

Fig. 8.9 Design variant II

The stress analysis results are summarised in *Table 8.3*. The roller bearings are then stated and the FEM analysis results follow.

Table 8.3 Design variant II – stress analysis results

Shaft		**Reference element**			
σ_{B2A} [MPa]	109	σ_{B2C} [MPa]	60	τ_{S2C} [MPa]	11.6
σ_{B3A} [MPa]	271	σ_{B3C} [MPa]	151	τ_{S3C} [MPa]	29
s_{B2A}	1.6	s_{B2C}	2.77	s_{S2C}	8.2
s_{B3A}	1.27	s_{B3C}	2.28	s_{S3C}	12.1

Roller bearings chosen based on calculations (5.40) to (5.44) from *TIMKEN*'s catalogue are recorded in *Table 8.2*.

Table 8.4 Design variant II – types of bearing

Bearing *A*	**Bearing *B***	**Bearing *C***	**Bearing *D***
22320 spherical roller bearing	23224 spherical roller bearing	22228 spherical roller bearing	22228 spherical roller bearing

FEM analysis

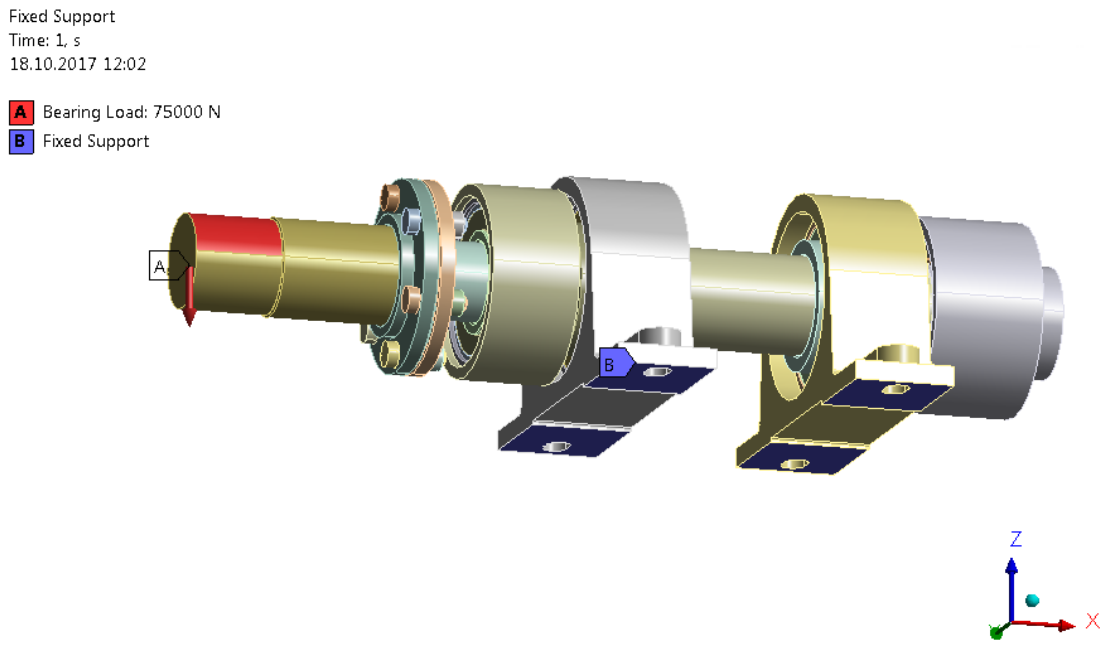

Fig. 8.10 Design variant II – load and boundary values

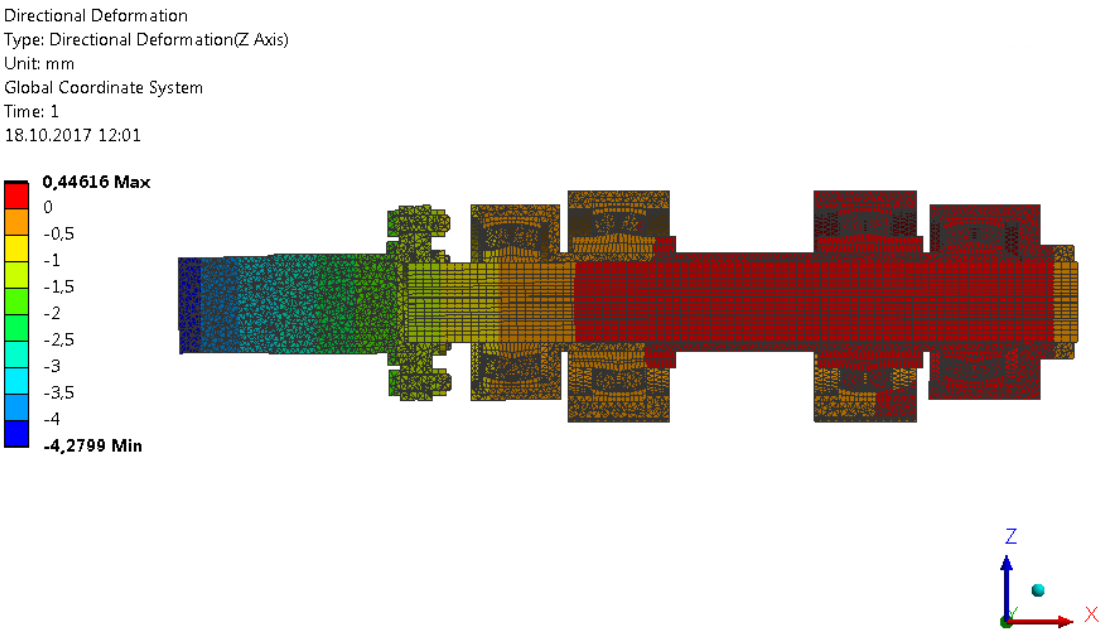

Fig. 8.11 Design variant II – deflection

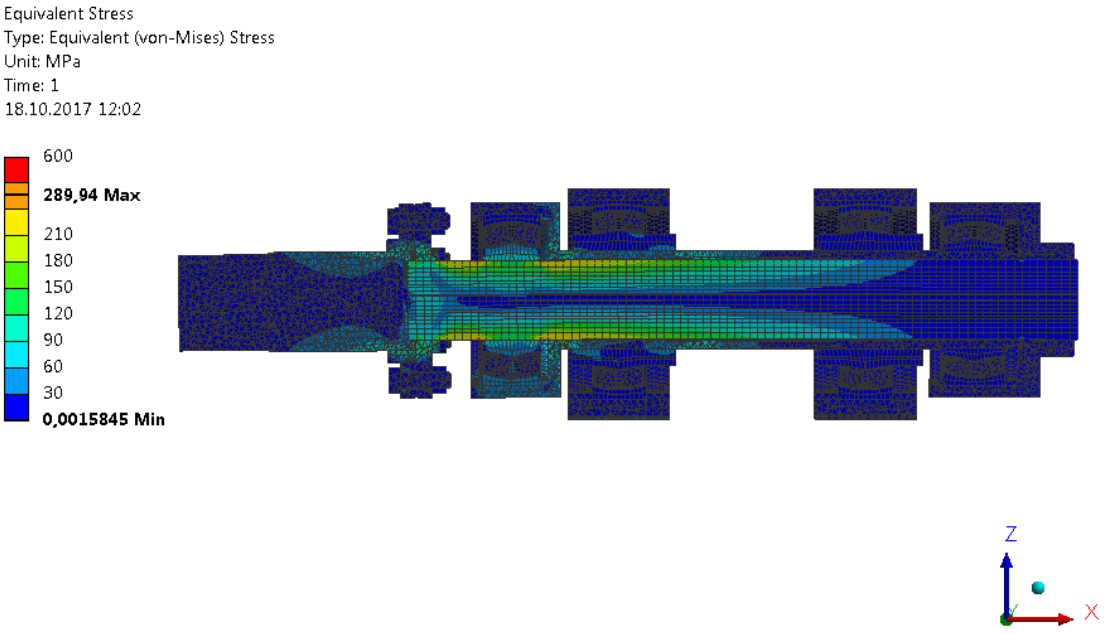

Fig. 8.12 Design variant II – equivalent stress (according to von Mises)

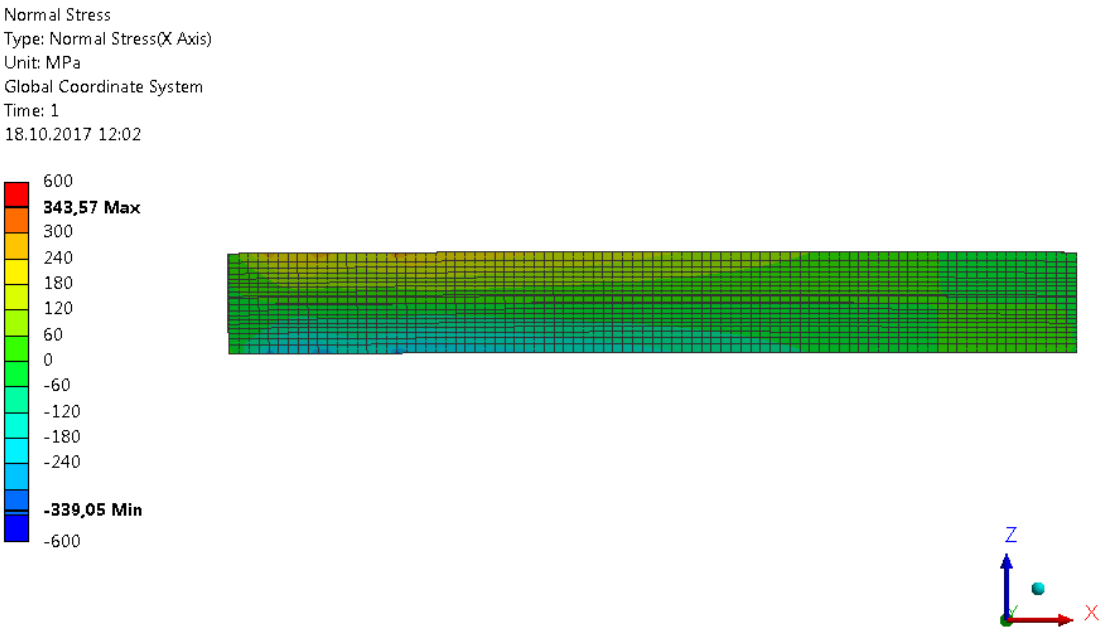

Fig. 8.13 Design variant II – normal stress along x axis – shaft

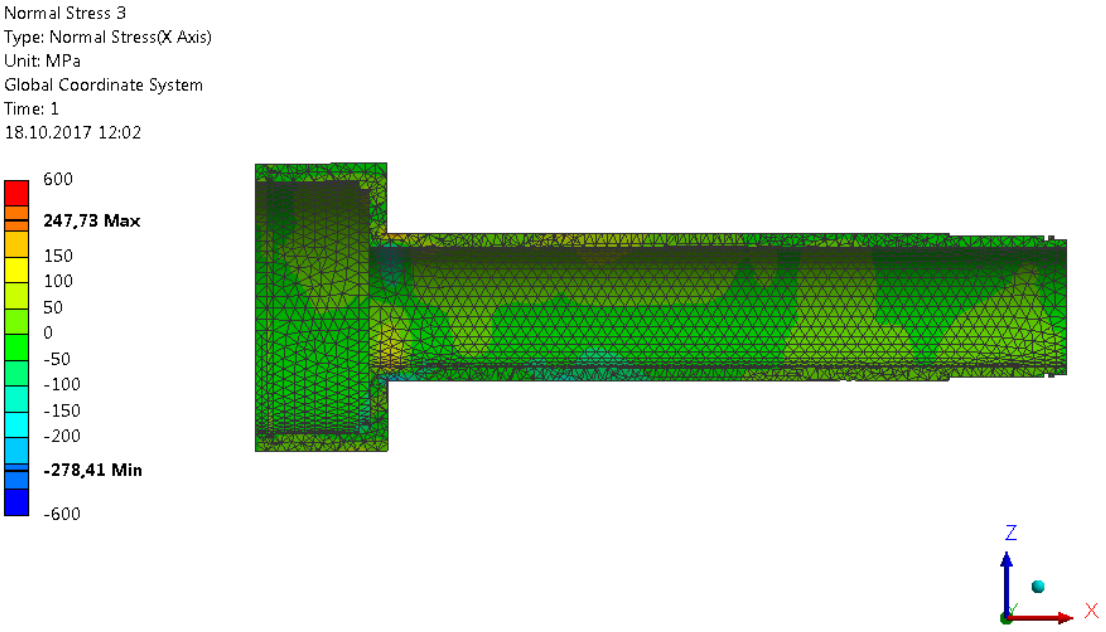

Fig. 8.14 Design variant II – normal stress along x axis – reference element

8.3.3 Design variant III

The third design variant is a compromise between the first and second variants. At the same time, it is the solution where the smallest number of components needs to be produced. The one-piece reference element incorporates roller bearing *B*, and a part of the coupling is integrated into the housing of bearing *A*. Three different types of bearing are used in this design of the sprocket shaft bearing assembly. As in the second design variant, bearings *A* and *B* are not the same due to their different inner diameters.

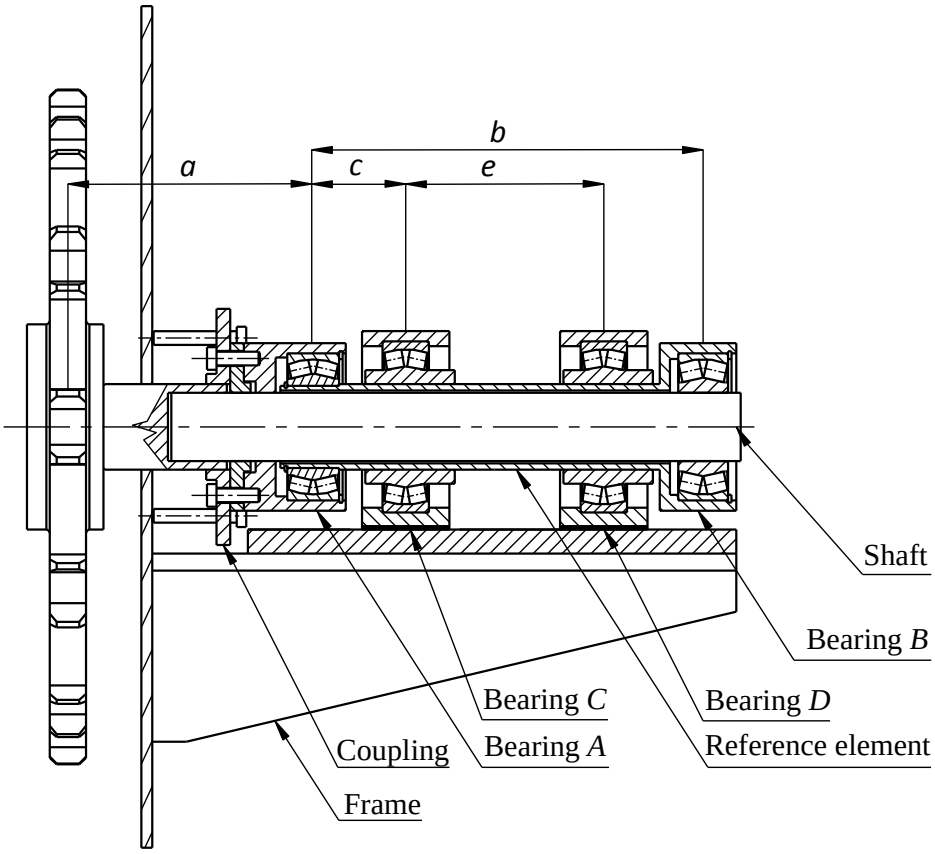

Fig. 8.15 Design variant III

The stress analysis results are summarised in *Table 8.3*. The roller bearings are then stated and the FEM analysis results follow.

Table 8.5 Design variant III – stress analysis results

Shaft		**Reference element**			
σ_{B2A} [MPa]	106	σ_{B2C} [MPa]	58	τ_{S2C} [MPa]	11.6
σ_{B3A} [MPa]	265	σ_{B3C} [MPa]	151	τ_{S3C} [MPa]	29
s_{B2A}	1.6	s_{B2C}	3	s_{S2C}	8.1
s_{B3A}	1.3	s_{B3C}	2.28	s_{S3C}	12.1

Roller bearings chosen based on calculations (5.40) to (5.44) from *TIMKEN*'s catalogue are recorded in *Table 8.6*.

Table 8.6 Design variant III – types of bearing

Bearing *A*	**Bearing *B***	**Bearing *C***	**Bearing *D***
23224 spherical roller bearing	22320 spherical roller bearing	22228 spherical roller bearing	22228 spherical roller bearing

FEM analysis

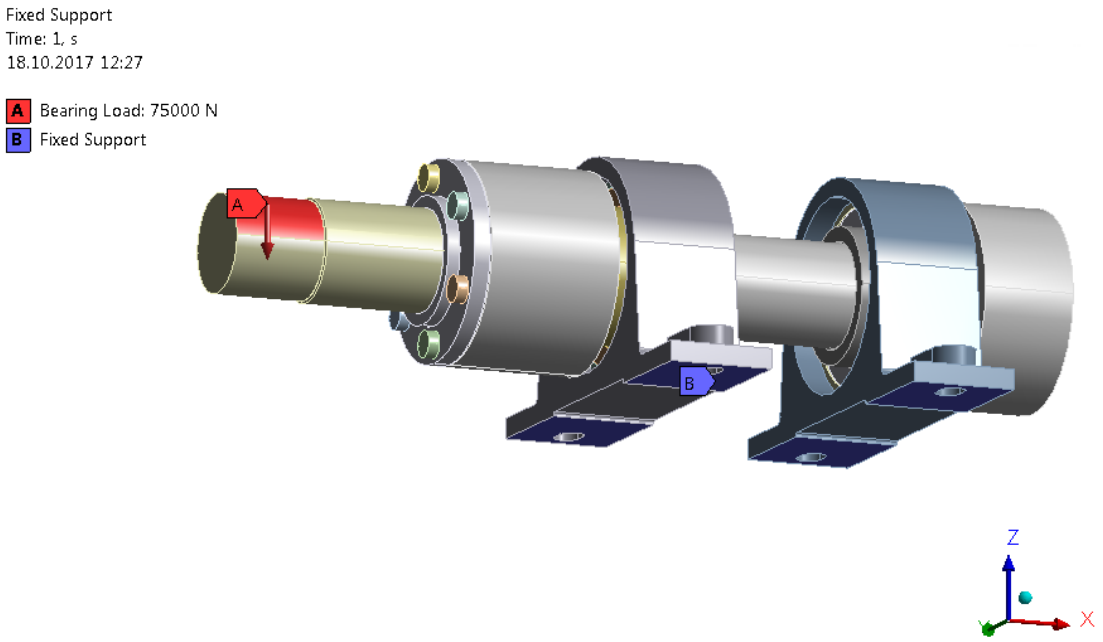

Fig. 8.16 Design variant III – load and boundary values

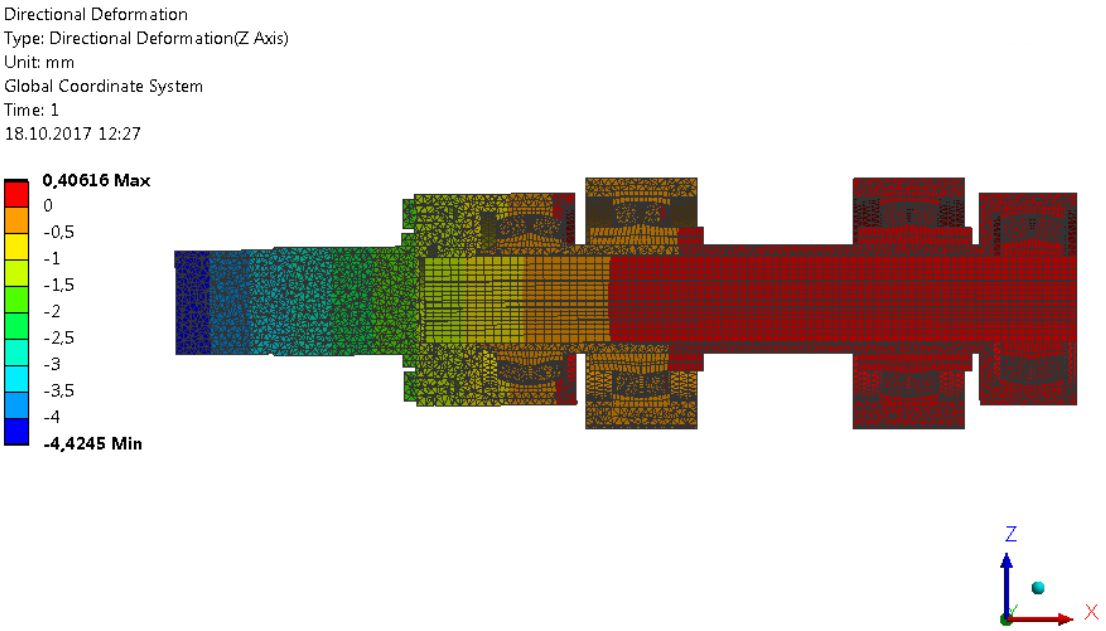

Fig. 8.17 Design variant III – deflection

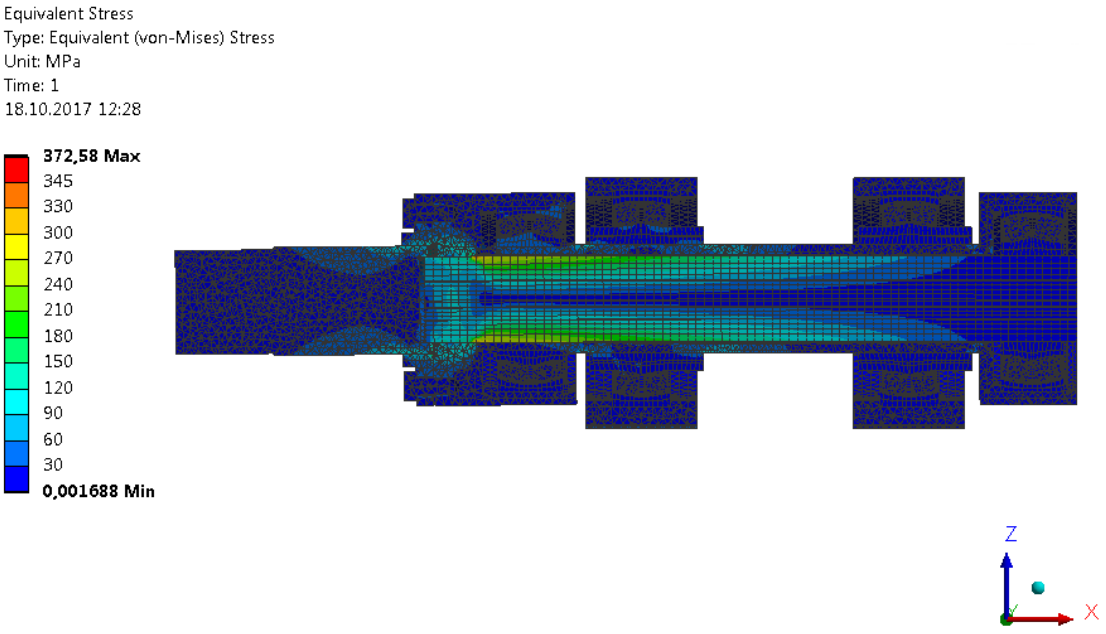

Fig. 8.18 Design variant III – equivalent stress (according to von Mises)

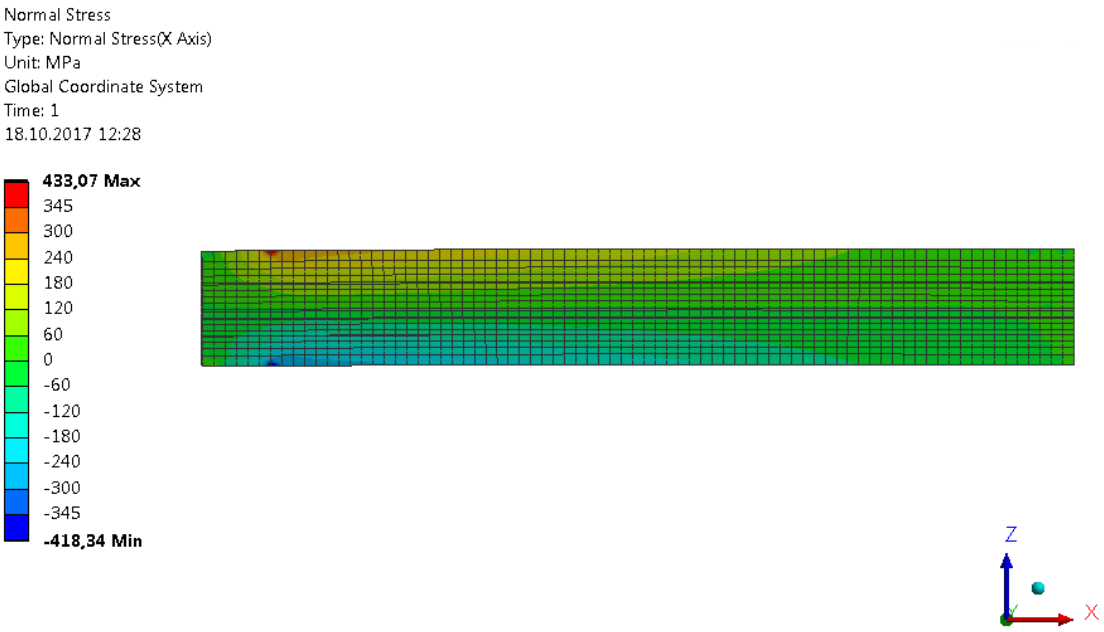

Fig. 8.19 Design variant III – normal stress along x axis – shaft

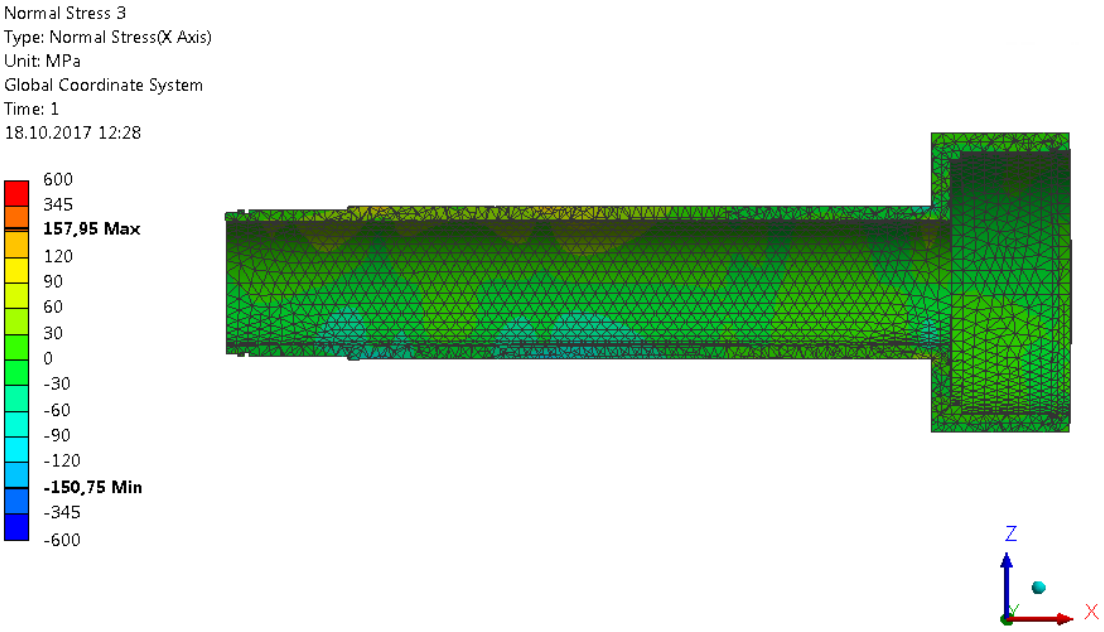

Fig. 8.20 Design variant III – normal stress along x axis – reference element

8.3.4 Assessment of the design variants

Design variant I

The stress analysis performed using the finite element method shows flaws in the relatively slender design of the sprocket shaft bearing assembly seen in design variant I. This relates to a shaft deflection of 4.6 mm (*Fig. 8.5*). In addition, local stress values as per *Fig. 8.6* and *Fig. 8.8* show that the yield strength of the steel used has been exceeded.

Design variant II

The result of the stress analysis for design variant II shows an increase in strength of the entire structure. The deflection of the shaft reduces to 4.3 mm (*Fig. 8.11*) and the stresses in the individual components do not exceed the yield strength (*Fig. 8.12*, *Fig. 8.13* and *Fig. 8.14*).

Design variant III

The FEM analysis for design variant III shows that the strength of the entire assembly lies between that of design variants I and II. *Fig. 8.17* shows a shaft deflection of 4.3 mm. As with the first design variant however, the yield strength of the steel used is exceeded locally (*Fig. 8.18* and *Fig. 8.19*).

Comparison of the design variants

The FEM analyses for the relevant structural sections of the different sprocket shaft bearing assembly variants were performed on simplified 3D models. These analyses have shown that design variant II is best suited in terms of strength.

However, in all variants it seems advantageous to reduce the bending moment by reducing the distance between the sprocket and the neighbouring roller bearing. It is also preferable to reduce the distance between roller bearings A and C as well as between roller bearings B and D. In any case, the distance a, where the shaft coupling is located, must also be considerably reduced and a compact design for the coupling must be found.

8.4 Optimised design variant of the sprocket shaft bearing assembly

The optimised design for the sprocket shaft bearing assembly is based on design variant II and focuses on a change to the coupling for joining the shaft.

8.4.1 Design variant II, optimised

With this derived design, the coupling, in which the shaft is fitted and connected using an axial screw (*Fig. 8.21*), has been optimised. Further properties of this design are identical to design variant II (section 8.3.2).

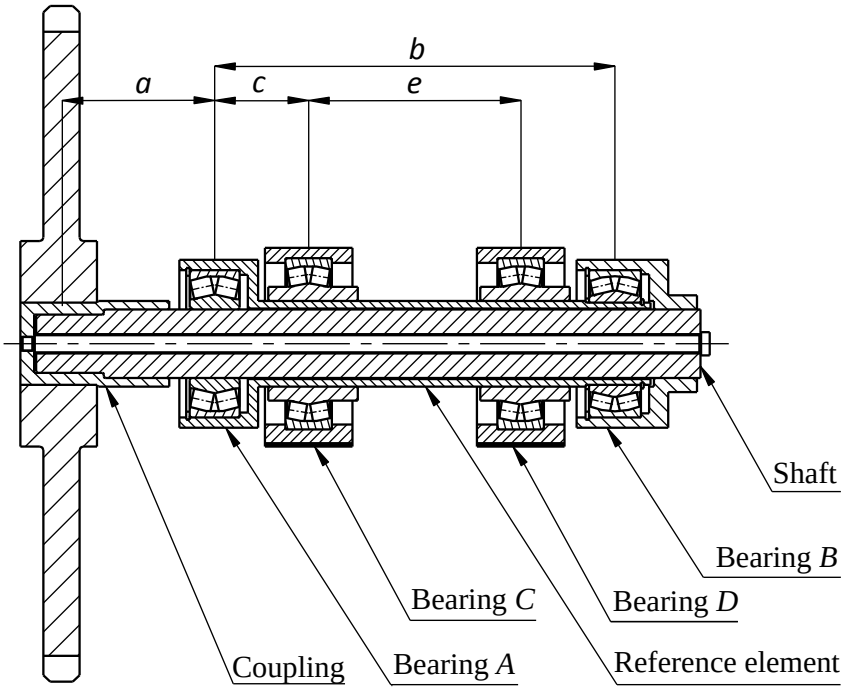

Fig. 8.21 Design variant II, optimised

The stress analysis results are summarised in *Table 8.7*.

Table 8.7 Design variant II, optimised – stress analysis results

Shaft		**Reference element**			
σ_{B2A} [MPa]	68	σ_{B2C} [MPa]	53	τ_{S2C} [MPa]	10
σ_{B3A} [MPa]	170	σ_{B3C} [MPa]	132	τ_{S3C} [MPa]	25
s_{B2A}	2.56	s_{B2C}	3.3	s_{S2C}	9.33
s_{B3A}	2.02	s_{B3C}	2.61	s_{S3C}	13.77

Roller bearings chosen based on calculations (5.40) to (5.44) from *TIMKEN*'s catalogue are recorded in *Table 8.8*.

Table 8.8 Design variant II, optimised – types of bearing

Bearing *A*	**Bearing *B***	**Bearing *C***	**Bearing *D***
22320 spherical roller bearing	23224 spherical roller bearing	22228 spherical roller bearing	22228 spherical roller bearing

FEM analysis

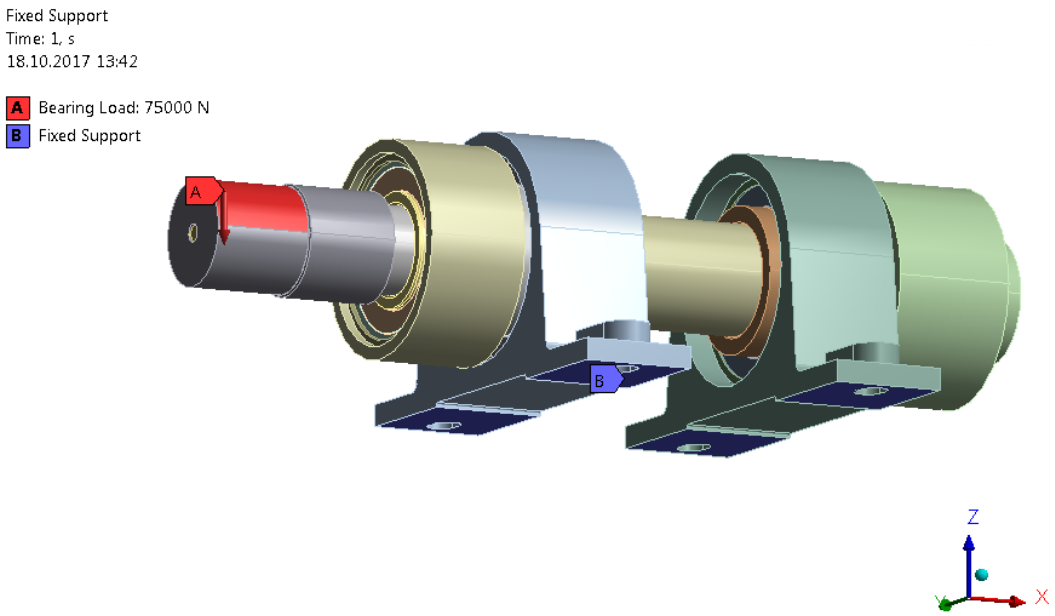

Fig. 8.22 Design variant II, optimised – load and boundary values

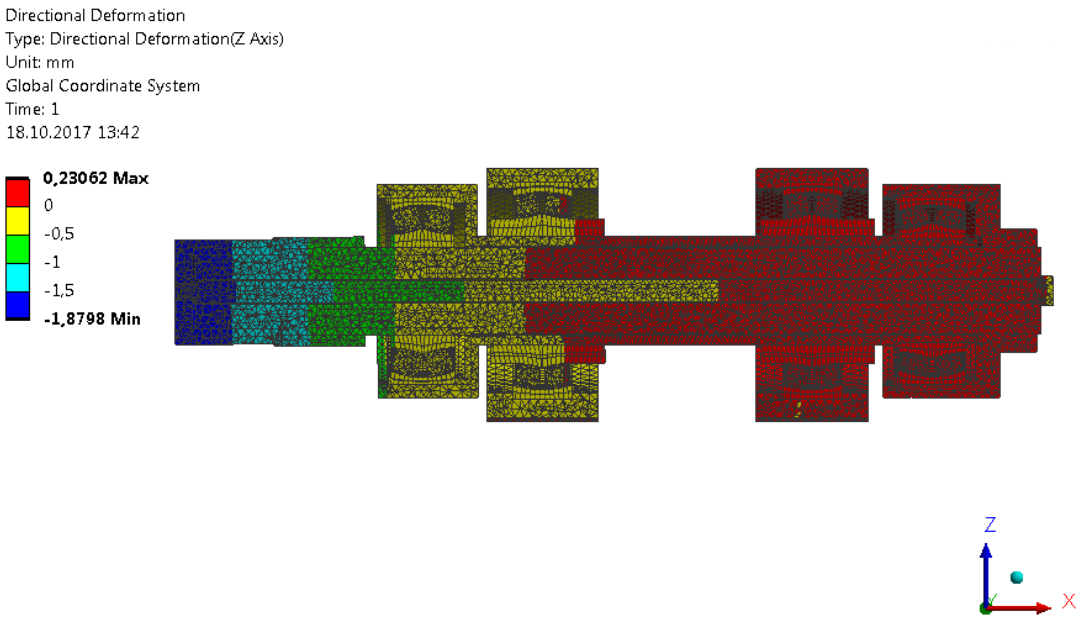

Fig. 8.23 Design variant II, optimised – deflection

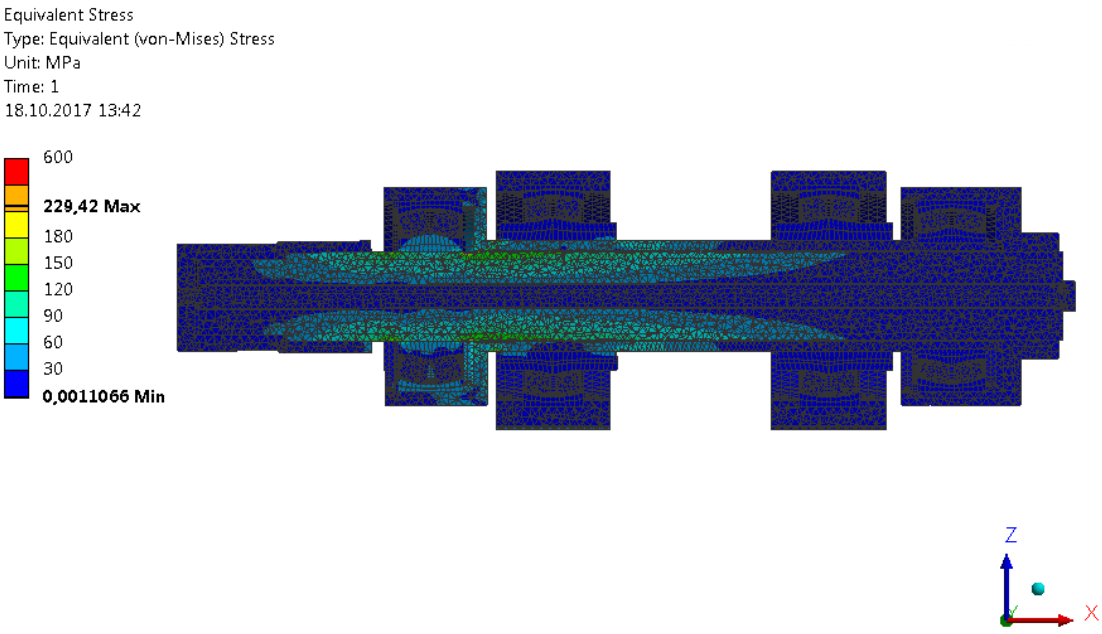

Fig. 8.24 Design variant II, optimised – equivalent stress (according to von Mises)

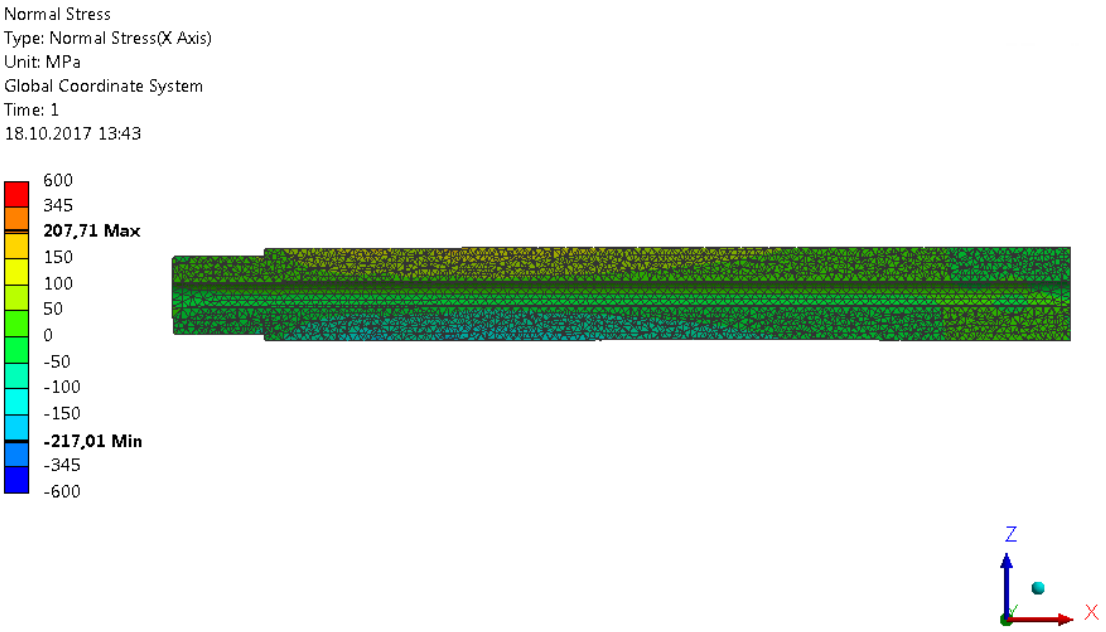

Fig. 8.25 Design variant II, optimised – normal stress along x axis – shaft

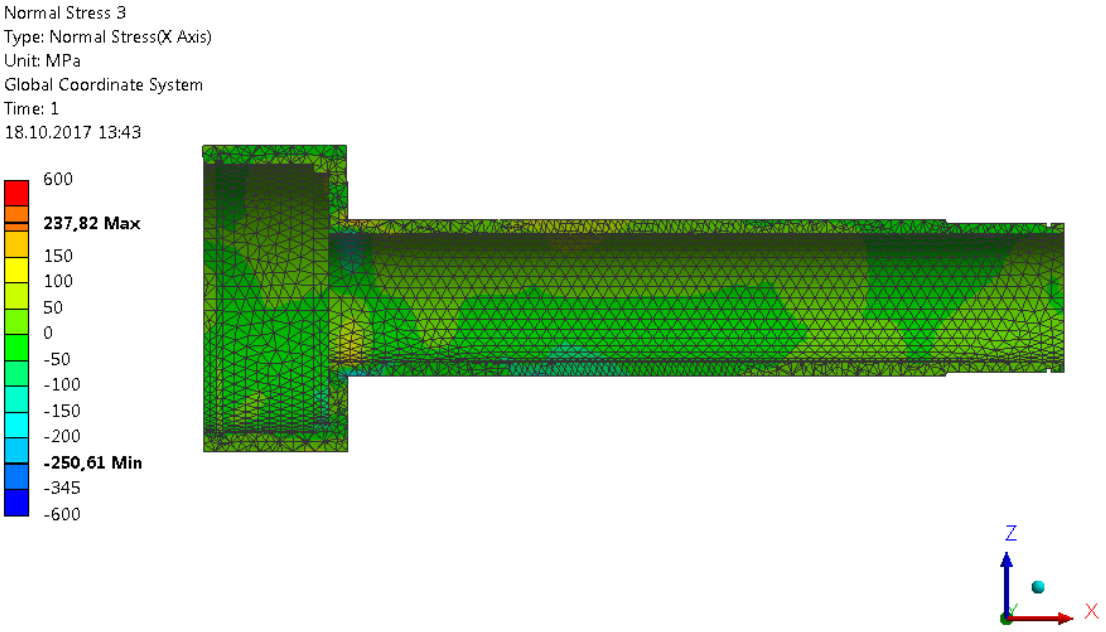

Fig. 8.26 Design variant II, optimised – normal stress along x axis – reference element

8.4.2 Assessment of the optimised design variant

In comparison to the original design variant II, the stress analysis for the optimised version of design variant II exhibits a considerable improvement in the strength of the new structure (*Fig. 8.23*). The deflection of the sprocket shaft has reduced to 1.9 mm. The stress analysis has shown satisfactory values. There are no longer any stresses approaching the yield strength of the steel used.

8.5 Design of the optimised sprocket shaft bearing assembly

The design of the optimised sprocket shaft bearing assembly can be seen in *Fig. 8.27*. The shaft consists of two components that are joined and connected to one another using an axial shaft coupling stud. One part of the shaft is firmly attached to the sprocket using a conical adapter and the second part of the shaft is connected to the reference element using two spherical roller bearings. The reference element is mounted using two further spherical roller bearings, which are positioned on a baseplate and are bolted to an installation frame. The shaft seal in the side wall of the installation frame consists of a seal assembly with braided packing.

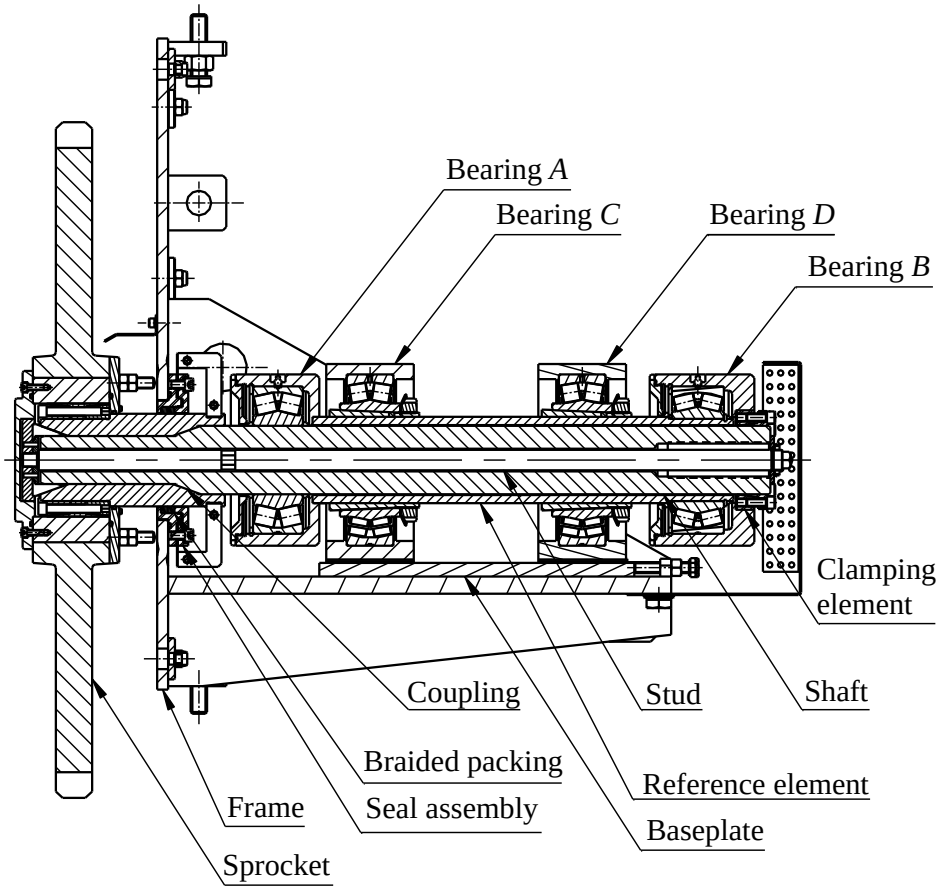

Fig. 8.27 Design of the optimised sprocket shaft bearing assembly

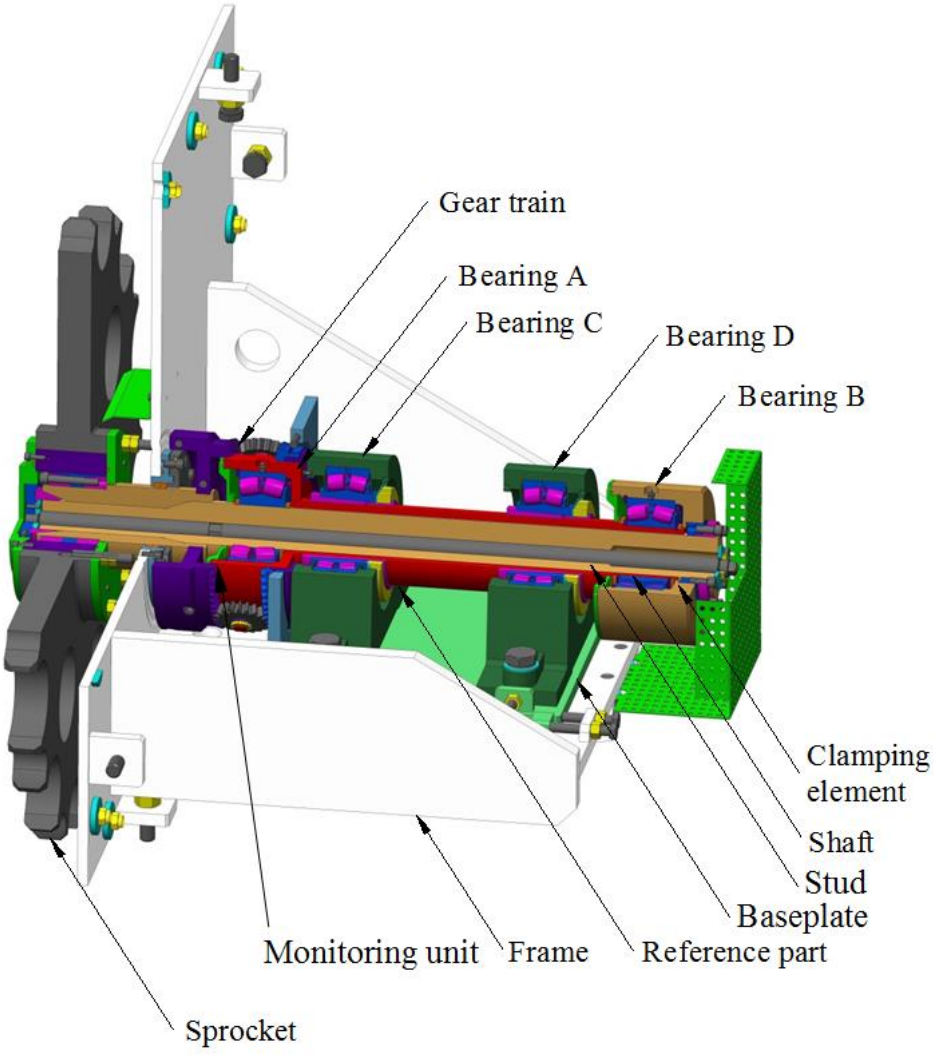

Fig. 8.28 Design of the optimised sprocket shaft bearing assembly including monitoring unit

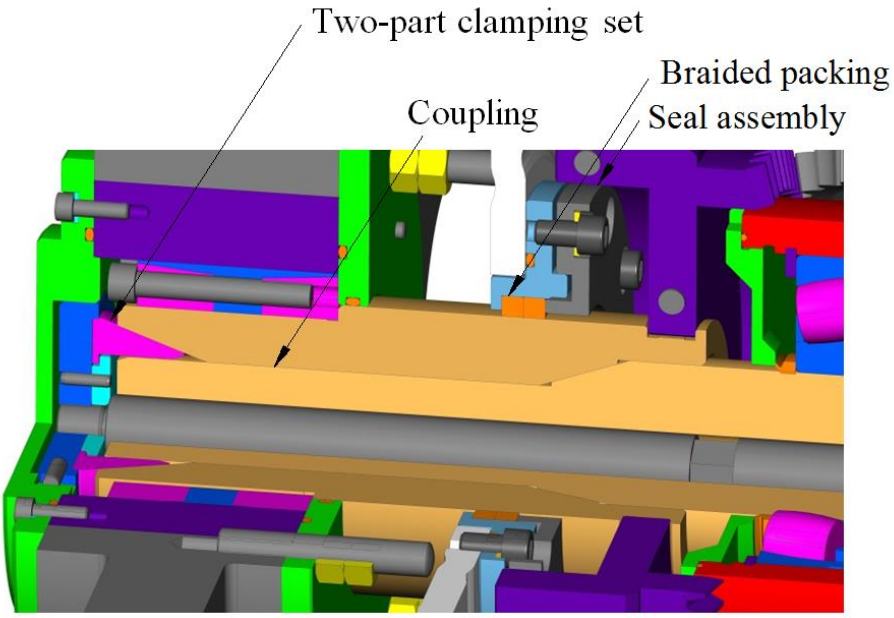

Fig. 8.29 Design of the sprocket shaft coupling

8.5.1 Parameters of the spherical roller bearing

The sprocket shaft bearing assembly incorporates four TIMKEN spherical roller bearings.

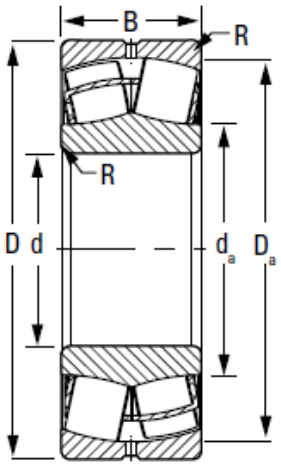

Fig. 8.30 Basic dimensions of the TIMKEN spherical roller bearing

Bearing *A* – TIMKEN 22320 spherical roller bearing with the parameters according to *Table 8.9.*

Table 8.9 Parameters of the TIMKEN 22320 roller bearing

Outer diameter	$D = 215$ mm
Inner diameter	$d = 100$ mm
Width	$B = 73$ mm
Weight	$m = 12.8$ kg
Dynamic load rating	$C = 768000$ N
Static load rating	$C_0 = 853000$ N

Bearing *B* – TIMKEN 23224 spherical roller bearing with the parameters according to *Table 8.10.*

Table 8.10 Parameters of the TIMKEN 23224 roller bearing

Outer diameter	$D = 215$ mm
Inner diameter	$d = 120$ mm
Width	$B = 76$ mm
Weight	$m = 11.8$ kg
Dynamic load rating	$C = 824000$ N
Static load rating	$C_0 = 1040000$ N

Bearing *C* and *D* – TIMKEN TAPN28K125S bearing assembly with integrated 22228 spherical roller bearing and H2328 adapter sleeve.

Table 8.11 Parameters of the TIMKEN 22228 bearing

Outer diameter	$D = 250$ mm
Inner diameter	$d = 140$ mm
Width	$B = 68$ mm
Weight	$m = 14.2$ kg
Dynamic load rating	$C = 863000$ N
Static load rating	$C_0 = 1060000$ N

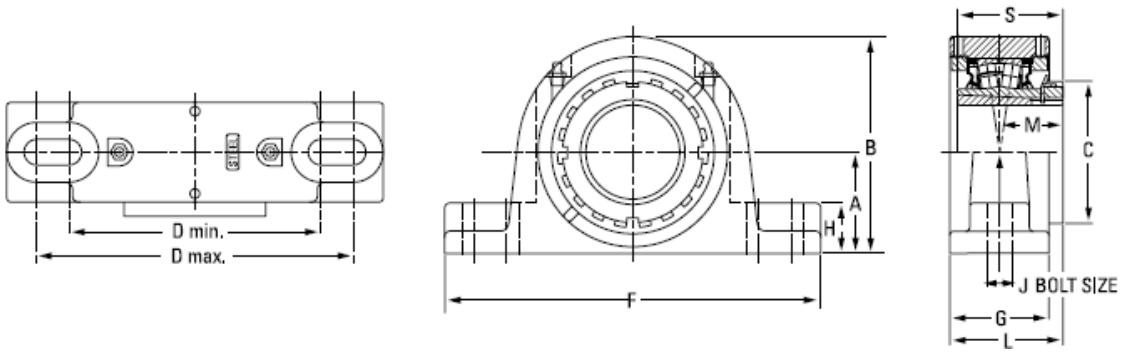

Fig. 8.31 Dimensions of the TIMKEN TAPN28K125S bearing assembly

Table 8.12 Parameters of the TIMKEN TAPN28K125S bearing assembly

Dimensions	$B = 288.5$ mm
	$F = 499.9$ mm
	$L = 120.4$ mm
Weight	$m = 61.8$ kg

8.5.2 Replacing the bearings in the event of repair

The roller bearings in this optimised design variant are replaced after disassembling the entire reference element unit.

Before disassembly, the sprocket including the coupling connected to it must be secured in the frame. For this purpose, a two-part clamping set is used. This shaft-hub-connection is fixed to the coupling and makes it possible for the sprocket to be secured to the side wall of the installation frame using clamping screws (*Fig. 8.32*). The side wall has a circular groove on both sides (*Fig. 8.32*). These grooves help to keep the clamping screws at their points of contact in the defined positions. In order to reduce the exposed length between the clamping set and side wall of the installation frame of all of the clamping set's screws to zero, the baseplate's adjusting screws must first be loosened and then the fixing bolts for frame bearings *C* and *D* removed (*Fig. 8.32*).

A removal tool is used for disassembling the reference element unit with the frame bearings. After removing the nut from the end of the shaft coupling stud, the removal tool is attached and, using the external thread, is screwed into the internal thread of the shaft. Thus, the shaft with the reference element unit is pulled outwards and detached from the coupling. Using an inserted extension piece, the assembly is pulled outwards until the hexagon of the shaft coupling stud (*Fig. 8.33*) is freely accessible. Using the hexagon, the shaft coupling stud is unscrewed from the coupling and the entire reference element unit can be removed.

Conversely, installing the reference element unit including the frame bearings is performed using an installation tool, which is attached to the shaft and is screwed together with the shaft coupling stud. The two parts, i.e. the shaft and the coupling, are reconnected and tightened using a hexagonal nut on the external thread.

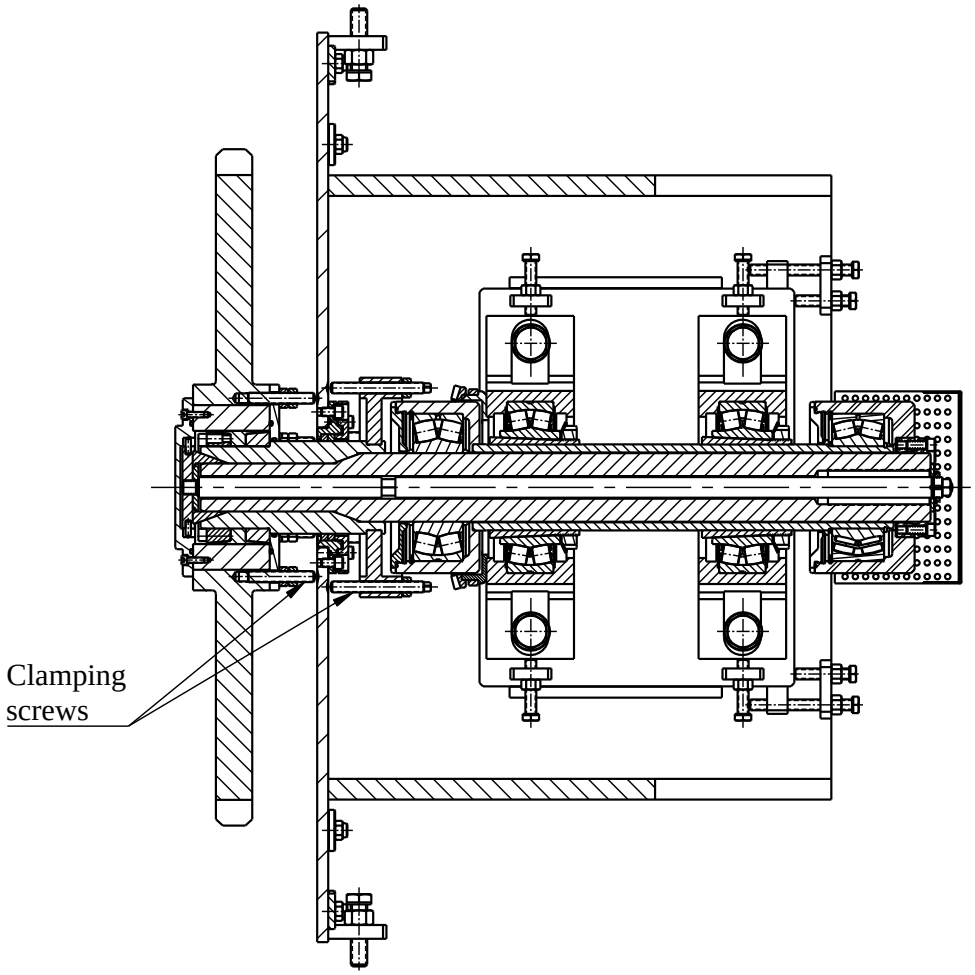

Fig. 8.32 Removing the reference element unit

This design solution also makes it relatively easy to replace the shaft seal located in the side wall of the installation frame without having to remove the entire shaft with the sprocket. This has been made possible due to the use of 10-mm-thick braided packing with a square cross section. Another advantage of this shaft seal is that it is less vulnerable to dry running and that it forms a better seal with the shaft than a seal ring.

Another special feature of this design is the connection of the coupling to the side wall of the installation frame using the CLAMPEX KTR 203 clamping set.

Using bearing grease, the braided packing used as the seal between the coupling and the reference element unit provides sufficient sealing properties.

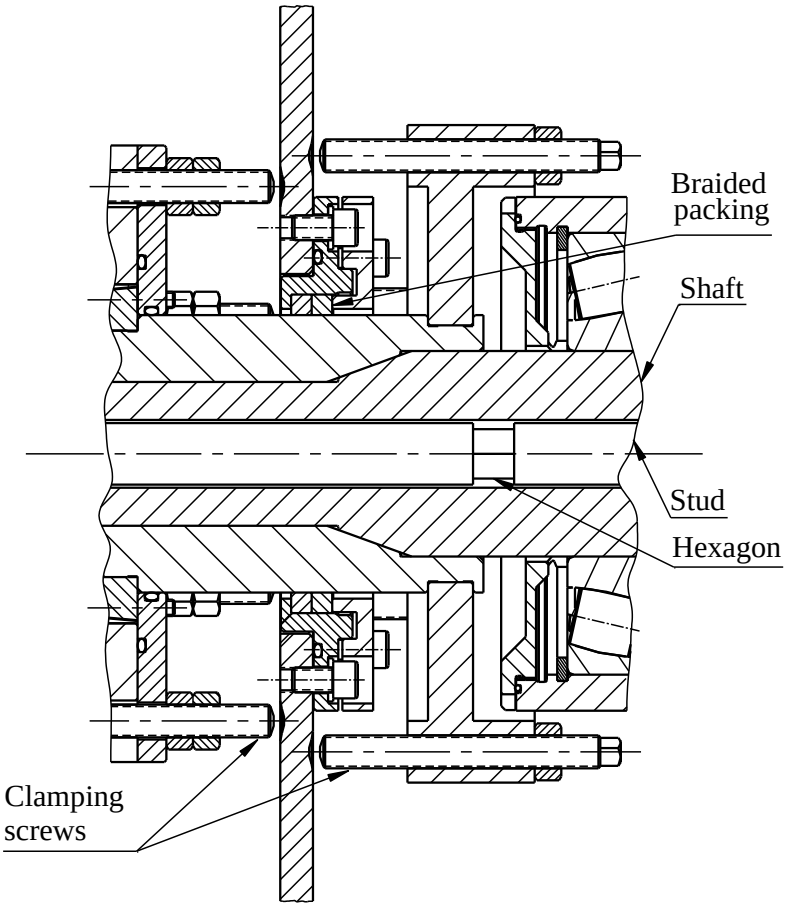

Fig. 8.33 Detail of the design solution

The change to the design makes maintenance simpler and replacing the seals easier, and provides a better seal position in relation to the coupling, and thus has excellent sealing properties.

9 Laboratory test of the diagnostic device

Two prototypes of the sprocket shaft bearing assembly were produced. The first prototype without monitoring unit was tested for fatigue and subsequently exposed to maximum load. The second prototype with monitoring unit was used for the diagnostic test. In both cases, the shaft was driven by a gearbox using an electric motor.

9.1 Fatigue test on the first prototype

The aim of the fatigue test on the first prototype of the sprocket shaft bearing assembly was to verify the design and functionality of the proposed solution.

During this test, the first prototype operated under 60% of the maximum load, i.e. a load of 4.5 tonnes at a shaft speed of 3.3 rpm. This test was carried out continuously over 1000 hours.

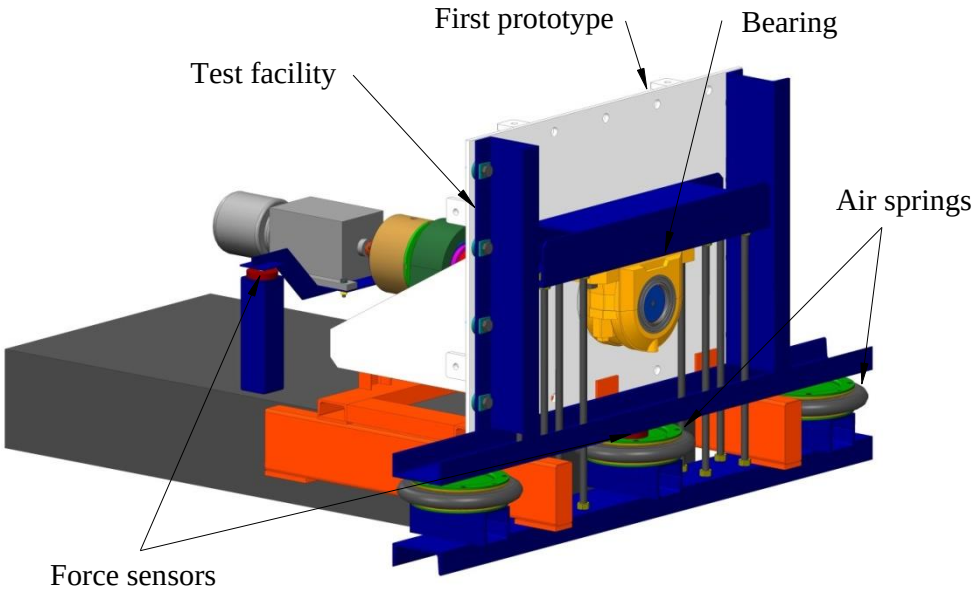

Fig. 9.1 Fatigue test on the first prototype

Fig. 9.1 illustrates the fatigue test on the first prototype.

The load on the shaft at the sprocket was absorbed by three 14-inch pneumatic springs via an FAG SCHAEFFLER 22228-E1-K roller bearing with an H3128 adapter sleeve mounted in an SNV250 bearing housing.

An electric motor was used to drive the first prototype and the motor's gearbox was connected to the sprocket shaft via a clutch (*Fig. 9.2*).

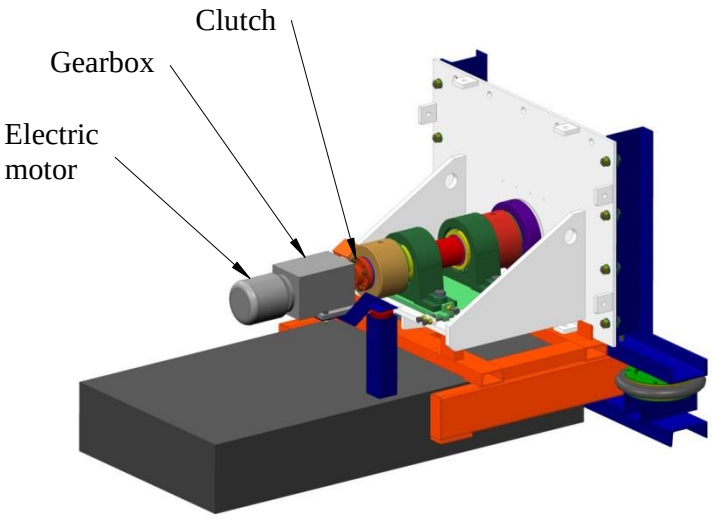

Fig. 9.2 Drive system for the first prototype's sprocket shaft during the fatigue test

During the load test, the sprocket shaft's load and torque were continuously measured.

Before the test commenced, it became apparent that there was almost no clearance between the shaft and the metal ring used for positioning the braided packing. Once the sprocket shaft was subjected to a load of 4.5 tonnes at the position of the sprocket, the ring came into contact with the shaft. Subsequently, the inner diameter of the metal ring for the braided packing assembly was increased by 4 mm.

The fatigue test was then conducted over 1000 hours. There was no sign of damage during this laboratory test, which was also confirmed by a constant level of shaft torque when idling.

9.2 Load test on the first prototype

The aim of the load test was to determine the maximum load on the sprocket shaft bearing assembly, which led to a total failure. During the laboratory test, the load on the first prototype was gradually increased until it was destroyed at a rotational speed of 3.3 rpm.

During the test, the force resulting from the torque, the deflection of the sprocket shaft and the load on the pneumatic springs (*Fig. 9.3*) were all measured. The data was recorded using a DEWETRON DEWE 5000 unit and DEWESoft 7.3 software.

Fig. 9.3 shows the design of the load test on the first prototype. The load on the shaft at the sprocket was absorbed by three 14-inch pneumatic springs via an FAG

SCHAEFFLER 22228-E1-K roller bearing with an H3128 adapter sleeve mounted in an SNV250 bearing housing.

Just like with the fatigue test, an electric motor was used to drive the first prototype and the motor's gearbox was connected to the sprocket shaft via a clutch (*Fig. 9.4*).

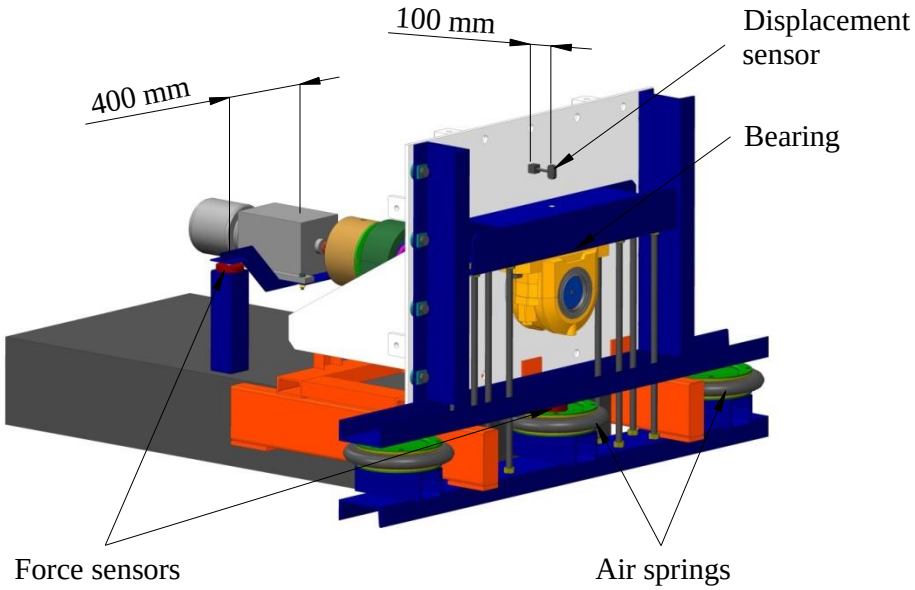

Fig. 9.3 Load test on the first prototype

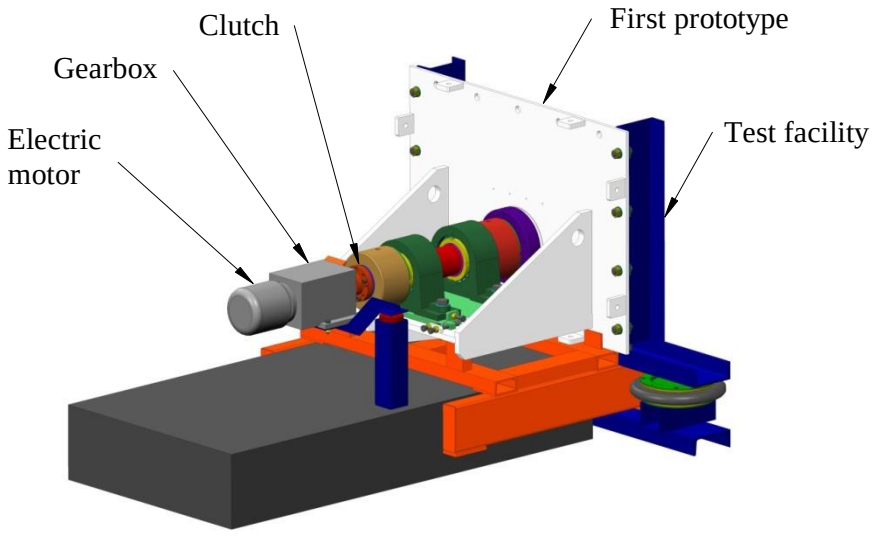

Fig. 9.4 Drive system for the first prototype's sprocket shaft during the load test

Fig. 9.5 shows a graph of all the measured data. The green line indicates the force in kN that corresponds to the sprocket shaft's driving torque. The vertical deflection of the shaft in mm at the load acceptance point is indicated by the red line. The blue line shows the load on the pneumatic springs in kN.

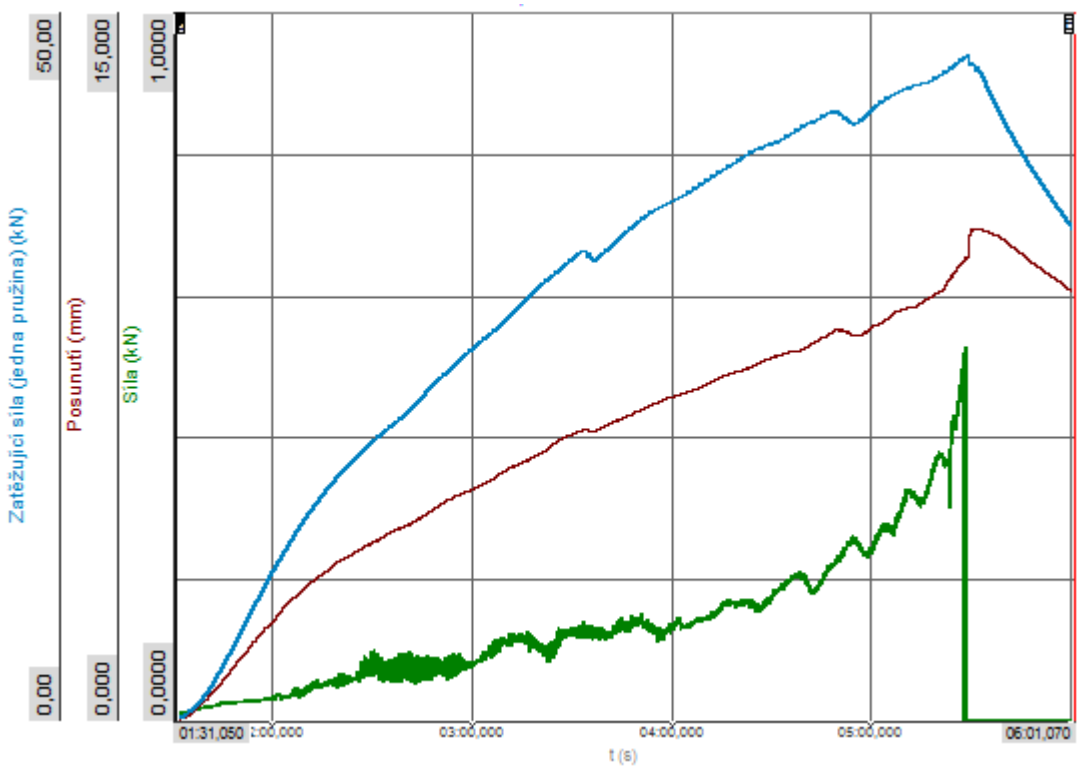

Fig. 9.5 Graph of all the measured data

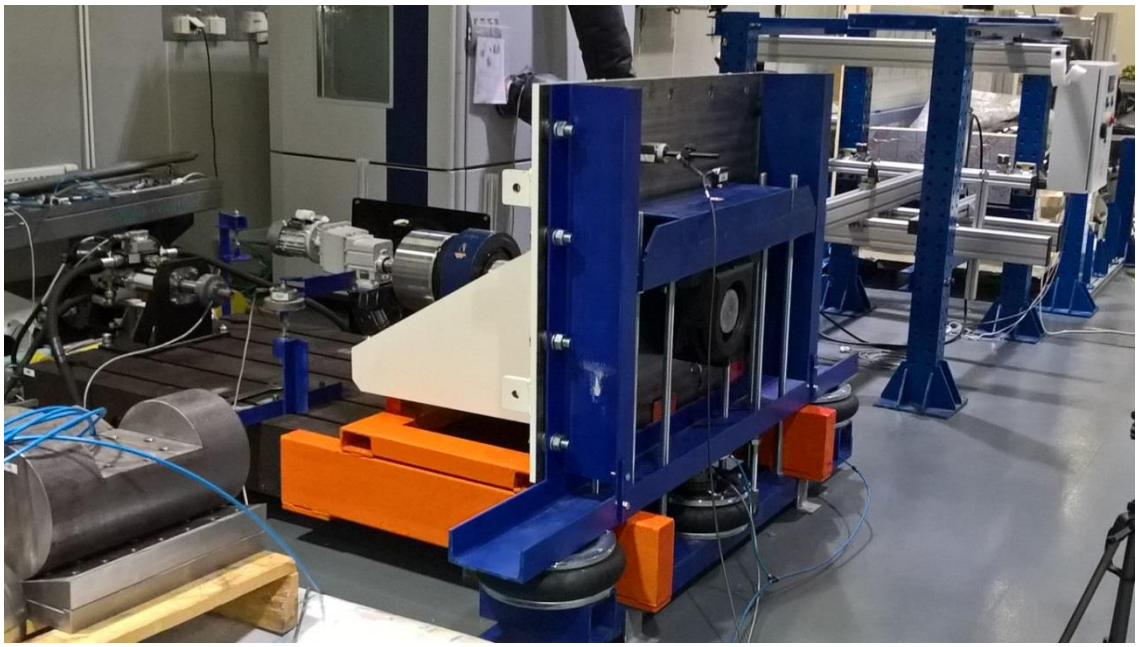

Fig. 9.6 Laboratory experiment using the first prototype

During the load test, two videos were shot of the first prototype – one from the front and one from the side.

Fig. 9.7 shows the evaluated measurements with their maximum values. In addition, the values for the sprocket shaft's vertical deflection and the torque of the drive unit are given at 4.5 tonnes and 7.5 tonnes. The green line shows the shaft's torque in Nm. The sprocket shaft's deflection in mm is illustrated by the red line and the load on the pneumatic springs in tonnes by the blue line.

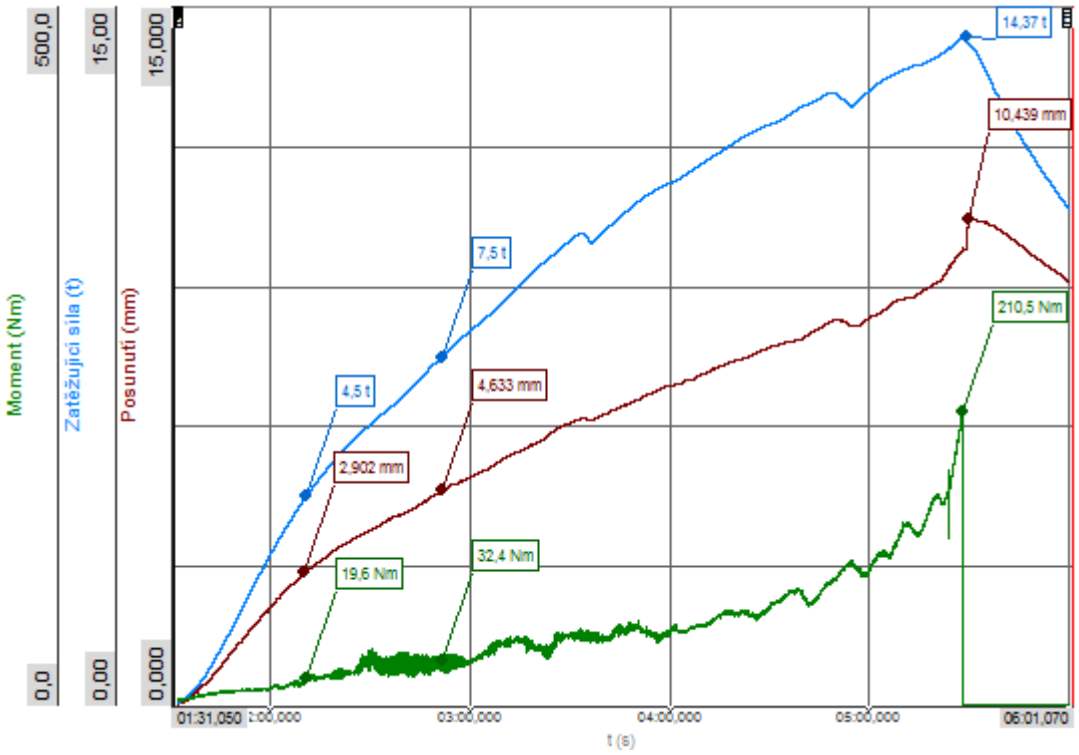

Fig. 9.7 Evaluation of all measured data

In the laboratory test, the load on the shaft at the position of the sprocket was increased to 14.37 tonnes. This led to a sprocket shaft deflection that was so great that the shaft interfered with the metal ring used for positioning the braided packing. As a result, the drive unit's torque increased to such an extent that the gearbox was destroyed.

The laboratory test demonstrated that the load rating of the design solution for the sprocket shaft bearing assembly was sufficient. At a load of 14.37 tonnes, no components were completely destroyed. However, at the end of the laboratory test, the sprocket shaft deflection exhibited a plastic deformation of 1.875 mm, which was measured with a dial indicator (*Fig. 9.8*).

Fig. 9.8 Measurement of the sprocket shaft's deflection

In addition, damage occurred on the surface of the shaft coupling stud (*Fig. 9.9)* during the laboratory test due to the extent of the sprocket shaft's deflection.

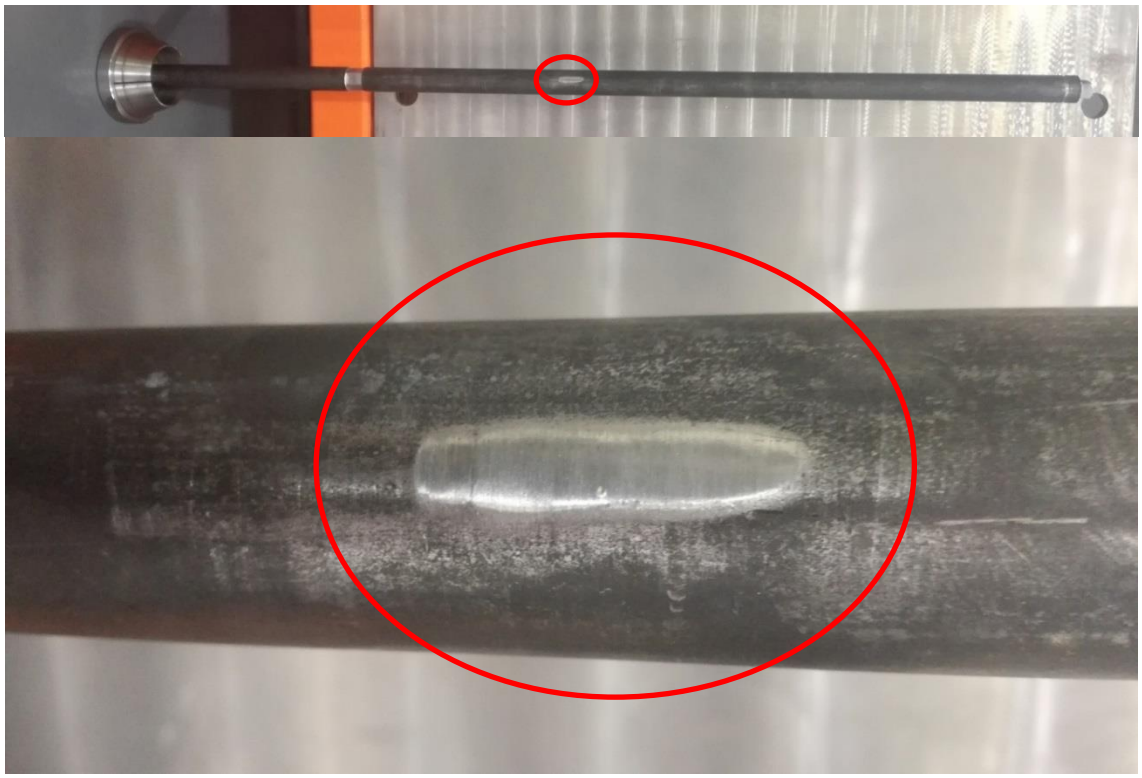

Fig. 9.9 Bending force on the shaft coupling stud

9.3 Diagnostic test on the second prototype

The aim of the diagnostic test was to test the function of the monitoring unit for damage to low-speed bearings. To this end, a second prototype of the sprocket shaft bearing assembly with a monitoring unit was used. The laboratory test consisted of the simulation of a bearing failure under a load of 4.5 tonnes (60% of the maximum load) at a sprocket shaft speed of 3.3 rpm.

Fig. 9.10 shows the experimental setup of the diagnostic test for the second prototype. Again, the load on the shaft at the sprocket was absorbed by three 14-inch pneumatic springs via an FAG SCHAEFFLER 22228-E1-K roller bearing with an H3128 adapter sleeve mounted in an SNV250 bearing housing.

An electric motor was used to drive the second prototype and the motor's gearbox was connected to the sprocket shaft via a clutch.

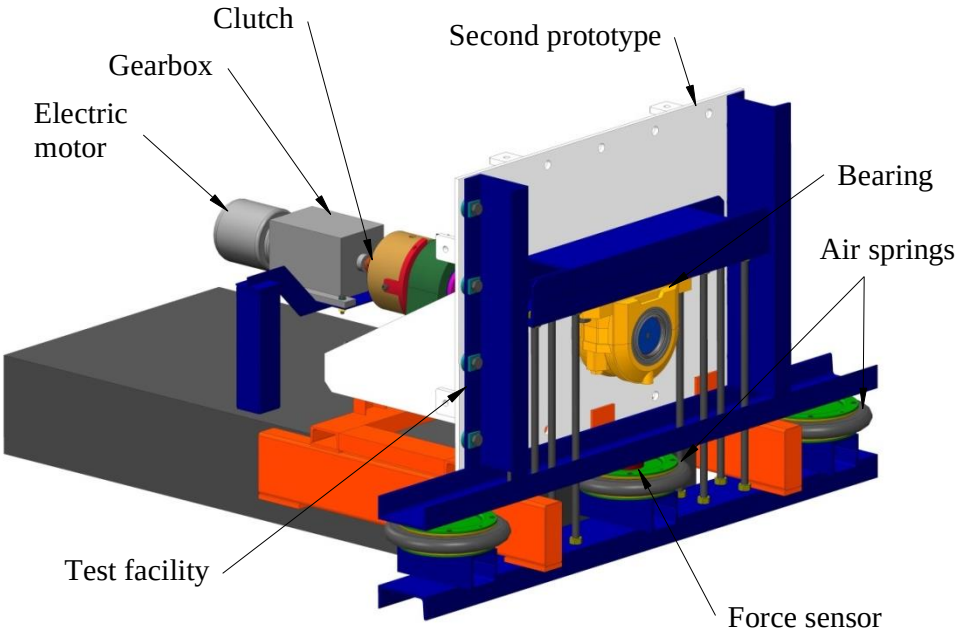

Fig. 9.10 Diagnostic test on the second prototype

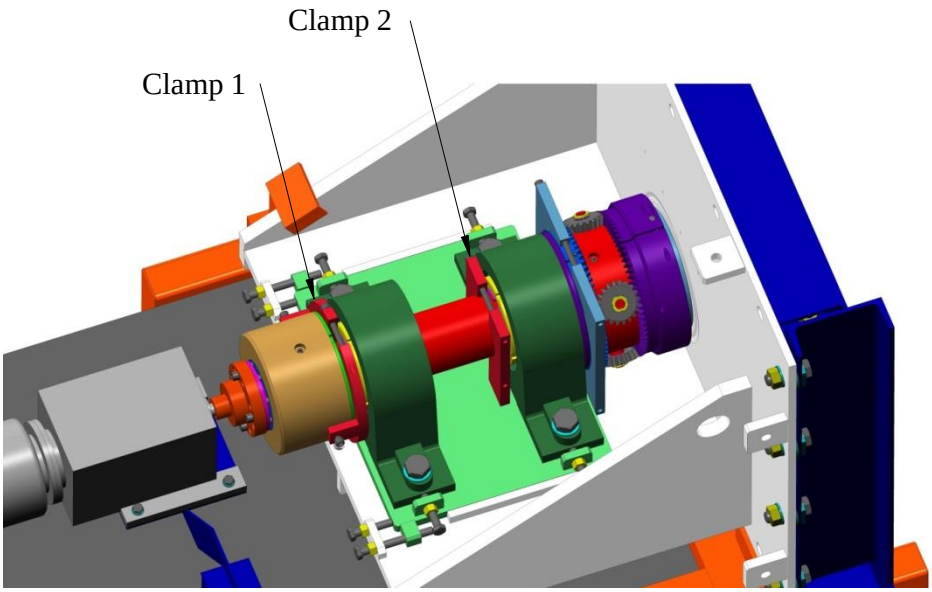

Fig. 9.11 Diagnostic test design for the second prototype

Fig. 9.11 shows the principle of the bearing failure simulation. When clamping the reference element to the sprocket shaft using clamping device 1, the movement between the shaft and the reference element is prevented, which simulates the failure of one of the shaft bearings located between the shaft and the reference element.

When clamping the reference element to the bearing housing using clamping device 2, the movement between the reference element and the installation frame is prevented, which simulates the failure of one of the frame bearings located between the reference element and the installation frame.

The diagnostic test of the functionality of the monitoring unit in the sprocket shaft bearing assembly showed no faults and thus proved the full functionality of the monitoring unit.

10 Conclusion

This thesis addresses a very topical issue relating to the running of diagnostics on low-speed bearings. In practice to this day, there is no reliable method, which can deliver acceptable results for the prediction of damage to these components in state-of-the-art production systems.

Whilst diagnostics have successfully been run on high-speed bearings in industry practice using vibration diagnostics, this method cannot be used for low-speed bearings. Running diagnostics on low-speed bearings therefore poses a great challenge for experts and engineers. This is a significant problem area with regard to reliable production without stoppages due to unexpected breakdowns, particularly for manufacturers of production lines.

This thesis resolves the specific issue of running diagnostics on low-speed bearings in the sprocket shaft bearing assemblies used in a chain conveyor in the pretreatment line at the ŠKODA AUTO a.s. paint shop in Mladá Boleslav. Due to negative experiences with failing bearings, and the significant financial losses associated with these failures, this thesis and the resulting findings are of great importance to ŠKODA.

Under the given circumstances, there has been a relatively high degree of flexibility in design when developing a solution to this problem. Following an analytical description of the chain conveyor's operating conditions, two different concepts for running diagnostics on low-speed bearings were developed. The basic idea behind these solutions was introducing a reference element into the sprocket shaft bearing assembly.

Using a pair of shaft and frame bearings each, this component can rotate both around the shaft and within the frame. As a result, the reference element has a degree of rotational freedom and can rotate independently. This degree of freedom can be used to technically run diagnostics on low-speed bearings in two different ways.

Firstly, it is possible to rotate the reference element at a high speed and to measure the vibrations that occur as a result of bearing damage. The rotational speed of the reference element can be defined and, if necessary, changed to correlate with the desired excitation frequency that, in the frequency spectrum of the vibrations measured at the bearing assembly, corresponds to the relevant damage. This makes the diagnostic method incredibly reliable. This solution has been successfully patented at a European level.

Secondly, if the bearings are undamaged, the reference element should be able to rotate freely and without resistance. If the moment of resistance increases, it means that one of the bearings is damaged. This method of running diagnostics is considerably simpler in terms of the design and work required, and is also more cost effective. Over the course of this thesis, this second method has been developed at length, all the way through to a

prototype. In the process, three different variants for the sprocket shaft bearing assembly were designed. One of the variants was chosen and then optimised until it was suitable for production.

The monitoring unit, which is based on detecting an increase in the moment of resistance, was realised using a planetary gear system and was also patented. Subsequently the entire sprocket shaft bearing assembly including the monitoring unit was manufactured and tested at length under laboratory conditions. Following successful test results, this design solution was installed in the ŠKODA AUTO a.s. paint shop in Mladá Boleslav in summer 2018 and put into operation.

Literature

[1] MISHRA, Chandrabhanu, SAMANTARAY, Arun Kumar, CHAKRABORTY, Goutam. Rolling element bearing fault diagnosis under slow speed operation using wavelet de-noising. *MEASUREMENT*. 2017, 103, 77-86. ISSN 0036-9942.

[2] HUANG, Hsin-Cheng, CRESSIE, Noel. Deterministic/stochastic wavelet decomposition for recovery of signal from noisy data. *TECHNOMETRICS*. 2000, 42 (3), 262-276. ISSN 0040-1706.

[3] HE, Miao, HE, David. Deep Learning Based Approach for Bearing Fault Diagnosis. *IEEE TRANSACTIONS ON INDUSTRY APPLICATIONS*. 2017, 53 (3), 3057-3065. ISSN 0093-9994.

[4] SAKO, Takashi a YOSHIE, Osamu. Diagnostic method of low speed rolling element bearing using AE envelope waveform. In: *TENCON 2010: 2010 IEEE REGION 10 CONFERENCE*. New York: IEEE, 2010, s. 724-729. ISBN 978-1-4244-6890-4

[5] SONG, Liuyang, WANG, Huaqing, CHEN, Peng. Vibration-Based Intelligent Fault Diagnosis for Roller Bearings in Low-Speed Rotating Machinery. *IEEE TRANSACTIONS ON INSTRUMENTATION AND MEASUREMENT*. 2018, 67 (8), 1887-1899. ISSN 0018-9456.

[6] ELFORJANI, Mohamed. Diagnosis and prognosis of slow speed bearing behaviour under grease starvation condition. *STRUCTURAL HEALTH MONITORING-AN INTERNATIONAL JOURNAL*. 2018, 17 (3), 532-548. ISSN 1475-9217.

[7] SUTRISNO, Edwin, OH, Hyunseok, VASAN, Arvind Sai Sarathi a PECHT, Michael. Estimation of remaining useful life of ball bearings using data driven methodologies. In: *PHM 2012: 2012 IEEE International Conference on Prognostics and Health Management*. Denver, 2012, s. 18-21. ISBN: 978-1-4673-0356-9.

[8] HITACHI BUILDING SYSTEMS CO. LTD. Method of diagnosing anomalies in low speed rotational bearing of elevator. JP application JP 2013224853 A. 31.10.2013.

[9] NIPPON STEEL SUMIKIN CO. LTD. Abnormality diagnosis method for low-speed rotary machine bearing, apparatus and program. JP grant JP 5640999 B2. 17.12.2014.

[10] NIPPON STEEL AND SUMITOMO METAL CORP. Method and system for abnormality diagnosis of very low speed rotating machine. US grant US 8534128 B2. 17.9.2013.

[11] NIPPON STEEL SUMIKIN CO. LTD. a POSCO. Acoustic sensor device. JP grant JP 5178594 B2. 10.4.2013.

[12] *Hauptkatalog* SKF Group, 2007. 1134 s.

[13] DRESIG, Hans und HOLZWEISSIG, Franz, Maschinendynamik. 8. Auflage. Springer Berlin. 2007. ISBN: 978-3-540-72032-4.

[14] ŠKODA AUTO a.s. A device for error diagnosis of low-speed bearings. Inventors: Michael OELJEKLAUS, Lubomír PEŠÍK and Marek JANCÁK. EP grant EP 3225967 B1. 4.10.2017.

[15] ŠKODA AUTO a.s. Vorrichtung zum Überwachen wenigstens einer Lagereinrichtung sowie Maschine mit wenigstens einer solchen Vorrichtung. Inventors: Michael OELJEKLAUS, Lubomír PEŠÍK a Marek JANCÁK. Anmeldung der Erfindung PV 2018-86. 21.02.2018.

List of authors publications

OELJEKLAUS, Michael, PEŠÍK, Lubomír. Kinematic similarity of rolling bearing with planetary gears – a review. *International Conference of Machine Design Departments ICMD 2017*. Praha, 2017, s. 276-279. ISBN 978-80-213-2769-6.

OELJEKLAUS, Michael, PEŠÍK, Lubomír. The diagnostic system of low speed bearings. *Experimental Stress Analysis EAN 2018*. Harrachov, 2018, s. 308-313. ISBN 978-80-270-4062-9.

OELJEKLAUS, Michael, PEŠÍK, Lubomír. Control system for slow running bearings. *Scientific Journal of Silesian University of Technology – Series Transport*. 2018, 100, 157-164. ISSN 0209-3324.

OELJEKLAUS, Michael, PEŠÍK, Lubomír. Kinematic similarity of rolling bearing with planetary gears – a review. *International Conference of Machine Design Departments ICMD 2018*. Demänovská Dolina.

Appendix

A On attached CD

Text of Dissertation thesis

- Dissertation thesis_2019_Michael_Oeljeklaus.pdf